

A Nicol

# National Tsunami Model: Stage 1 Final Report

B Fry WL Power L Hughes
E Lane YI Syed NA Horspool
A Howell A O'Kane Y-WM Liao

**CA Williams** 

GNS Science Report 2025/09 Revised September 2025

# **Earth Sciences**New Zealand

#### **DISCLAIMER**

The Institute of Geological and Nuclear Sciences Limited (GNS Science) and its funders give no warranties of any kind concerning the accuracy, completeness, timeliness or fitness for purpose of the contents of this report. GNS Science accepts no responsibility for any actions taken based on, or reliance placed on the contents of this report and GNS Science and its funders exclude to the full extent permitted by law liability for any loss, damage or expense, direct or indirect, and however caused, whether through negligence or otherwise, resulting from any person's or organisation's use of, or reliance on, the contents of this report.

#### **BIBLIOGRAPHIC REFERENCE**

Fry B, Power WL, Hughes L, Lane E, Syed YI, Horspool NA, Howell A, O'Kane A, Liao Y-WM, Nicol A, et al. 2025. National Tsunami Model: Stage 1 final report (Rev. ed.). Lower Hutt (NZ): GNS Science. 32 p. (GNS Science report 2025/09). https://doi.org/10.21420/FE6N-0E17

B Fry, GNS Science, PO Box 30368, Lower Hutt 5040, Aotearoa New Zealand
WL Power, GNS Science, PO Box 30368, Lower Hutt 5040, Aotearoa New Zealand
L Hughes, GNS Science, PO Box 30368, Lower Hutt 5040, Aotearoa New Zealand
E Lane, National Institute of Water & Atmospheric Research, PO Box 8602, Christchurch 8440,
Aotearoa New Zealand

YI Syed, GNS Science, PO Box 30368, Lower Hutt 5040, Aotearoa New Zealand NA Horspool, GNS Science, PO Box 30368, Lower Hutt 5040, Aotearoa New Zealand A Howell, GNS Science, PO Box 30368, Lower Hutt 5040, Aotearoa New Zealand A O'Kane, GNS Science, PO Box 30368, Lower Hutt 5040, Aotearoa New Zealand Y-WM Liao, GNS Science, PO Box 30368, Lower Hutt 5040, Aotearoa New Zealand A Nicol, University of Canterbury, Private Bag 4800, Christchurch 8140, Aotearoa New Zealand CA Williams, GNS Science, PO Box 30368, Lower Hutt 5040, Aotearoa New Zealand

# **CONTENTS**

Abstr	act		v
Keyw	ords		v
Fund	ing Ack	nowledgement	v
1.0	Intro	ductionduction	1
2.0	Stage	e 2: National Tsunami Model Framework	2
	2.1	Modular Approach	
	2.2	Source Model	
	2.3	Wave Propagation and Inundation	6
	2.4	Impacts	6
	2.5	Workflow	7
	2.6	Testing	8
3.0	Te W	hanganui-a-Tara / Wellington Region Tsunami Model	9
	3.1	Vertical Deformation and Tsunami Initial Conditions	. 10
	3.2	Hydrodynamic Modelling and Coastal Hazard	. 11
	3.3	Inundation	.14
4.0	Build	ing Loss Calculations	19
	4.1	Relationship between Tsunami Events and Building Loss	. 19
	4.2	Annualised Loss	. 20
	4.3	Deaggregation of Loss	. 21
	4.4	Risk from Distant Events	. 27
5.0	Sum	mary	30
6.0	Ackn	owledgements	31
7.0	Refe	rences	31
		FIGURES	
Figure	2.1	Working model of a framework for a physics-based National Tsunami Model	2
Figure	2.2	Hybrid workflow for a physics-based National Tsunami Model	3
Figure		Each row represents an earthquake source for a tsunami scenario modelled for Stage 1	
Figure	2.4	Source-model generation, including both physics-based (synthetic seismicity, e.g. Robinson and Benites [1996]) and traditional (stochastic) branches	
Figure	2.5	Ongoing work to define circum-Pacific subduction-zone sources	5
Figure	2.6	Modelling framework in which source models feed into hydrodynamic models to calculate	
		inundation and flow velocity for every scenario	
Figure		Map of impact calculation, including loss and risk, as well as scenario analysis.	
Figure	2.8	Cylc workflow showing tasks (circles) and dependencies (arrows) as it progresses through tir	
Figure	3.1	Spatial distribution of earthquakes from the RSQSim catalogue comprising the Stage 1 sourc	e
Figure	3.2	Coastal-tsunami-hazard generated using all earthquakes with a magnitude greater than M <sub>W</sub> 7	7.5

Figure 3.3	Tsunami hazard for the Chatham Islands generated using all earthquakes with a magnitude greater than $M_W$ 7.5	13
Figure 3.4	Tsunami hazard around the Greater Wellington region generated using all earthquakes with a magnitude greater than $M_W$ 7.5 and earthquakes between $M_W$ 6.5 and 7.5 that generate deformation with 500 km of Te Whanganui-a-Tara / Wellington Region	
Figure 3.5	Example of coastal amplitude and inundation modelling of an earthquake from the catalogue	15
Figure 3.6	Inundation across Te Whanganui-a-Tara / Wellington Region calculated for different return periods	17
Figure 3.7	Summary of the inundation across Te Whanganui-a-Tara / Wellington Region	
Figure 4.1	Expected loss at different return periods	19
Figure 4.2	Distribution of the average annualised losses for different time segments of the entire 30,000-year earthquake catalogue	-
Figure 4.3	Event loss versus magnitude for events that only rupture the subduction megathrust	22
Figure 4.4	Annualised loss for events that only rupture the subduction megathrust	22
Figure 4.5	Event loss versus magnitude for subduction megathrust plus Wellington Fault events	23
Figure 4.6	Annualised loss for subduction megathrust plus Wellington Fault events	23
Figure 4.7	Event loss versus magnitude for subduction megathrust plus Wairarapa Fault events	24
Figure 4.8	Annualised loss for subduction megathrust plus Wairarapa Fault events	24
Figure 4.9	Event loss versus magnitude for subduction megathrust plus Alpine Fault events	25
Figure 4.10	Annualised loss for pure subduction megathrust events	25
Figure 4.11	Event loss versus magnitude for events that only rupture the Wellington Fault	26
Figure 4.12	Annualised loss of events that only rupture the Wellington Fault	26
Figure 4.13	Inundation generated by a selection of nine distant source earthquakes taken from the New Zealand Tsunami Threat-Level Database	27
Figure 4.14	Relationship between earthquake magnitude and the total loss for each event	29
	TABLES	
Table 3.1	Nested grid used in COMCOT to undertake the coastal amplitude simulations	11
Table 3.2	Boundaries of the nested grids used in COMCOT to undertake the coastal amplitude simulations.	11
Table 3.3	Nested grids in COMCOT for inundation modelling	16
Table 3.4	Boundaries of the nested grids used for inundation modelling	16
Table 4.1	Summary of how the average annualised loss changes depending on which sub-set of earthquakes is analysed.	
Table 4.2	Summary of the variability in the average annualised loss when the entire model space is sampled at different-length sub-sets of the earthquake catalogue are analysed	20
Table 4.3	Summary of the inundation statistics and total loss generated by a selection of distant-source earthquakes taken from the New Zealand Tsunami Threat-Level Database	е

# **APPENDICES**

APPENDIX 1	National Tsunami Model Stage 1.a	35
A1.1	Introduction	35
A1.2	Peer Review of the Physics-Based Source Model	35
A1.3	Technical Advisory Group	
A1.4	Comparison of NTM Stage 1 and NTHM	
	A1.4.1 Scenario Selection and Simulations	
	A1.4.2 Hazard and Loss Comparison	
	A1.4.3 Return Period Hazard Comparison	
	A1.4.4 Loss Comparison	
	A1.4.5 16 <sup>th</sup> , 50 <sup>th</sup> and 84 <sup>th</sup> Percentile Comparisons	
	A1.4.6 Comparison of Sensitivity to Sea Level, Friction and Model Resolution between the NTHM and NTM Stage 1 Events	n
	A1.4.7 Simulations at Mean High Water Springs	
	A1.4.8 Simulations Run with Different Resolutions and Roughness Coefficients	
A1.5	Discussion of Differences between NTM Stage 1 and NTHM	
711.0	A1.5.1 Hikurangi Subduction Margin Events	
	A1.5.2 Wairarapa Fault Events	
	A1.5.3 Jordan-Kekerengu-Needles Fault Events	
	A1.5.4 Hope-Te Rapa Fault Events	
A1.6	IT Infrastructure Necessary for Nation-Wide Probabilistic Tsunami Risk Calculation	55
A1.0	with Hydrodynamic Tsunami Simulations	54
A1.7	Summary	
	APPENDIX FIGURES	
Figure A1.1	Maps of the inundation generated at different return periods when the simulator events are used and when the traditional approach to hazard is used	
Figure A1.2	Comparison of the exceedance curves for total loss (calculated using RiskScape) for the two alternative approaches.	
Figure A1.3	Comparison of the total loss exceedance curve (calculated using RiskScape) for the two alternative approaches.	40
Figure A1.4	Comparison of the total loss exceedance curves (calculated using RiskScape) for the Simula approach (black) and the weighted mean of the losses in the traditional approach (yellow) at each return period.	
Figure A1.5	Comparison of the total loss exceedance curves (calculated using RiskScape) for the two alternative approaches (simulator and traditional composite hazard).	44
Figure A1.6	Maps of the inundation generated at different return periods when the simulator events are used and when the traditional approach to hazard is used, and modelling is undertaken at me high water spring (mean sea level + 0.68 m).	
Figure A1.7	Comparison of the total loss exceedance curves (calculated using RiskScape) for the two alternative approaches, when modelling is undertaken at mean high water springs (mean sea level + 0.68 m).	
Figure A1.8	Comparison of the losses that are generated by the two approaches when modelling is undertaken at both mean sea level and mean high water springs.	. 47
Figure A1.9	Comparison of the losses that are calculated when different modelling resolutions and friction coefficients are used.	n

Figure A1.10	Initial surface displacements for the different scenarios modelled (Hikurangi)	50	
Figure A1.11	Initial surface displacements for the different scenarios modelled (Wairarapa and Wharekauhau)	51	
Figure A1.12	Initial surface displacements for the different scenarios modelled (Jordan-Kekerengu-Needles	•	
Figure A1.13	Initial surface displacements for the different scenarios modelled (Hope – Te Rapa)	54	
	APPENDIX TABLES		
Table A1.1	Summary of the losses for each event, and their associated weights, divided based on percentile of uncertainty and return period.	41	
Table A1.2	Summary of the Hikurangi earthquake magnitudes from the traditional approach and the simulator.	49	
Table A1.3	Summary of the Wairarapa earthquake magnitudes from the traditional approach and the simulator.	51	
Table A1.4	Summary of the Jordan-Kekerengu-Needles earthquake magnitudes from the traditional approach and the simulator.	52	
Table A1.5 Summary of the Hope-Te Rapa earthquake magnitudes from the traditional approach simulator.			

## **ABSTRACT**

In this report, we present the outcomes of Stage 1 of the National Tsunami Model. Central to this work is the use of physics-based source catalogues and hydrodynamic modelling of tsunami impacts. Drawing upon this work, and in consultation with the wider Aotearoa New Zealand research community, we have developed a strategy for a nationally consistent model of tsunami hazard and risk. We apply this approach to Te Whanganui-a-Tara / Wellington Region. In this framework, we use physics-informed models of the earthquake cycle to generate a catalogue of 30,000 years of synthetic earthquakes. We analyse this catalogue and create hydrodynamic models of inundation for the events that create significant loss. Loss is then calculated with the RiskScape™ platform. We conclude by presenting a new model of tsunami hazard and risk that includes the critically important effects of complex, multi-fault rupture.

# **KEYWORDS**

Tsunami risk model, tsunami scenarios, tsunami loss, synthetic seismicity

# **Funding Acknowledgement**

The National Tsunami Model, Stage 1 and 1.a are the direct result of funding from the Natural Hazards Commission Toka Tū Ake (NHC) under contract #4133. Work builds upon the Resilience to Nature's Challenges (RNC) National Science Challenge Earthquake and Tsunami Programme. Stage 1 and 1a also draw upon previous funded work including the Tsunami impact and loss modelling in Hawkes Bay project (contract #20/LM773) a study funded by the NHC (then the Earthquake Commission).

This page left intentionally blank.

## 1.0 Introduction

Aotearoa New Zealand does not currently have a National Tsunami Inundation Model (NTIM) or National Tsunami Risk Model (NTRM). This constitutes a critical gap in Aotearoa New Zealand's disaster risk reduction. Advanced, nationally consistent tsunami risk models allow us to (1) reduce the impacts of future tsunami through better estimation of the impact to people and property, including financial and societal losses, leading to better strategies for risk management; and (2) develop appropriate credible-event scenarios to test our response systems and provide insight into ways that these systems can be strengthened.

To address this critical gap, we have begun a three-stage National Tsunami Model programme to provide a nationally consistent NTIM and NTRM. This report documents the completion of Stage 1 of the National Tsunami Model. We report against the eight milestones contracted for Stage 1. Stage 1 comprises the application of synthetic seismicity earthquake-cycle modelling developed during the Earthquake and Tsunami Programme of the Resilience to Nature's Challenges (RNC2) National Science Challenge to provide risk metrics for tsunami loss in Te Whanganui-a-Tara / Wellington Region. We build upon the successful proof-of-concept work within the EQC Toka Tū Ake (now Natural Hazards Commission [NHC] Toka Tū Ake) project #20773 that applied a similar approach to Hawke's Bay and the Stage 1 interim report (Fry et al. 2024).

We report against the successful completion of all eight contracted milestones:

- 1. Framework for an Aotearoa New Zealand -wide physics-based probabilistic tsunami risk model (reported in Section 2).
- 2. A 30,000-year catalogue of ruptures affecting Wellington, including multi-fault events (reported in Section 3).
- 3. Vertical surface deformation for the 30,000-year catalogue (reported in Section 3.1).
- 4. Coastal wave amplitudes in Wellington from the 30,000-year catalogue (reported in Section 3.2).
- 5. Inundation estimates from significant tsunami loss events within the catalogue (reported in Section 3.3).
- 6. Loss calculations for the events modelled in milestone 5 (reported in Section 4).
- 7. Probabilistic risk metrics for losses modelled in milestone 6 (reported in Section 4).
- 8. Meetings as requested by NHC to communicate progress and interim outputs (fulfilled all requested meetings throughout the project duration).

# 2.0 Stage 2: National Tsunami Model Framework

**Milestone 1:** The development of a framework for an Aotearoa-New-Zealand-wide physics-based probabilistic tsunami risk model, highlighting any existing scientific challenges.

Building upon the success of RNC2 and the EQC Toka Tū Ake project #20773 (Tsunami Impact and Loss Modelling in Hawke's Bay), we have continued to develop the use of earthquake-cycle simulators to underpin tsunami-hazard calculations. We present this framework in Figure 2.1, noting that further work in Stage 2 will continue to (a) test assumptions and (b) improve the workflow through scientific validation and optimisation of the individual components.

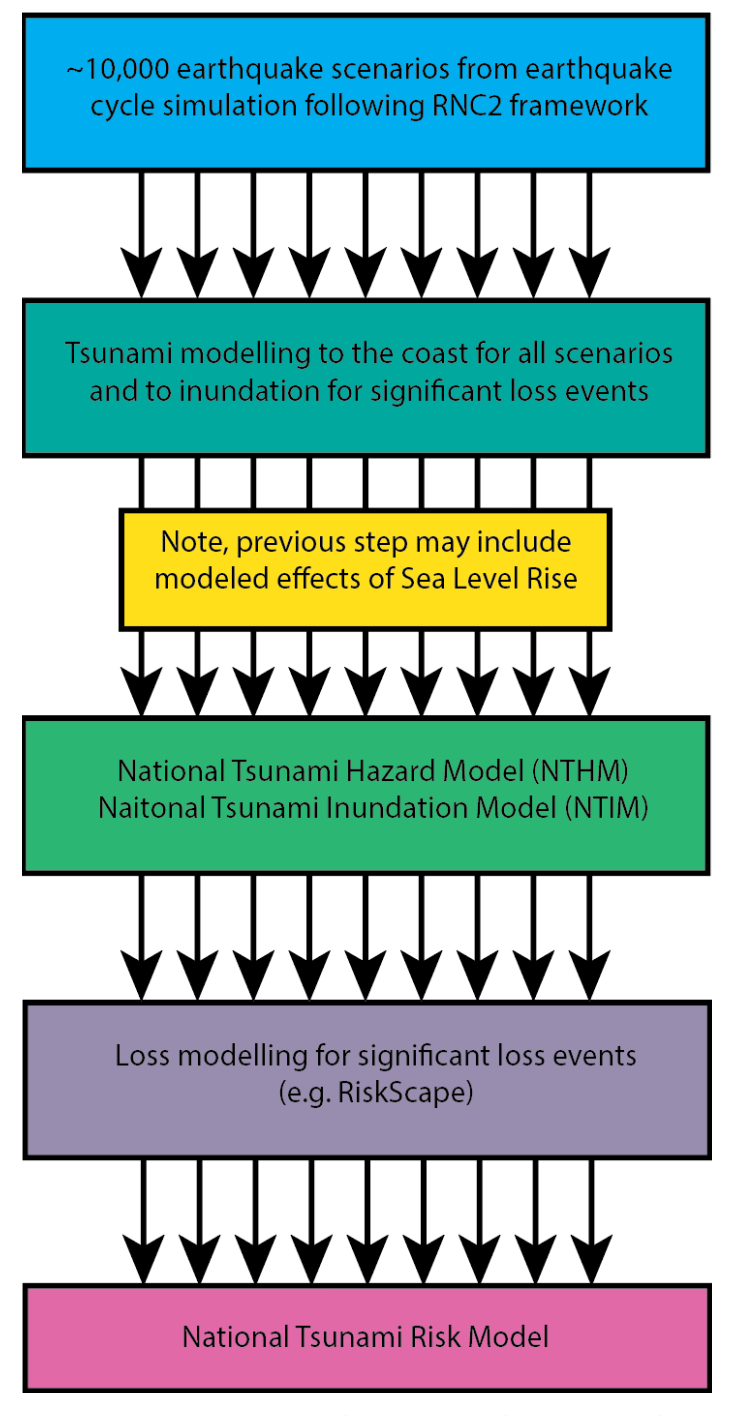


Figure 2.1 Working model of a framework for a physics-based National Tsunami Model.

One key component of the workflow is the end-to-end inundation and loss modelling of each event in the catalogue. This allows us to, at any stage, extract probabilistic metrics from the catalogue, as opposed to analysing a return period hazard and using the 'average event' at a given return interval to calculate the 'average impact'. This approach also provides the foundation for incorporating the National Tsunami Model into future multi-hazard/multi-risk models and digital twins. We note that work has begun to develop a cascading multi-risk model from the Te Whanganui-a-Tara / Wellington test case presented here.

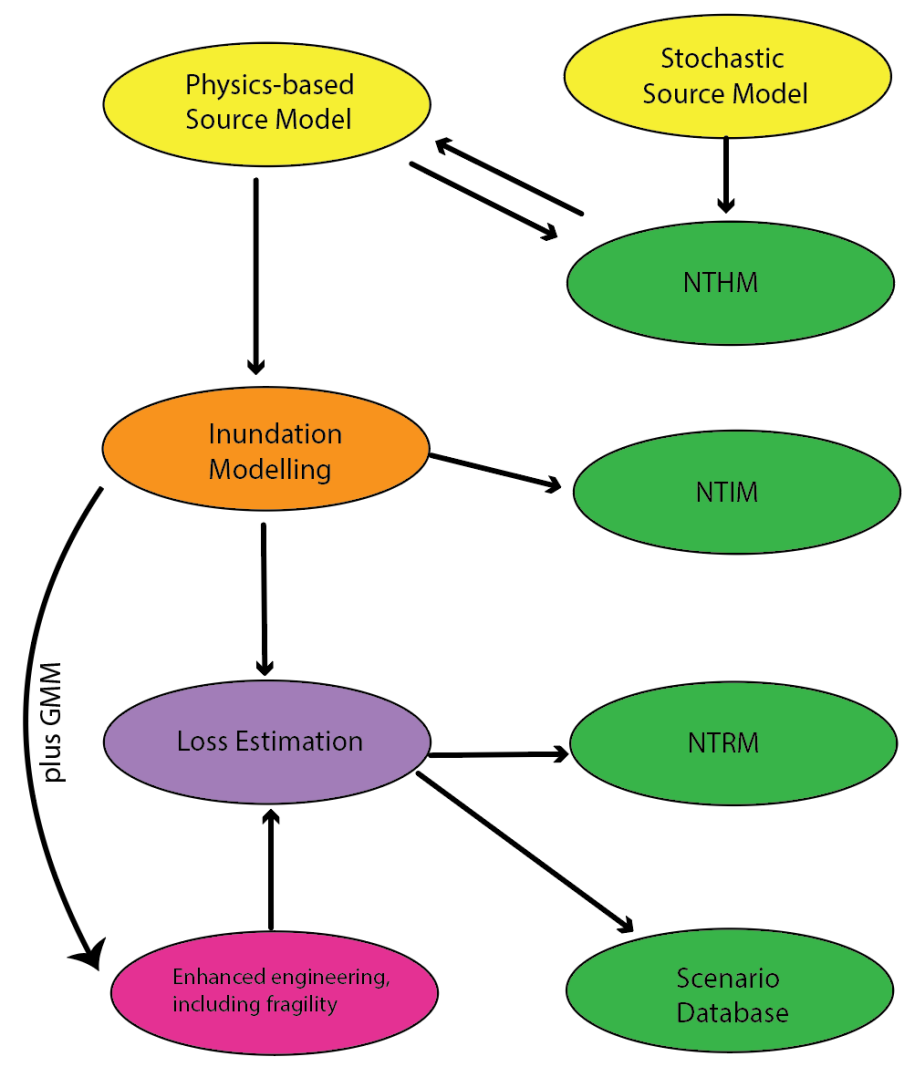


Figure 2.2 Hybrid workflow for a physics-based National Tsunami Model, with outputs shown in green ellipses.

# 2.1 Modular Approach

The workflow is designed to be modular, allowing for testing of multiple modelling approaches as well as providing a mechanism to test each component separately. The modularity is well-suited to community collaboration, allowing multiple scientific approaches to be applied at each step. It also permits application of traditional logic-tree approaches, in which branches can include alternate source, impact and loss modelling, and these can be weighted. In many ways, this is similar to the existing National Tsunami Hazard Model (NTHM) and National Seismic Hazard Model (NSHM) approaches. However, our workflow diverges from these previous models in that it is underpinned by a physics-based source model, described in Sections 1.2 and 2.2.

## 2.2 Source Model

A significant outcome of the RNC2 Earthquake and Tsunami programme was the understanding that many large (M8+) subduction earthquakes in Aotearoa New Zealand are likely to be accompanied by co-seismic triggering of subsidiary crustal faults. Consideration of these crustal faults is important because, in many cases, they can either contribute to the tsunamigenic potential of the earthquake or change the elevation of the coastline, thereby altering the pattern of inundation. We present two such possibilities in Figure 2.3.

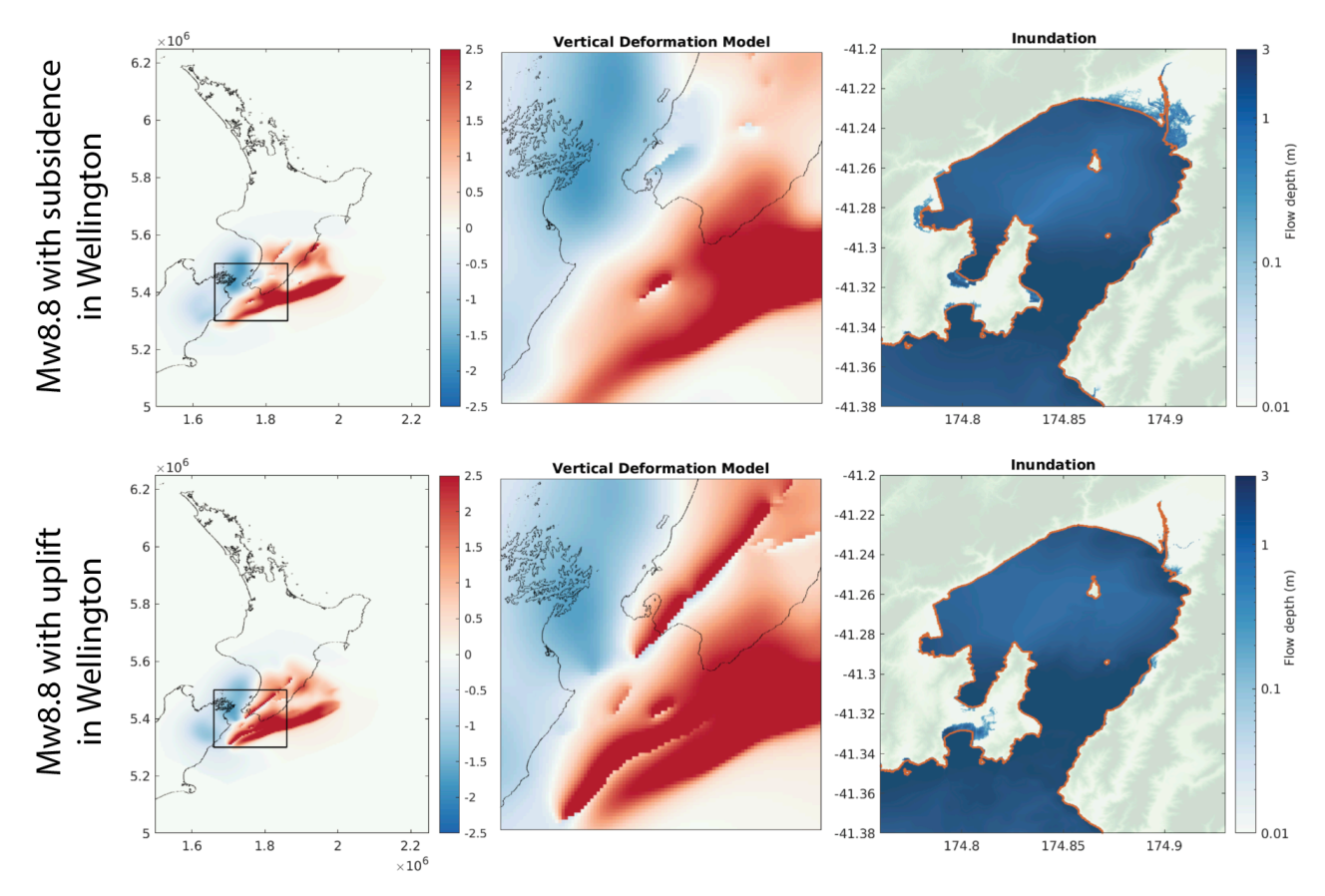


Figure 2.3 Each row represents an earthquake source for a tsunami scenario modelled for Stage 1. Left and centre: vertical-deformation models in metres. Right: inundation model, showing the offshore wave amplitudes and onshore flow depths (in metres). Note that both scenarios are of similar magnitude, yet the top scenario generates initial subsidence (due to the rupture of the Wellington Fault; subsidence is shown in blue) around Te Whanganui-a-Tara / Wellington Harbour and the bottom scenario generates initial uplift (due to the rupture of the Wairarapa Fault; subsidence is shown in red).

To account for this variation in the natural process of tsunami inundation, our framework employs a physics-based source model. Using such a source model allows us to better address many crucial details that are difficult or intractable in traditional probabilistic source models. These include but are not limited to (1) addressing complex, multi-fault earthquakes, involving the subduction megathrust and co-seismic movement on crustal faults capable of producing vertical land motion of the coast; (2) including tidal cycles into inundation modelling; and (3) providing the opportunity to address cascading multi-hazard peril. However, it is possible that existing probabilistic source models contain complementary information and this will be explored (Figure 2.2).

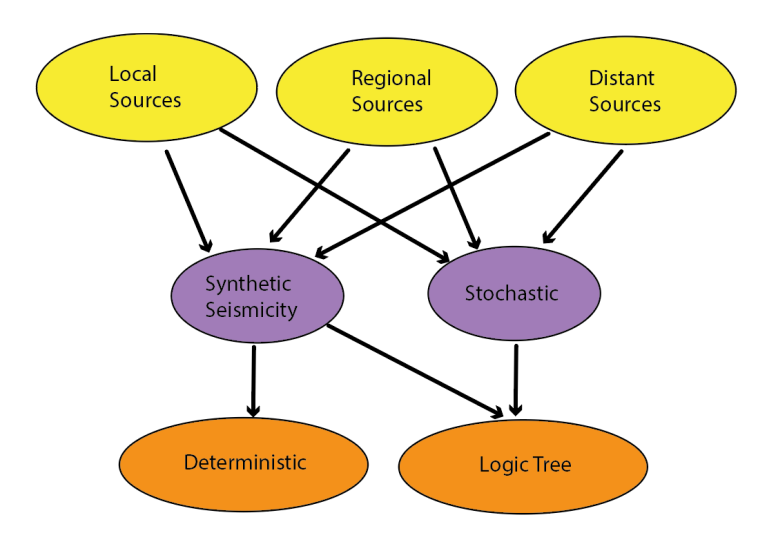


Figure 2.4 Source-model generation, including both physics-based (synthetic seismicity, e.g. Robinson and Benites [1996]) and traditional (stochastic) branches. We note that while both the Logic Tree and Deterministic outcomes provide traditional hazard and risk metrics, the deterministic branch creates a clear path toward digital twins of tsunami that can be utilised for many disaster-risk-reduction purposes outside the benefits of a NTRM.

To fully account for tsunami hazard, it is necessary to consider local, regional and distant sources (Figure 2.4). These classes are typically based on travel times, with local events having travel times less than an hour, regional events having travel times between one and three hours and distant events having travel times longer than three hours. As the source distance grows, the sensitivity of local inundation to source complexity decreases. For local sources, it is imperative to account for source complexity. For distant sources (Figure 2.5), it is less crucial. It is possible that we can utilise this feature to reduce computation and scientific resources for generating distant-source models while retaining necessary complexity for local sources. Stage 1 includes results from modelling local sources, which are appropriate for capturing the main characteristics of hazard and risk in Te Whanganui-a-Tara / Wellington Region due to its specific geographic and bathymetric features.

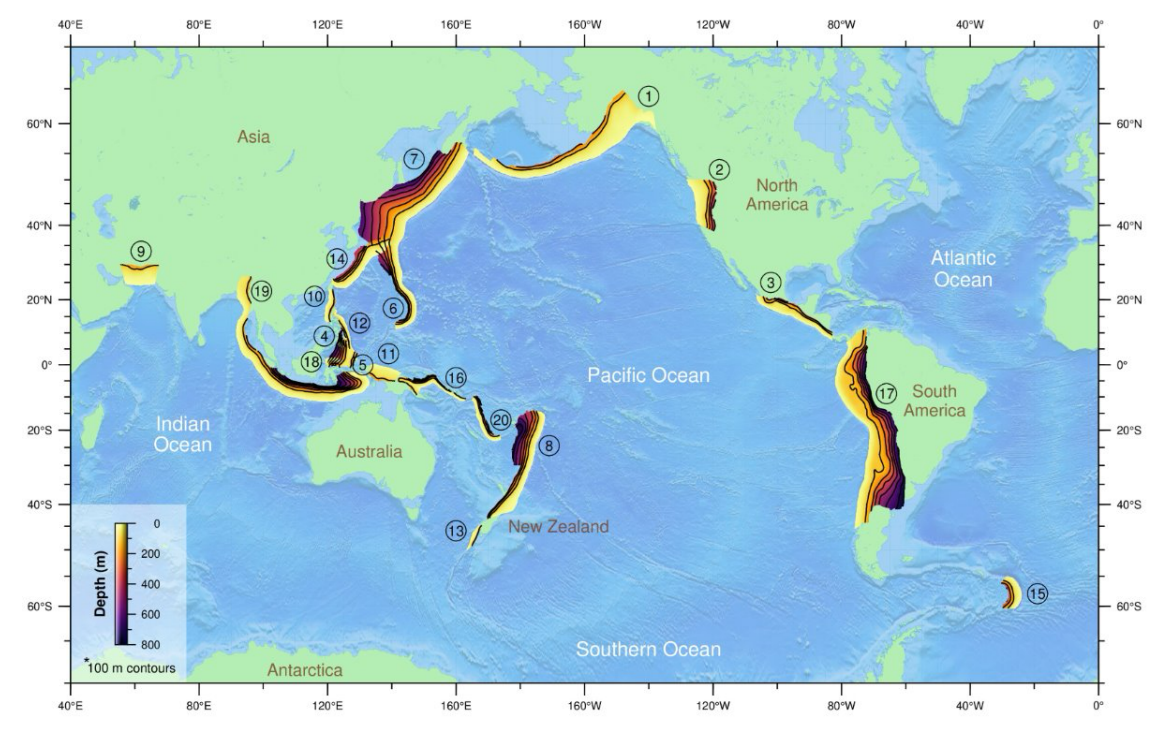


Figure 2.5 Ongoing work to define circum-Pacific subduction-zone sources. The map represents the computational mesh used in our earthquake-cycle modelling. Extensive research into complexities in regions 8 and 20 has been undertaken within the RNC2 programme (Liao et al. 2024).

# 2.3 Wave Propagation and Inundation

Hydrodynamic modelling is necessary to account for hazard due to complex sources and near-shore effects, such as harbour resonance and non-linear wave propagation. We have identified three candidate models to calculate wave propagation and inundation (Figure 2.6). Of these, both HySEA (Hyperbolic Systems and Efficient Algorithms; Macías et al. 2016) and BGFlood (Block-adaptive GPU [graphics processing unit] -capable Flood model¹) are currently GPU -based and with efficiencies potentially capable of supporting inundation modelling on the scale of tens of thousands of events with only moderate computational resources. To test the utility of using engineering approximations for inundation mapping, it is possible to extract coastal amplitude from each of the hydrodynamic models to provide initial conditions. We note that these types of approaches were largely created to address challenges in modelling inundation prior to the advent of GPU hydrodynamic computing and for areas of the earth for which high-resolution bathymetric mapping does not exist.

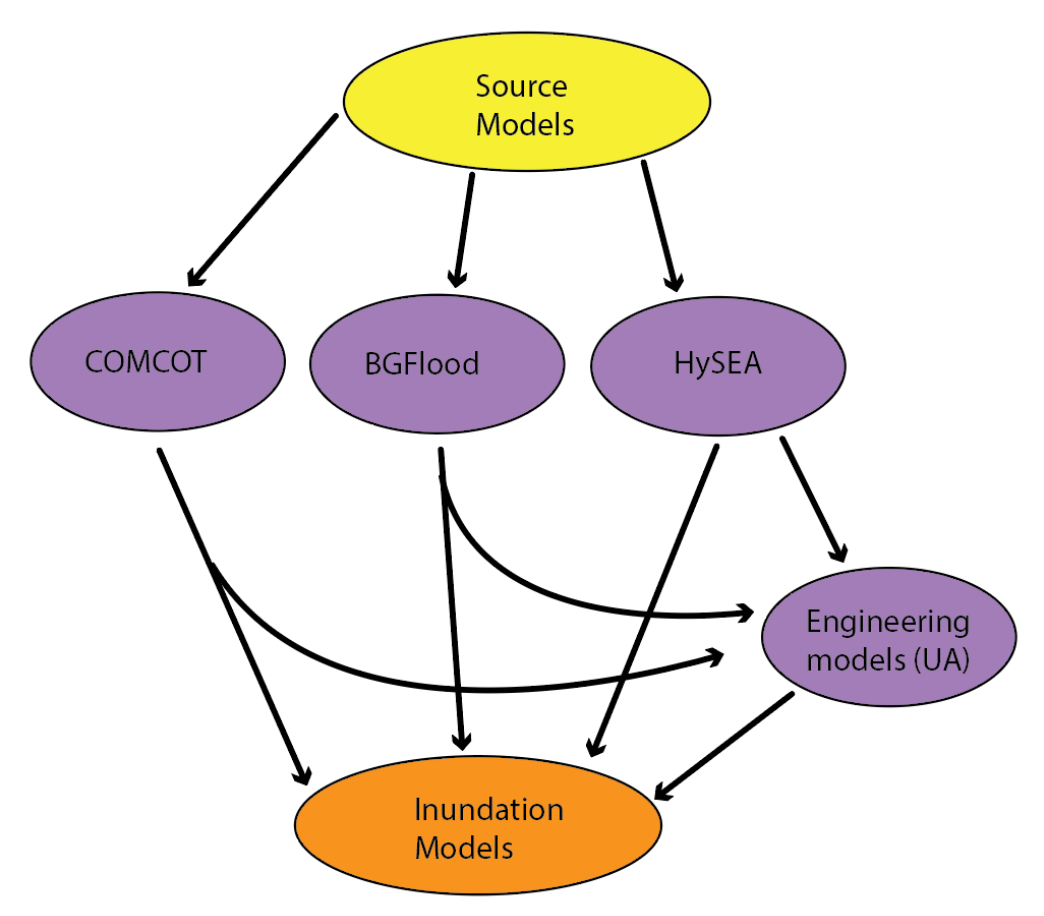


Figure 2.6 Modelling framework in which source models feed into hydrodynamic models to calculate inundation and flow velocity for every scenario. COMCOT = COrnell Multi-grid COupled Tsunami model (Wang and Power 2011). BGFlood and HySEA noted in above text.

## 2.4 Impacts

Once the physical impacts (inundation and flow velocities) of each scenario are calculated, loss modelling for each scenario can reasonably be accomplished with the RiskScape<sup>™</sup> platform, with analysis of the results yielding probabilistic risk models. The RiskScape<sup>™</sup> environment has been configured for Stage 1 (see Sections 6.1 and 6.2). However, extensive work to develop exposure data is likely necessary and needs to be aligned with work in other ongoing and future research efforts to ensure inter-operability and maximum leveraging.

<sup>1</sup> Open source: <a href="https://aliceharang.github.io/index.html#autotoc\_md0">https://aliceharang.github.io/index.html#autotoc\_md0</a>

We emphasise the power of our physics-based modular approach to incorporate advances across tsunami hazard into the National Tsunami Model. These could be agent-based evacuation modelling or transport and erosion modelling (Figure 2.7). Our modular approach also allows for inclusion of dynamic exposure, which will be crucially important as our coastlines see the effects of climate change manifest as coastal erosion and aggradation and as our communities implement mitigation measures.

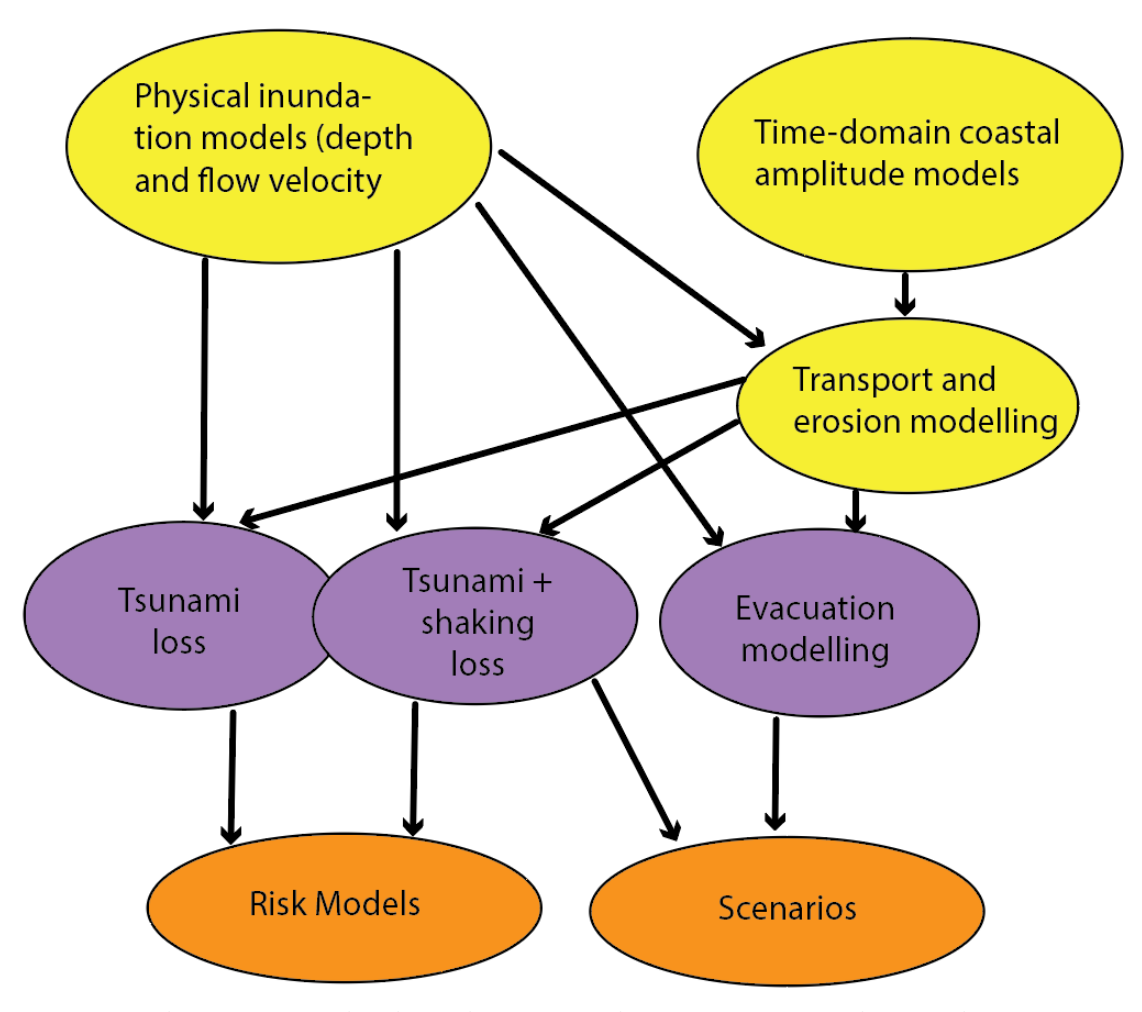


Figure 2.7 Map of impact calculation, including loss and risk, as well as scenario analysis.

## 2.5 Workflow

Modelling tsunami inundation and impacts at a national scale will involve integrating a chain of models over multiple events and for multiple locations. This can be very intensive because of the requirements of keeping track of the models and transferring data between these, dealing with scheduling, inevitable bugs and IT failures, etc., that are part of a large project.

Employing scheduling software to allow the system process to be broken down into smaller (often repeated) sub-tasks and modular units can dramatically improve repeatability and future use of the modelling chain. One possible scheduling option is the Cylc software<sup>2</sup>, originally developed at the National Institute of Water & Atmospheric Research (NIWA). Cylc has been previously used to develop a workflow schedule and run the national flood inundation model for Aotearoa New Zealand as part of Mā te Haumaru ō te Wai: Flood Resilience Aotearoa.

<sup>2 &</sup>lt;a href="https://cylc.github.io/cylc-doc/stable/html/index.html">https://cylc.github.io/cylc-doc/stable/html/index.html</a>

Cylc is a workflow engine; a system that automatically executes tasks according to schedules and dependencies. In a Cylc workflow, each step is a computational task. It runs each task as soon as it is appropriate to do so (Figure 2.8), and it can automatically:

- Submit tasks across computer systems and resource managers.
- Recover from failures.
- Repeat workflows.

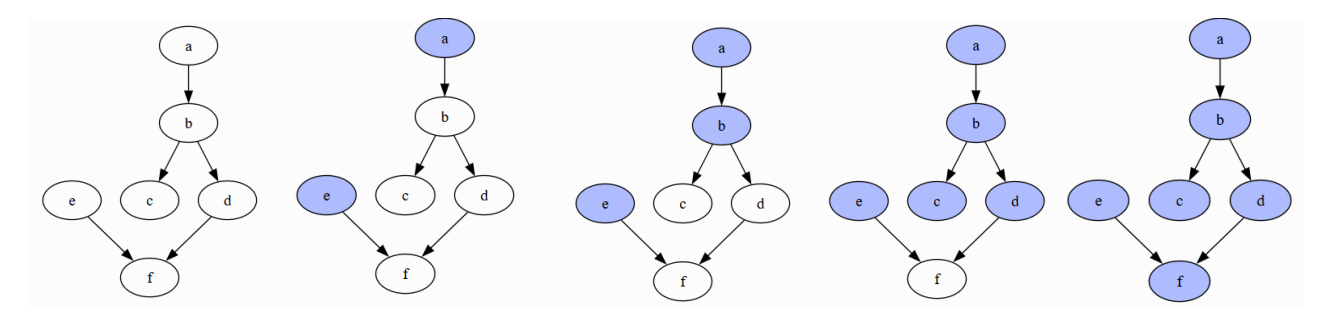


Figure 2.8 Cylc workflow showing tasks (circles) and dependencies (arrows) as it progresses through time. Each task is automatically run after its pre-requisite task is finished (blue).

Cylc tasks are ideally broken down into their smallest component steps to assist keeping track of workflow progress and allow substitution of modules representing modelling advances, such as better inundation and loss modelling or improved input data, such as bathymetry or sea-level rise models. Tasks are hierarchical, so child tasks inherit the features of their parent task unless otherwise specified. Tasks can be cycled through multiple times, or different instances of a similar task can be spawned and run simultaneously.

## 2.6 Testing

The modular approach of the National Tsunami Model facilitates testing of the various individual components that make up a workflow, as well as comparison of the results from workflows based on different combinations of components.

Testing and comparison of components is very important because different approaches have different strengths and weaknesses. For example, inundation models using GPUs may be much quicker than those that run on CPUs (central processing units), but these may be less mature in their development and potentially less accurate. Hence, it is important to test different models against established benchmarks, against the outputs of other models and, as far as possible, against real-world datasets. Testing should include features that may be specific requirements of the Aotearoa New Zealand context; for example, tsunami-propagation models should remain accurate when tsunami energy propagates at the very high latitudes close to Antarctica, as this is the case for some important South American tsunami sources.

Testing should be applicable to all stages in the workflow. For example, the earthquake simulator shows a high proportion of multi-fault ruptures, especially for events involving the plate interface. This should be checked for consistency with the known geological dating of fault ruptures. Loss-estimation approaches should be tested against past events and checked for appropriateness to the Aotearoa New Zealand context; for example, there should be assessment of the applicability of fragility functions that link hazard to loss that are derived from impacts of events in countries that use different building techniques.

# 3.0 Te Whanganui-a-Tara / Wellington Region Tsunami Model

**Milestone 2:** Development of an ~30,000-year catalogue of earthquake scenarios affecting Wellington, including multi-fault events.

Drawing on the results of the RNC2 Earthquake and Tsunami Programme (Shaw et al. 2022; Liao et al. 2024), we have applied physical models of the earthquake process to simulate the earthquake cycle in Aotearoa New Zealand by computationally modelling the effects of tectonic stressing on active faults contained in the New Zealand Community Fault Model (Seebeck et al. 2022) using the RSQSim software package. The resulting catalogue contains about 3700 M6+ complex earthquake-source models and ~2500 events that either have a magnitude greater than  $M_W$  7.5 regionally or magnitudes of  $M_W$  6.5–7.5 with an epicentre within 500 km of Te Whanganui-a-Tara / Wellington Region. The character of and inundation from local-source tsunami (tsunami travel-times of <60 minutes) is dependent on complexities of the earthquake source, including slip heterogeneities and multi-fault ruptures. Our earthquake simulators are capable of exploring the variability of these two facets of the earthquake source, making them well-suited to generating source models for studies of probabilistic inundation and risk. We have further improved our tsunami-source catalogue of the Kermadec Subduction Zone by testing the sensitivity of the subduction zone to initial stress conditions in Liao et al. (2024).

We believe that this synthetic catalogue samples much of the stochastic variation of the earthquake process in Aotearoa New Zealand and highlights some of the cascading and broadly reaching hazards of events that pose significant hazard for Te Whanganui-a-Tara / Wellington. In this catalogue, we see striking complexity in the largest earthquake. This complexity happens more often than not, meaning that most large events in the catalogue are complex. This observation is consistent with very limited historical complexity of events in Aotearoa New Zealand. Using synthetic catalogues to generate scenarios for response system stress-testing is not only insightful but necessary to consider the wealth of variation in natural stochastic earthquake systems.

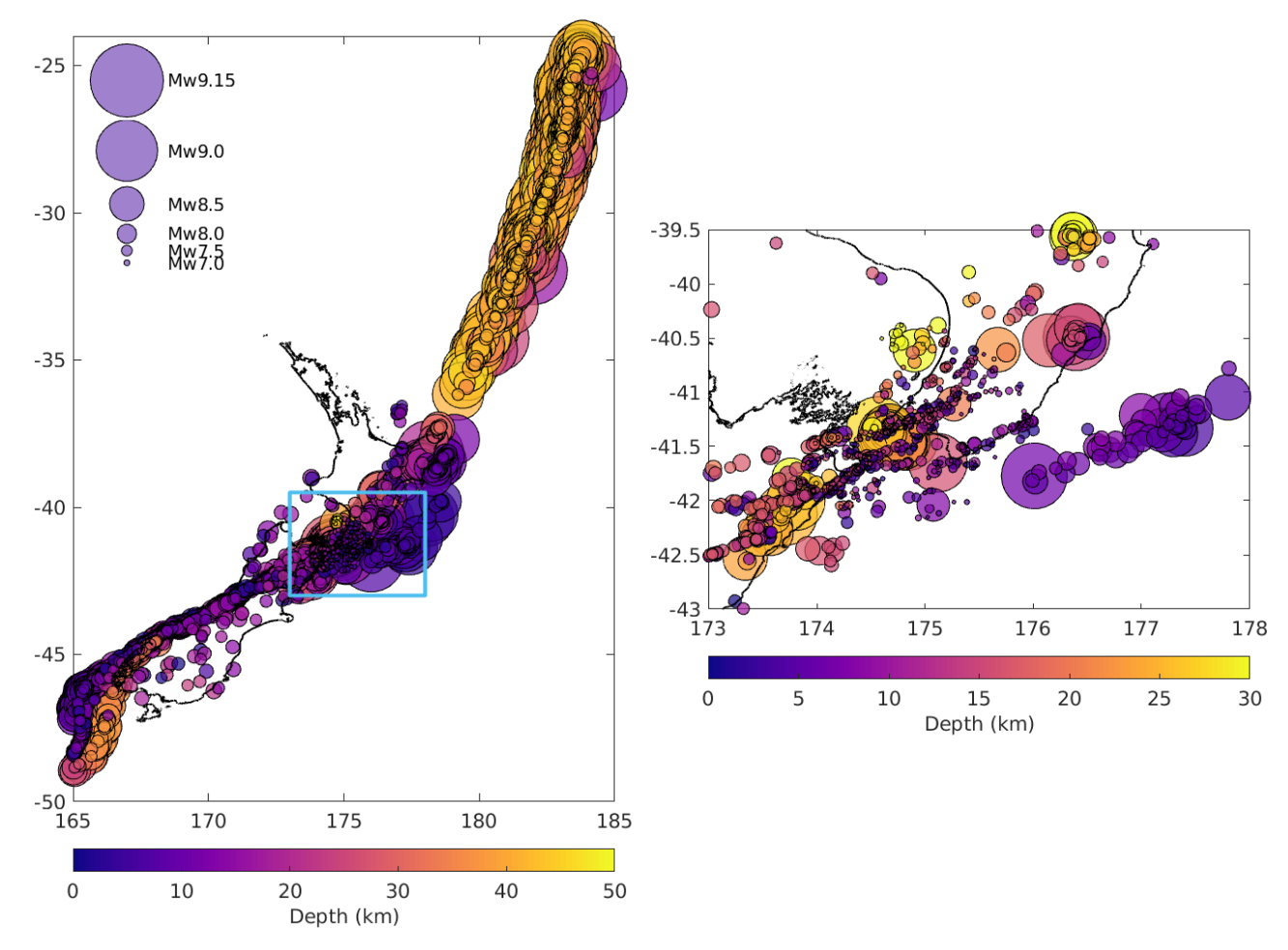


Figure 3.1 Spatial distribution of earthquakes from the RSQSim catalogue comprising the Stage 1 source model. Events are coloured by nucleation depth and sized by moment magnitude. Left: Distribution of all earthquakes in the catalogue. The blue square shows the area of the zoomed in plot. Right: Distribution of earthquakes that occur around central Aotearoa New Zealand that are likely to impact Te Whanganui-a-Tara / Wellington Region. Note: Earthquakes have a magnitude range of  $M_W 6.5-9.15$ .

## 3.1 Vertical Deformation and Tsunami Initial Conditions

Milestone 3: Models of vertical deformation from the catalogue.

It is necessary to generate vertical displacement models of each scenario. These models are used as initial conditions for the hydrodynamic modelling. We have calculated vertical deformation models from the catalogue using a simple Okada formulation in a half-space following the procedure documented in Hughes et al. (2023, 2024). For each event, we limit the calculation to areas within 100 km from the fault rupture because vertical deformation at farther distances is negligible. Stage 1 work has raised an interesting question about trade-off between resolution of these vertical-deformation models and inundation-model uncertainty. In the work presented in Hughes et al. (2023) and Power and Fry (2023), vertical deformation was calculated on a 5 km cartesian grid. Because Te Whanganui-a-Tara / Wellington lies in the extreme near-field of several faults (e.g. Wellington Fault), it is possible that higher-resolution surface-deformation modelling is useful for the purpose of modelling inundation. Deformation models were generated on a 2 km grid focused on Te Whanganui-a-Tara / Wellington Region and a 5 km grid that covered the entire earthquake domain (50°S–24°S, 164°E–185°E). We are further exploring inundation differences with even higher-resolution initial conditions (1 km, 500 m and 100 m). This exploratory work will contribute to Stage 2.

## 3.2 Hydrodynamic Modelling and Coastal Hazard

**Milestone 4:** Calculation of coastal wave amplitudes in Wellington from significant events in the catalogue.

For the 2649 earthquakes in the local-source earthquake catalogue, coastal amplitude tsunami simulations were run using COMCOT (Cornell Multi-grid Coupled Tsunami; Wang and Power 2011). We chose to use COMCOT as it has been widely benchmarked and used by researchers worldwide to study various aspects of tsunami, including inundation, the aim of this study. Other modelling software, including GPU-based schemes, exist and will be utilised when our approach is extended to nationally consistent inundation modelling in Stages 2 and 3 of the National Tsunami Model.

COMCOT uses a modified staggered finite difference scheme to solve linear and non-linear shallow-water equations that typically govern tsunami, with shock capturing up-wind schemes, together with ad-hoc wave-breaking algorithms (Kennedy et al. 2000; Lynett 2022; Wang and Power 2011) for improved stability and to account for the energy-dissipation effects during run-up and inundation. A two-way nested grid configuration is implemented in the model to balance computational efficiency and numerical accuracy (Wang 2008; Wang and Power 2011). This allows us to efficiently move from low-resolution and large-scale grids, useful for modelling tsunami propagation, to high-resolution, smaller-scale grids necessary for modelling tsunami inundation.

For coastal amplitude modelling, we implement four nested grids that cover both Aotearoa New Zealand and the Chatham Islands (Wharekauri and Rangiāuria) (Tables 3.1 and 3.2).

Table 3.1 Nested grid used in COMCOT to undertake the coastal amplitude simulations.
--

Grid Layer	Refinement Level	Grid Size (arc-second)	Model	Boundary Condition
1	<b>1</b> <sup>st</sup>	240	Linear	Absorbing
2	2 <sup>nd</sup>	60	Linear	Two-way nested
3	3 <sup>rd</sup>	30	Non-Linear (n = 0.013)	Two-way nested, wall boundary condition at coast
4	3 <sup>rd</sup>	30	Non-Linear (n = 0.013)	Two-way nested, wall boundary condition at coast

Table 3.2 Boundaries of the nested grids used in COMCOT to undertake the coastal amplitude simulations.

Grid Layer	West	East	South	North
1	150	200	-60	-20
2	160	190	-49	-30
3	166	179	-48	-34
4	182.5	184.5	-45	-43

We run the simulations using a ~600 m grid spacing (Table 3.1). This spacing optimises both the time and computational requirements needed to run the simulations. Previous work using physics-based synthetic-earthquake catalogues showed that running the simulations for 16 hours (simulated time) ensured that the maximum wave amplitudes along all sections of Aotearoa New Zealand's coast were captured (Hughes et al. 2023, 2024). Therefore, for this study, we keep the simulation run-time at 16 hours.

We sample evenly distributed coastal points around Aotearoa New Zealand from the simulations. From all 2649 simulation results and for every coastal point, we sort the simulation tsunami- height results from largest to smallest. This allows us to identify the hazard at different return periods. As our catalogue covers a 30,000-year period of time, we can directly calculate the hazard at different return periods. To do this, we divide the length of our catalogue by the return period of interest to find the X<sup>th</sup> largest tsunami height from our sorted simulation results (X<sup>th</sup> largest tsunami height = return period of interest / length of the synthetic catalogue). For example, if we are interested in the 2500-year return period hazard, we would identify the 12<sup>th</sup> largest tsunami height for each coastal point (e.g.  $30,000 \div 2500 = 12$ ). This method allows us to investigate the hazard over a range of return periods. These simulations provided a database of tsunami heights for all coastal points around Aotearoa New Zealand and the Chatham Islands that we use as a reference for identifying events that contribute to the inundation hazard. With this approach, we develop a new tsunami hazard model for local earthquakes greater than M<sub>W</sub> 7.5 (Figure 3.2), noting that it does not include all regional and distant sources to be included in Stage 2 and is presented here only for illustration of the strength of our approach. The specific geography of the Wellington region makes it relatively insensitive to far regional and distant sources, with almost all of the tsunami risk derived from local events. We therefore consider our model a useful quantification of bulk risk in for the Wellington region. We note that future work under Stage 2 of the model will incorporate distant sources.

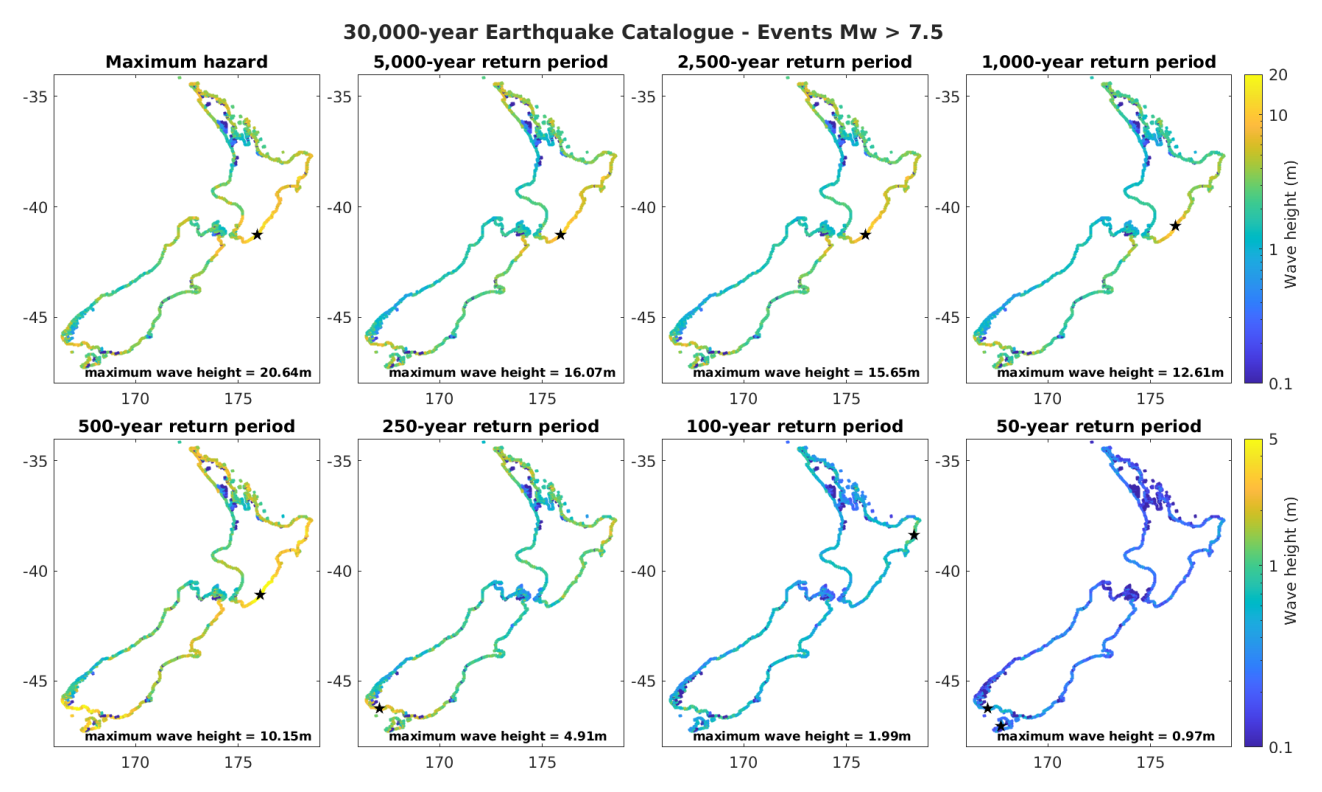


Figure 3.2 Coastal-tsunami-hazard generated using all earthquakes with a magnitude greater than  $M_W$  7.5. Stars show where the largest tsunami heights are recorded at the coast. Note: This is only the hazard posed by local-source earthquakes from 50°S to 25°S. Earthquakes with a magnitude between  $M_W$  6.5 and 7.5 are excluded, as these events are not modelled nationwide (only  $M_W$  6.5–7.5 events within 500 km of Te Whanganui-a-Tara / Wellington have currently been modelled).

For return periods longer than 500 years, the east coast of the North Island is likely to experience the largest tsunami heights, as the hazard is dominated by earthquakes that rupture the Hikurangi Subduction Zone (Figure 3.2). For the 100- and 50-year return periods, the hazard is smaller than that previously presented in the NTHM (Power et al. 2022). There are two reasons for this. The first is that we currently only use earthquakes that have a magnitude greater than  $M_W$  7.5, so are not including smaller magnitude earthquakes that rupture offshore but are close to the coast. These smaller-magnitude events all occur more frequently than larger-magnitude events. The second is that we are

not including distant earthquake sources in this preliminary hazard assessment, and it is known that the hazard at shorter return periods is dominated by distant sources, as there are more of these events occurring due to the larger region covered compared to the local sources. We find similar results for the hazard at different return periods for the Chatham Islands (Figure 3.3).

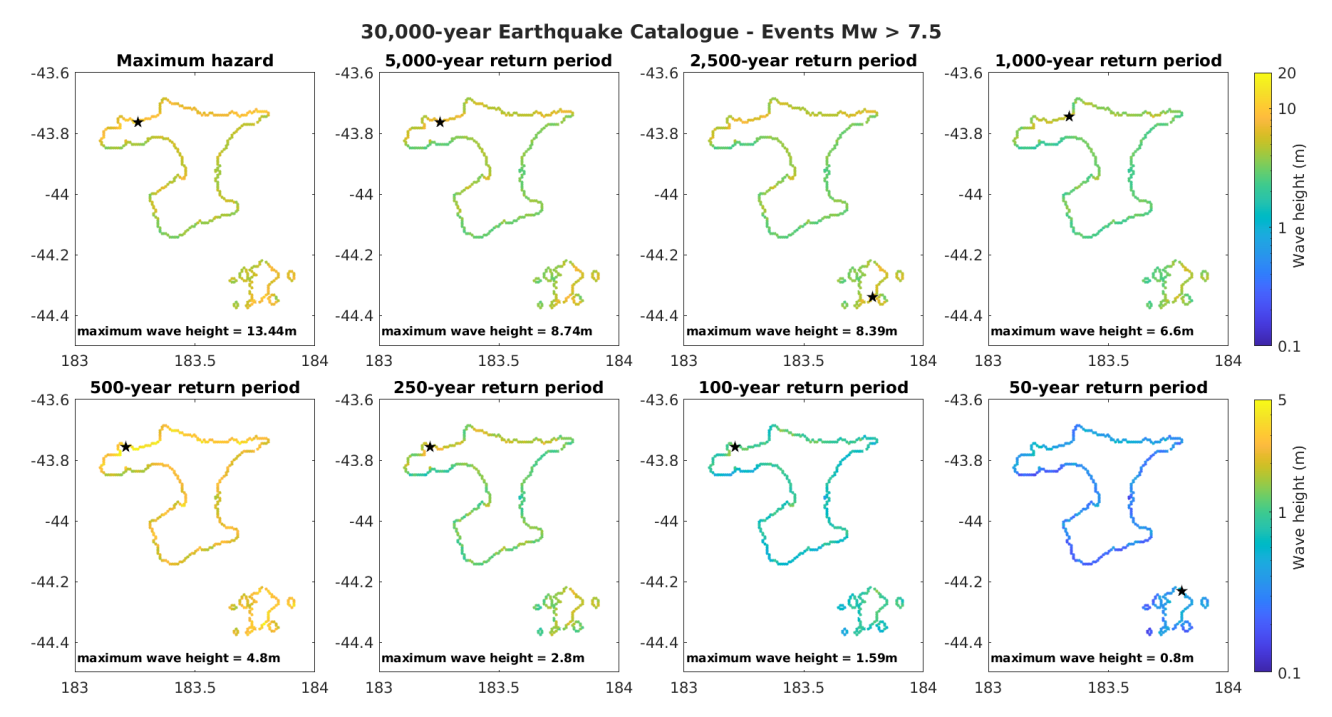


Figure 3.3 Tsunami hazard for the Chatham Islands generated using all earthquakes with a magnitude greater than  $M_W$  7.5. Stars show where the largest tsunami heights are recorded at the coast. Note: This is only the hazard posed by local-source earthquakes from 50°S to 25°S. Earthquakes with a magnitude between  $M_W$  6.5 and 7.5 are excluded, as these events are not modelled nationwide (only  $M_W$  6.5–7.5 events within 500 km of Te Whanganui-a-Tara / Wellington have currently been modelled).

While the maximum wave amplitudes recorded at the coast are smaller than those observed around Aotearoa New Zealand, the largest wave amplitudes are observed at the longer return periods. However, the hazard is likely lower than in the 2021 update of the NTHM (Power et al. 2022). Deaggreation of the hazard reveals that the major contributor of the hazard to the Chatham Islands are earthquakes that are generated along the Hikurangi Subduction Margin, the Kermadec Subduction Zone, the central Chile and Peru subduction zones, and the outer-rise faults of the Hikurangi Subduction Margin. Because Stage 1 is focused on Te Whanganui-a-Tara / Wellington, we are only modelling the megathrust earthquakes that rupture the Hikurangi Subduction Margin and Kermadec Subduction Zone, along with the Puysegur Subduction Zone and crustal faults.

While this earthquake catalogue provides a preliminary hazard assessment, the simulations also provide a database of local earthquake-source models and the resulting tsunami models. Using these data, we generate a methodology to identify the earthquakes capable of generating significant inundation. Te Whanganui-a-Tara / Wellington was chosen as the case study location for Stage 1 to test the methodology and construct the criteria for identifying events to run inundation models, largely because it is at low risk of significant inundation from distant events, as its hazard is predominantly from local sources (except possibly at the very shortest return periods, where little inundation is expected). This allows us to create a new inundation-hazard model for the region, with the preliminary to-coast model for Te Whanganui-a-Tara / Wellington Region shown in Figure 3.4.

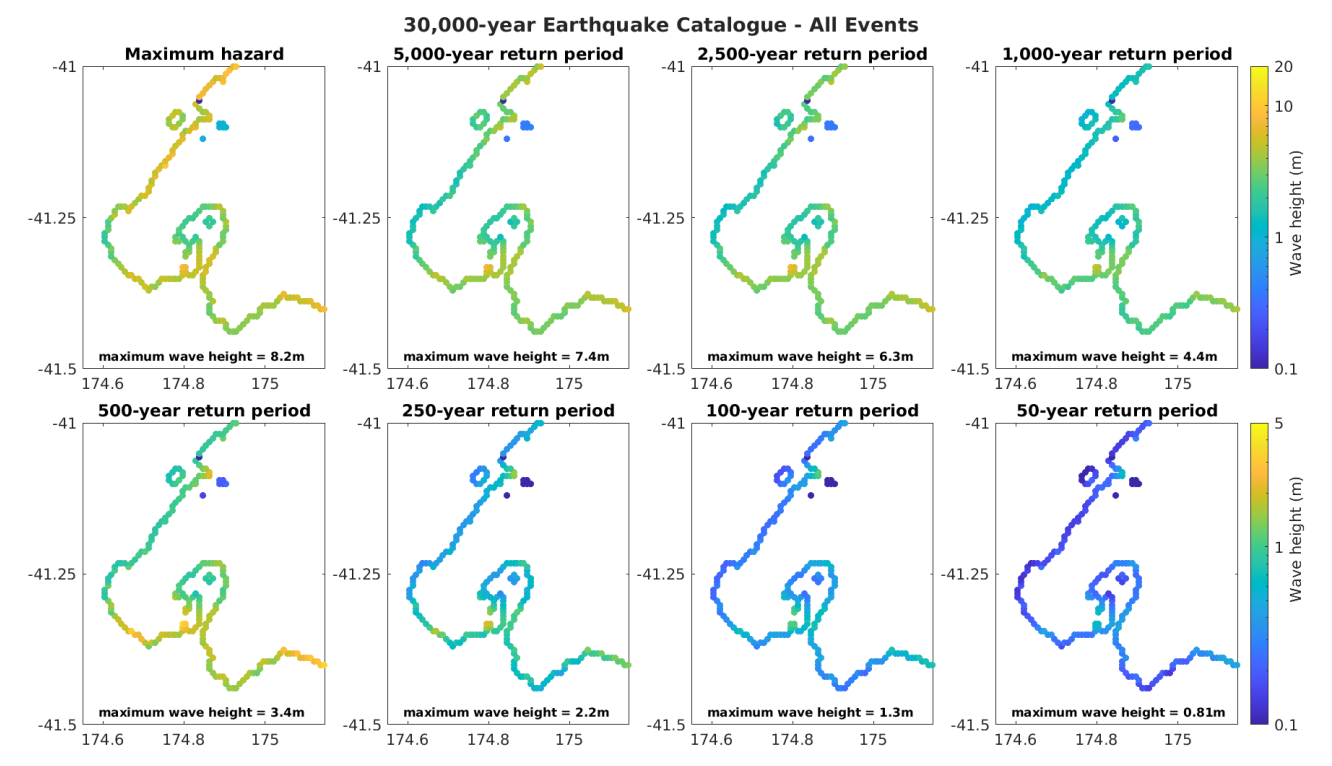


Figure 3.4 Tsunami hazard around the Greater Wellington region generated using all earthquakes with a magnitude greater than  $M_W$  7.5 and earthquakes between  $M_W$  6.5 and 7.5 that generate deformation with 500 km of Te Whanganui-a-Tara / Wellington Region. Note: This is only the hazard posed by local-source earthquakes from 50°S to 25°S, but, as discussed in text, includes the dominant hazard at longer return periods.

## 3.3 Inundation

Milestone 5: Inundation estimates from significant tsunami loss events in the catalogue

Following the approach taken in Hughes et al. (2023, 2024) and Hughes (2024) with the COMCOT software (Wang and Power 2011), we have completed inundation modelling of those events in the 30,000 year catalogue that pose a significant likelihood of inundation loss in Te Whanganui-a-Tara / Wellington Region, including:

- 100 events from the wider catalogue capable of generating significant inundation compatible with findings from Hughes (2024), as well as all of the events that rupture the Wellington Fault, as these events have not previously been investigated.
- Events that generated amplitudes in the Te Whanganui-a-Tara / Wellington warning zone polygon (MCDEM 2016) larger than 2 m (a further 99 events).
- Events that generated amplitudes in the Te Whanganui-a-Tara / Wellington warning zone polygon (MCDEM 2016) between 1.5 and 2 m (a further 101 events).

This includes large subduction-zone earthquakes and moderate (M>6.5) local earthquakes. We present an example of the inundation modelling in Figure 3.5.

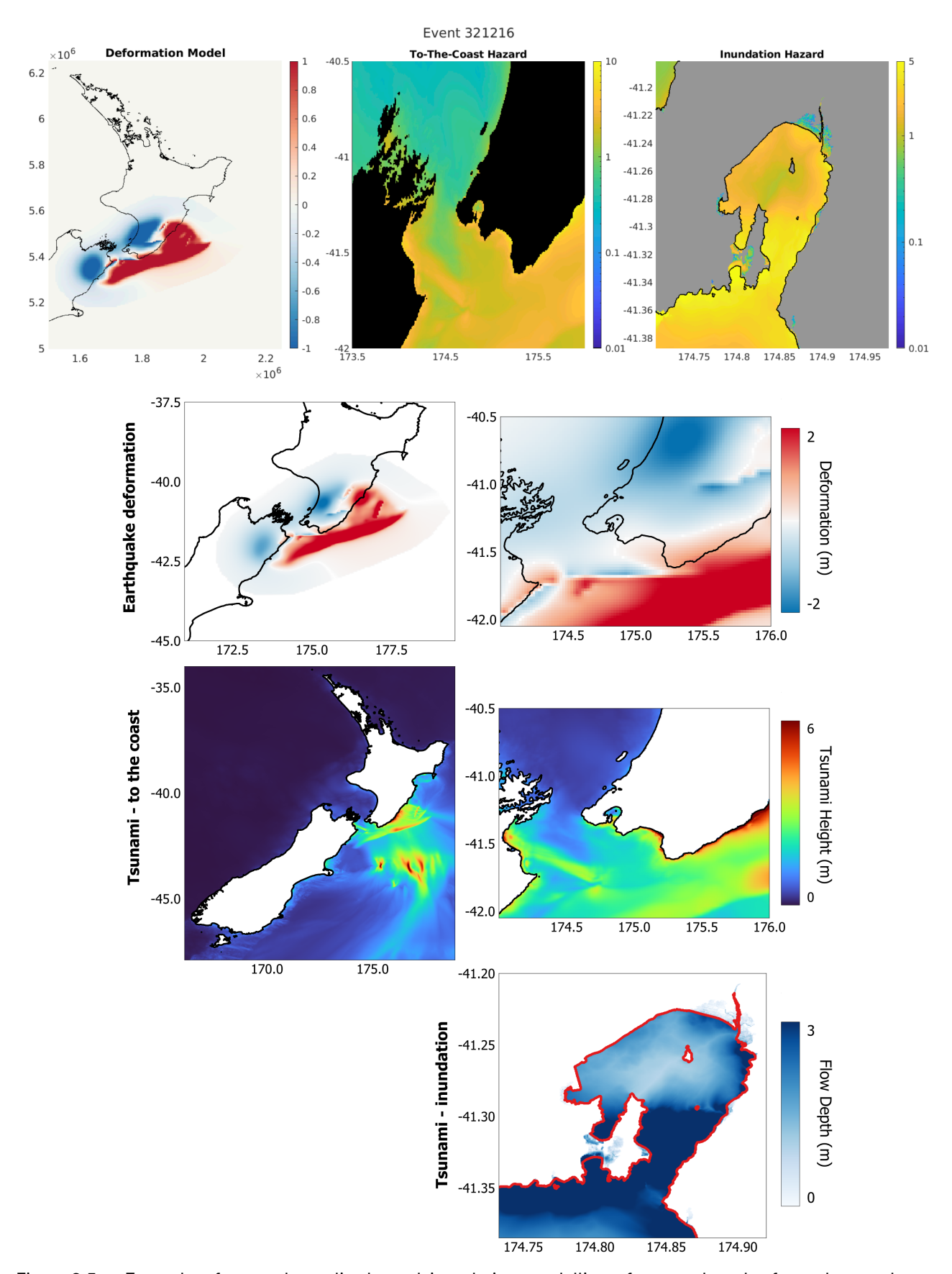


Figure 3.5 Example of coastal amplitude and inundation modelling of an earthquake from the catalogue. Top row: Initial earthquake deformation (blue is subsidence and red is uplift). The top middle and right panels show modelled tsunami heights in metres. Middle row: Tsunami height to the coast. Bottom row: Tsunami inundation. Left column: Aotearoa New Zealand view. Right column: Zoom-in of Te Whanganui-a-Tara / Wellington Region.

We used four nested grids for the inundation modelling, but these vary the grid spacing and boundary extents to ensure that the same model set-up can be implemented when distant-source events are included in the analysis (Tables 3.3 and 3.4).

Table 3.3 Nested grids in COMCOT for inundation modelling.

Grid Layer	Refinement Level	Grid Size (arc-second)	Model	Boundary Condition
1	1 <sup>st</sup>	120	Linear	Absorbing
2	2 <sup>nd</sup>	30	Linear	Two-way nested
3	3 <sup>rd</sup>	6	Linear	Two-way nested
4	<b>4</b> <sup>th</sup>	1.5	Non-Linear (n = 0.013)	Two-way nested

Table 3.4 Boundaries of the nested grids used for inundation modelling. Note: We change the bounds of grid layers 1 and 2 from the coastal amplitude simulations to ensure that we can use the same modelling set-up for future work, including distant sources.

Grid Layer	West	East	South	North
1	120.0	300.0	-65.0	65.0
2	166.0	180.0	-48.0	-34.0
3	174.49	175.15	-41.54	-41.03
4	174.704	174.979	-14.388	-41.181

We run the inundation simulations using a ~40 m grid spacing. This choice optimises the time and computational requirements necessary for Stage 1 modelling due to the limitations of CPU computing. Future National Tsunami Model calculations will employ GPU computing with reduced grid spacing. For all inundation simulations, we run each simulation for 10 hours of simulation time. This is sufficient to reach maximum inundation and flow velocity.

From all inundation simulations and for every point in the inundation grid, we sort the onshore flow depths / offshore wave heights from largest to smallest. We then calculate the hazard at different return periods by identifying the corresponding onshore flow depth/ offshore wave height (e.g. for the 2500-year return period hazard, we would identify the  $12^{th}$  largest tsunami height for each coastal point;  $30,000 \div 2500 = 12$ ). For each simulation, we also calculate the maximum area of inundation and maximum volume of inundation. To calculate these values, we assume that all areas inundate at the same time and that the flow depth in the cell remains constant throughout the simulation. We acknowledge that this is an approximation, but it allows us to compare each of the events like for like.

We combine all of the simulations to analyse the tsunami inundation, allowing us to create a probabilistic tsunami inundation model from local-source earthquakes for Te Whanganui-a-Tara / Wellington Region (Figure 3.6).

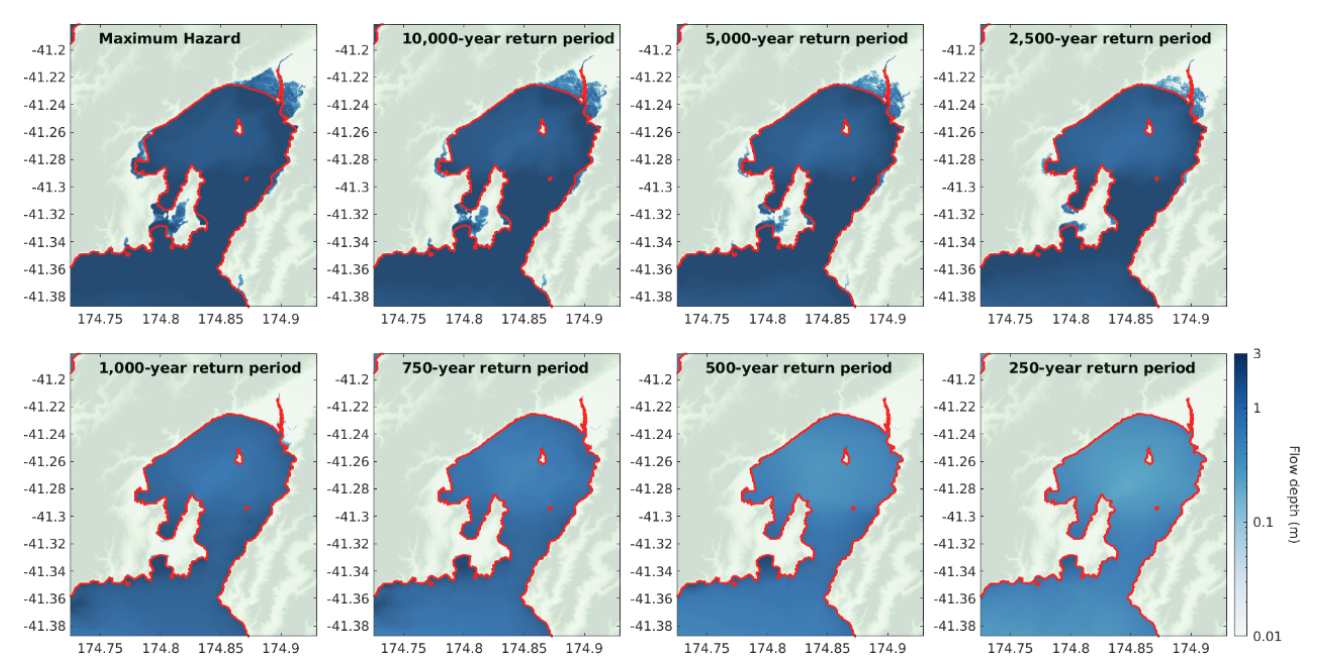


Figure 3.6 Inundation across Te Whanganui-a-Tara / Wellington Region calculated for different return periods. Note: The maximum hazard was calculated using one 30,000-year section of the earthquake catalogue, and, if a different section of the catalogue were to be used, then this result may differ due to different combinations of earthquakes.

As for the coastal hazard, the inundation hazard is largest when longer return periods are analysed. The greatest hazard is observed at return periods longer than 2500 years, with both large areas of inundation and flow depths of at least a 1 m being observed. However, there is a significant drop in the inundation hazard at shorter return periods. At shorter return periods, both the areas that become inundated and the onshore flow depths are significantly smaller and localised to small sections along the coast (Figures 2.14 and 2.15). This contrasts with the coastal amplitude hazard, which shows a steady reduction in hazard as the return period is reduced and reflects the importance of vertical movement of the coast on land inundation.

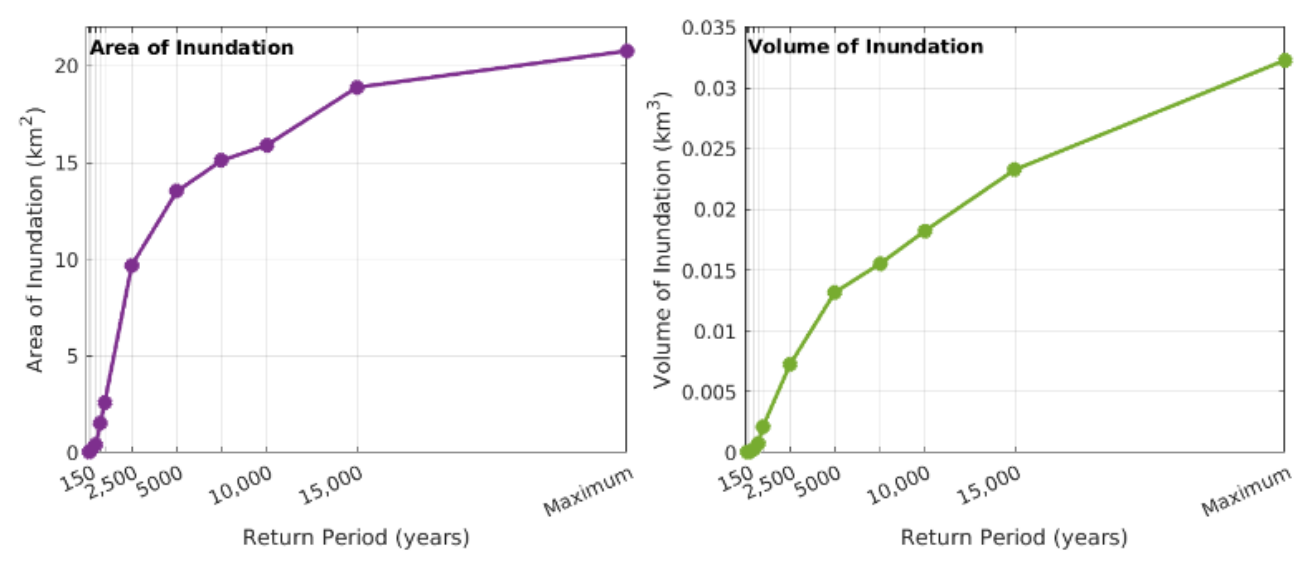


Figure 3.7 Summary of the inundation across Te Whanganui-a-Tara / Wellington Region. 'Area of inundation' is the area that is flooded at any point during the simulation. 'Volume of inundation' is the sum of the maximum flow depth recorded in the cell multiplied by the area of the cell. Note: The area and volume of inundation represent the maximum that is recorded over the simulations, and, due to the movement of the flow advancing and retreating, this maximum was not likely to occur all at one time.

The plots in Figure 3.7 further highlight this reduction, specifically when we are looking at the area of inundation. At 2500-year return periods, the area of inundation is 9.6 km² and the volume of inundation is 0.007 km³. At the 1000-year return periods, the area of inundation is 2.6 km² and the volume of inundation is 0.002 km³, which is a reduction of 72% and 71%, respectively. This highlights the need to model the largest events, which have longer recurrence intervals, because it is these events that contribute the most to the overall inundation hazard across Te Whanganui-a-Tara / Wellington Region.

While these results are able to provide an understanding about the scale of the event and which areas are likely to be the worst impacted, by extending the analysis into loss modelling we are able to see the scale of the damage that these events can cause.

# 4.0 Building Loss Calculations

Milestone 6: Loss calculations from the events modelled in Milestone 5

#### Milestone 7: Probabilistic risk metrics

Existing aligned work has provided the exposure data to model loss in Te Whanganui-a-Tara / Wellington Region from the simulated inundation (Magill 2024). We have utilised RiskScape $^{\text{TM}}$  software for this modelling.

The RiskScape<sup>™</sup> model calculates the estimated repair cost from tsunami-inundation-related damage. The RiskScape<sup>™</sup> pipeline calculates building repair cost on an asset-by-asset basis for each scenario inundation map. For each scenario map, the losses across the buildings are aggregated by suburb for visualisation purposes. The total loss for each scenario is calculated by summing the loss across all buildings.

The RiskScape<sup>™</sup> pipeline uses fragility functions (that relate damage state probability to flow depth) based on data from the 2011 Tōhoku Tsunami (Suppasri et al. 2013). These were coupled with a consequence function (that relates damage state to damage ratio – the ratio of repair cost to replacement cost of the building) by Horspool et al. (2015) to estimate the repair cost of the tsunami damage based on Aotearoa New Zealand data of flooding events. The primary building attributes used in the fragility functions are construction type (e.g. timber, reinforced concrete, steel, masonry) and number of storeys.

The exposure model is the NZ Building Exposure Dataset developed by Scheele et al. (2023). This contains building footprint polygons for all buildings in Aotearoa New Zealand. Each building has a number of attributes such as those used in the fragility function, as well as estimated replacement cost.

The RiskScape<sup>™</sup> model can easily be extended to include other asset types (e.g. infrastructure, people) or other fragility functions.

## 4.1 Relationship between Tsunami Events and Building Loss

For each of the events with inundation capable of generating loss, we calculated the total building loss with  $RiskScape^{TM}$  using vulnerability functions from Scheele et al. (2023). From these results, we calculated that the estimated total loss at different return periods (Figure 4.1).

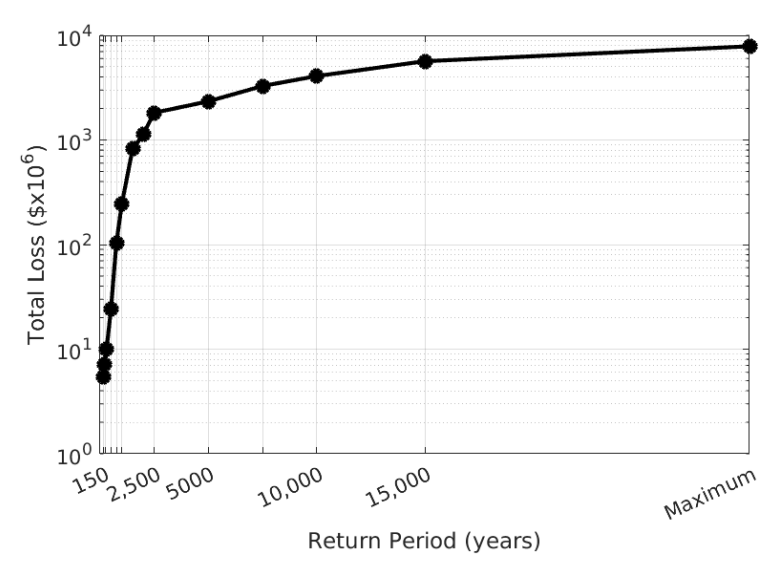


Figure 4.1 Expected loss at different return periods. Note: The maximum hazard is the worst-case scenario based on the 30,000-year earthquake catalogue that was analysed.

The greatest losses are expected at longer return periods (return periods greater than 2500 years). Both the hazard and total losses are significantly smaller at periods shorter than 2500 years. This supports the conclusion that there are many events that generate small losses while, very rarely, there is one event that generates losses that are exceedingly large.

#### 4.2 Annualised Loss

We calculate annualised loss by summing the total loss of all events modelled and dividing by the 30,000-year catalogue length ( $$5.56 \times 10^{10} / 30,000 = $1.85 \times 10^{6}$ ). This provides an estimated amount of loss expected each year; however, we do not expect a significant tsunami event every year. Table 4.1 shows how the average annualised loss varies depending on the subset of earthquakes that are used in the loss calculation.

Table 4.1 Summary of how the average annualised loss changes depending on which sub-set of earthquakes is analysed.

Scenario	Total Loss (All Events Modelled)	Total Loss of Events in Scenario	Average Annualised Loss
All events modelled through to inundation		\$5.56 x 10 <sup>10</sup>	\$1.85 x 10 <sup>6</sup>
50 earthquakes with the largest magnitude		\$4.72 x 10 <sup>10</sup>	\$1.57 x 10 <sup>6</sup>
50 earthquakes that generate the largest area of inundation	\$5.56 x 10 <sup>10</sup>	\$5.36 x 10 <sup>10</sup>	\$1.79 x 10 <sup>6</sup>
25 earthquakes that generate the largest area of inundation		\$5.03 x 10 <sup>10</sup>	\$1.68 x 10 <sup>6</sup>
10 earthquakes that generate the largest area of inundation		\$3.47 x 10 <sup>10</sup>	\$1.16 x 10 <sup>6</sup>

The 50 earthquakes that generate the largest areas of inundation contribute 96.8% of the total annualised loss, while the top 10 earthquakes that generate the largest areas of inundation constitute 63% of the total annualised loss. Using a similar process to that used to investigate the variability in individual event losses, we consider different time windows and calculate the average annualised loss for each of the segments. Using these values, we calculate the minimum, mean and maximum average annualised loss, along with the standard deviation (Table 4.2 and Figure 4.2).

Table 4.2 Summary of the variability in the average annualised loss when the entire model space is sampled at different-length sub-sets of the earthquake catalogue are analysed (i.e. the 30,000-year catalogue was sampled 60 times for the 500-year sub-set).

Length of Sub-Set (years)	Minimum Average Annualised Loss (\$ x 10°)	Mean Average Annualised Loss (\$ x 10°)	Maximum Average Annualised Loss (\$ x 10 <sup>6</sup> )	Standard Deviation Average Annualised Loss (\$ x 10°)
30,000	N/A	1.85	N/A	N/A
15,000	1.68	N/A	2.03	N/A
10,000	1.47	1.91	2.18	0.29
5000	1.01	1.85	3.05	0.64
2500	0.64	1.85	4.17	0.92
1000	0.14	1.84	8.84	1.82
500	0.016	1.92	16	2.95

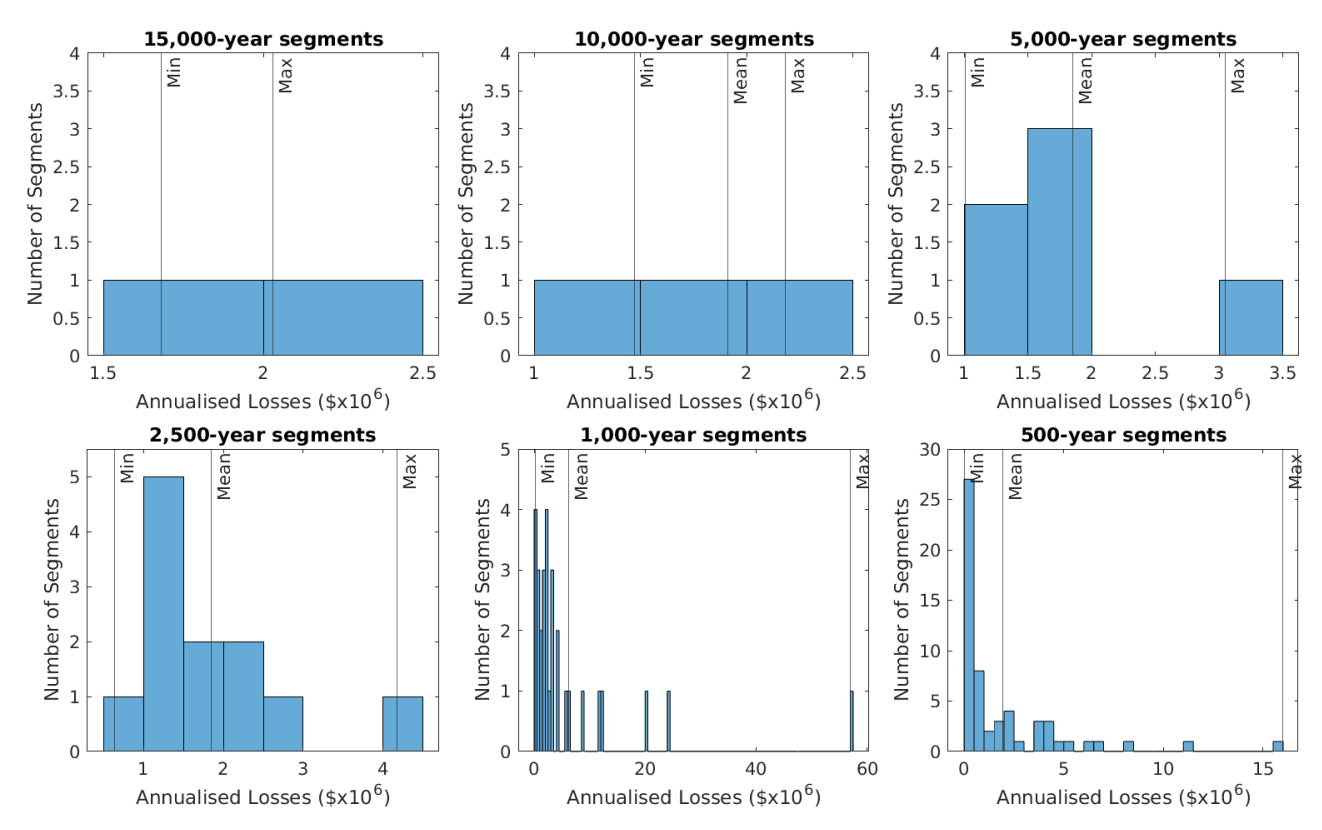


Figure 4.2 Distribution of the average annualised losses for different time segments of the entire 30,000-year earthquake catalogue.

The average annualised losses are skewed to the right, indicating that the majority of losses are small, while only a few events contribute to the largest averaged annualised loss. Further, this indicates that the expected losses are likely to be small in the different time segments, but, while rare, in some segments the losses are significantly larger than what has previously been observed.

## 4.3 Deaggregation of Loss

We have further investigated the contributions of key faults to the total loss (Figures 4.3–4.12). These include the Hikurangi and Kermadec megathrust faults, as well as the Wellington and Wairarapa crustal faults and Alpine Fault. Maximum losses are significantly higher when subduction zone events trigger co-seismic crustal faults, causing notable local coastal subsidence. This analysis highlights the need to consider complex events in risk modelling. Currently, physics-based modelling is the only method capable of creating the necessary complexity in the source model.

Due to the nature of multi-fault ruptures, we are unable to complete a full deaggregation of the losses. This is because it is very rare for events in our earthquake catalogue to rupture the subduction interface and only one crustal fault. For example, in our catalogue, only two events involve co-rupture of the Hikurangi Subduction Zone and Wairarapa Fault only, and no events involve co-rupture of the Hikurangi Subduction Zone and Wellington Fault only. Similarly, the events in the deaggregation plots titled 'Hikurangi-Kermadec + Rupture of the Wellington Fault' (Figure 4.5) and 'Hikurangi-Kermadec + Rupture of the Alpine Fault' (Figure 4.9) are also counted within the deaggregation of 'Hikurangi-Kermadec + Rupture of the Wairarapa Fault' (Figure 4.7), as all such events also ruptured the Wairarapa Fault.

## **Hikurangi-Kermadec-Only Ruptures**

From the 300 simulations, 37 scenarios rupture only the Hikurangi Subduction Margin. Eleven of these ruptures nucleate on the subduction interface to the south of Te Whanganui-a-Tara / Wellington and a further nine earthquakes nucleate along the southern Hikurangi Subduction Margin (between 41.8°S and 41.1°S). The deformation does not extend to Te Whanganui-a-Tara / Wellington Region and the remaining events nucleate along the southern segment of the Kermadec Subduction Zone. Due to these events not generating notable deformation around Te Whanganui-a-Tara / Wellington. the tsunami generated tend to result in limited inundation around Te Whanganui-a-Tara / Wellington.

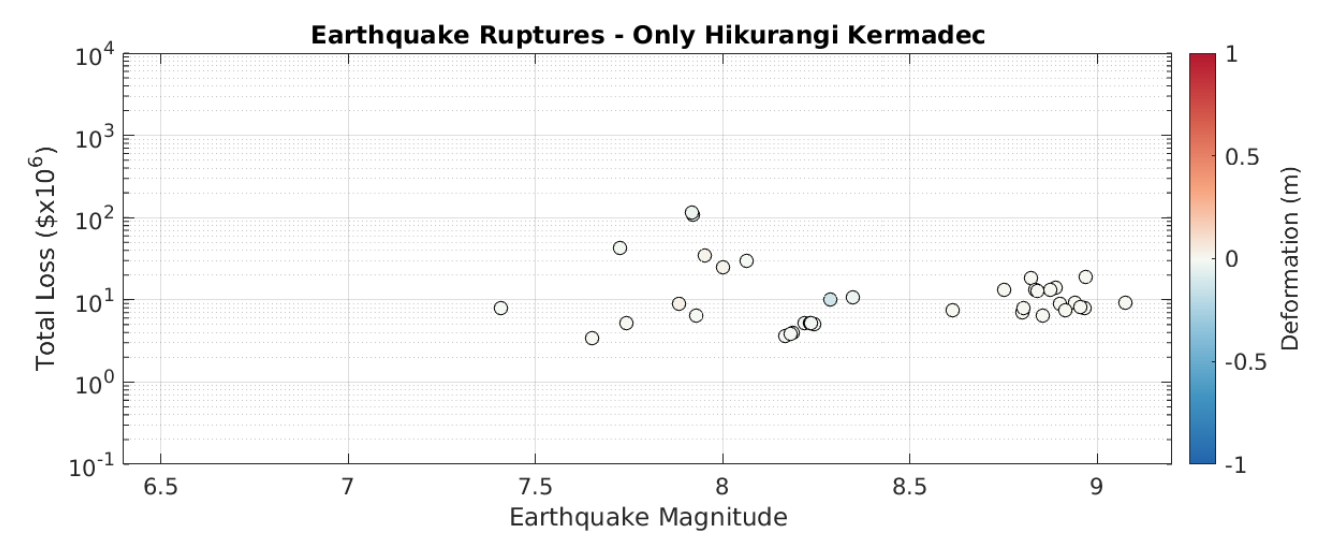


Figure 4.3 Event loss versus magnitude for events that only rupture the subduction megathrust.

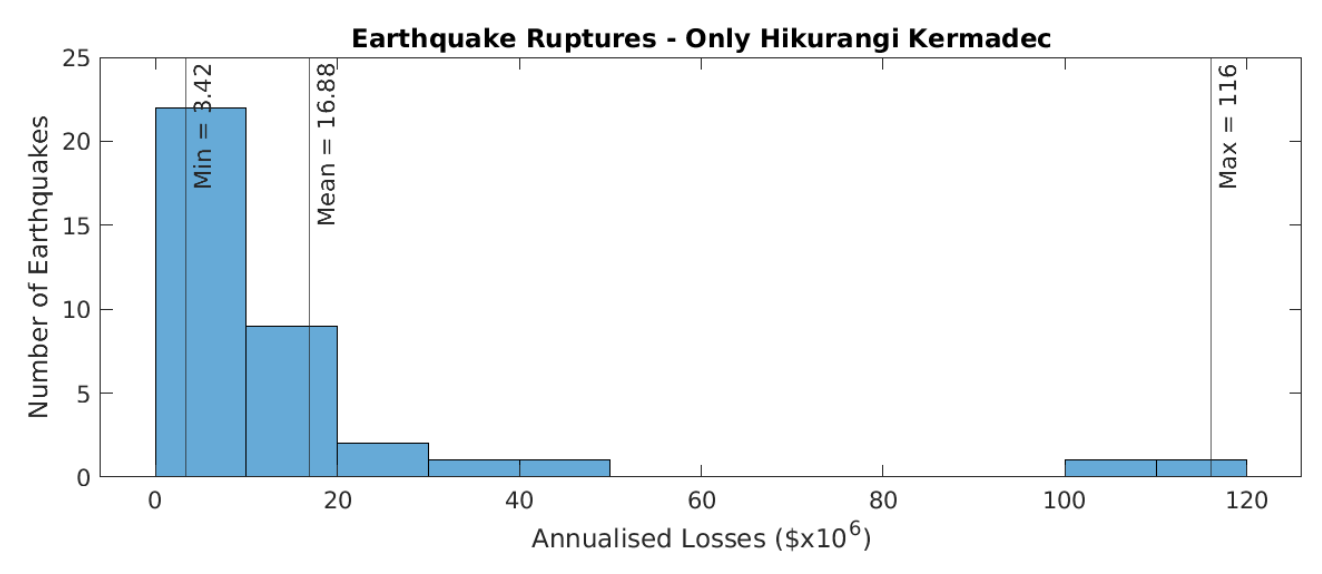


Figure 4.4 Annualised loss for events that only rupture the subduction megathrust.

# Hikurangi-Kermadec + Rupture of the Wellington Fault

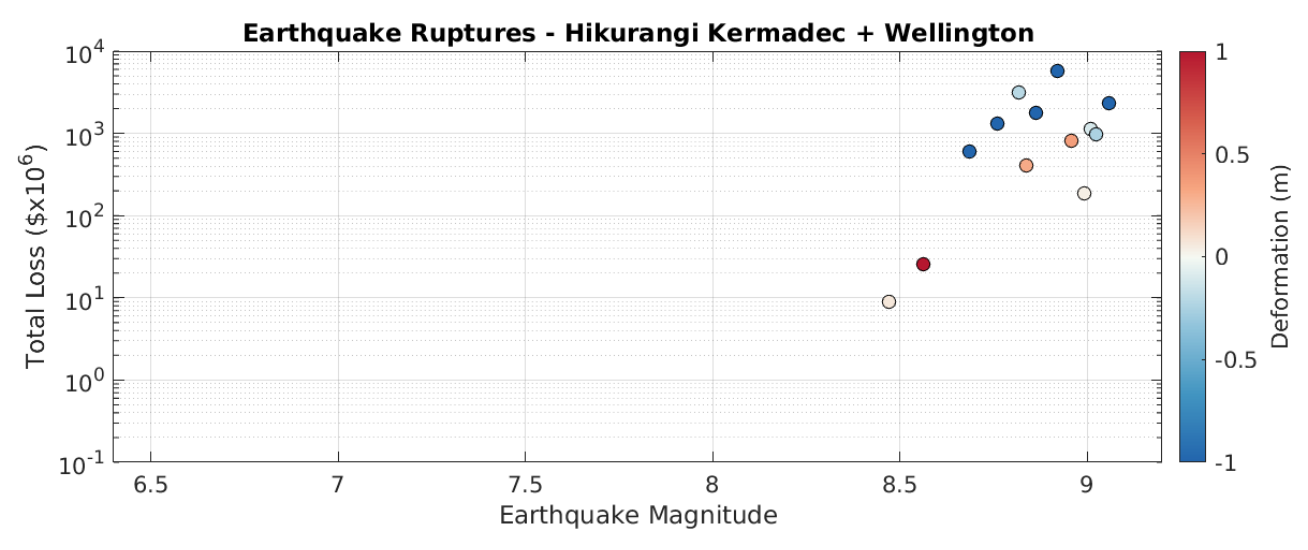


Figure 4.5 Event loss versus magnitude for subduction megathrust plus Wellington Fault events. Note: Other faults may also be rupturing at the same time, and these events are likely to be counted in the other deaggregation plots.

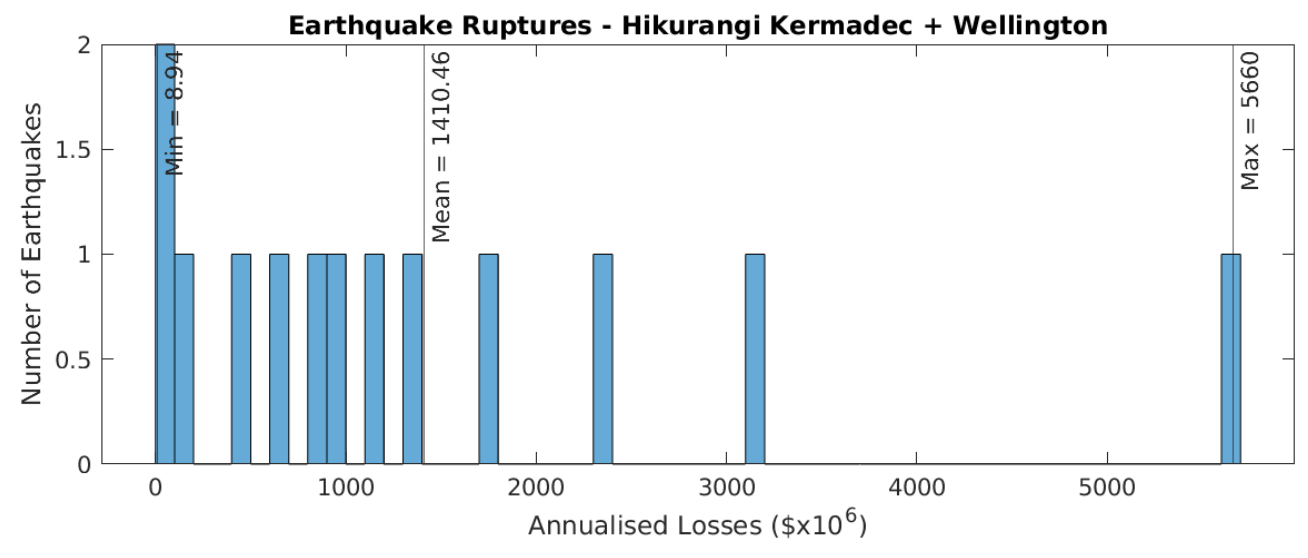


Figure 4.6 Annualised loss for subduction megathrust plus Wellington Fault events. Note: Other faults may also be rupturing at the same time, and these events are likely to be counted in the other deaggregation plots.

# Hikurangi-Kermadec + Rupture of the Wairarapa Fault

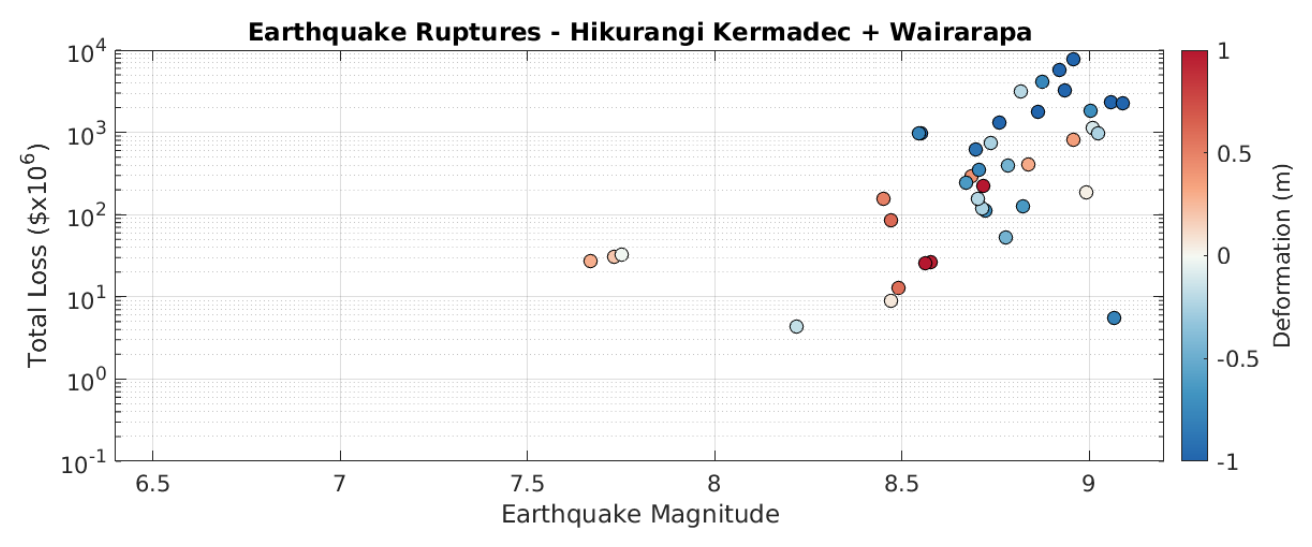


Figure 4.7 Event loss versus magnitude for subduction megathrust plus Wairarapa Fault events. Note: Other faults may also be rupturing at the same time, and these events are likely to be counted in the other deaggregation plots.

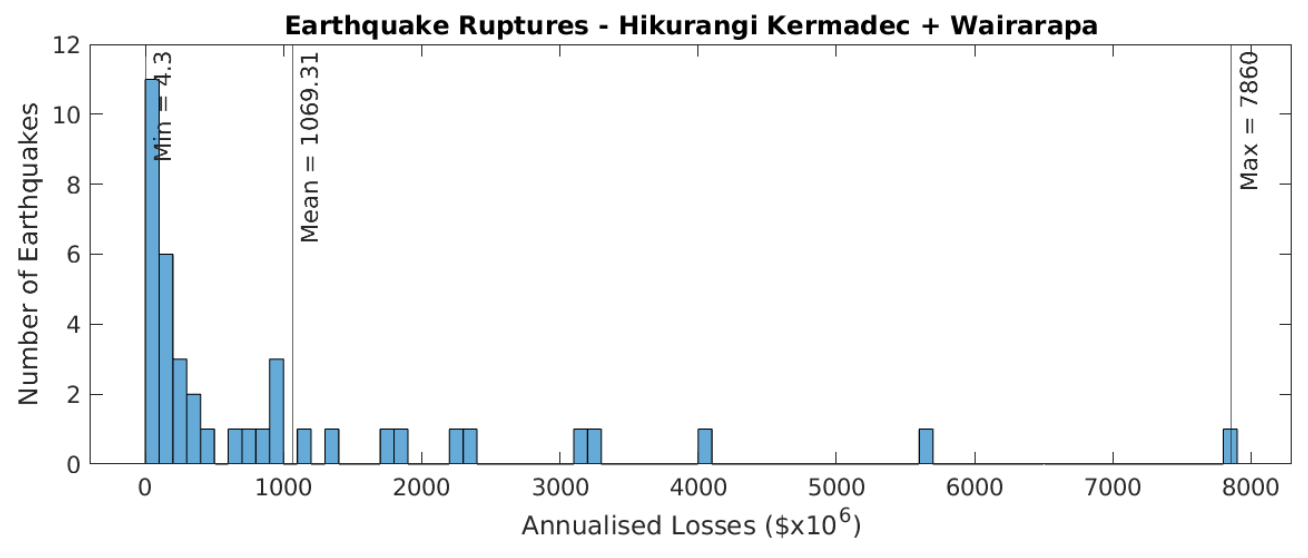


Figure 4.8 Annualised loss for subduction megathrust plus Wairarapa Fault events. Note: Other faults may also be rupturing at the same time, and these events are likely to be counted in the other deaggregation plots.

# Hikurangi-Kermadec + Rupture of the Alpine Fault

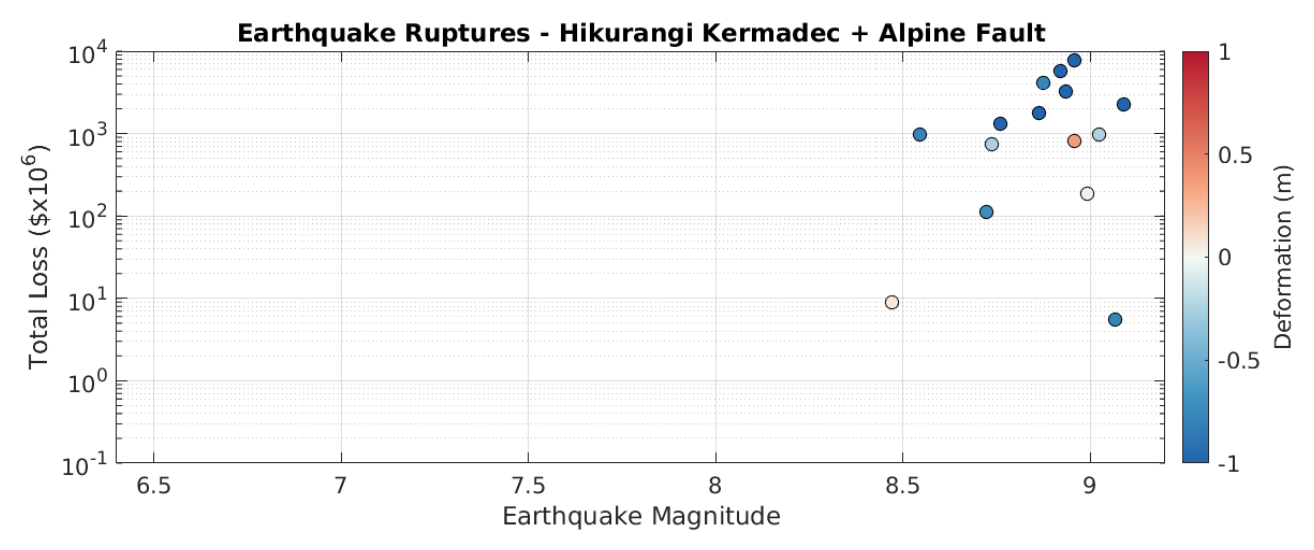


Figure 4.9 Event loss versus magnitude for subduction megathrust plus Alpine Fault events. Note: Other faults may also be rupturing at the same time, and these events are likely to be counted in the other deaggregation plots.

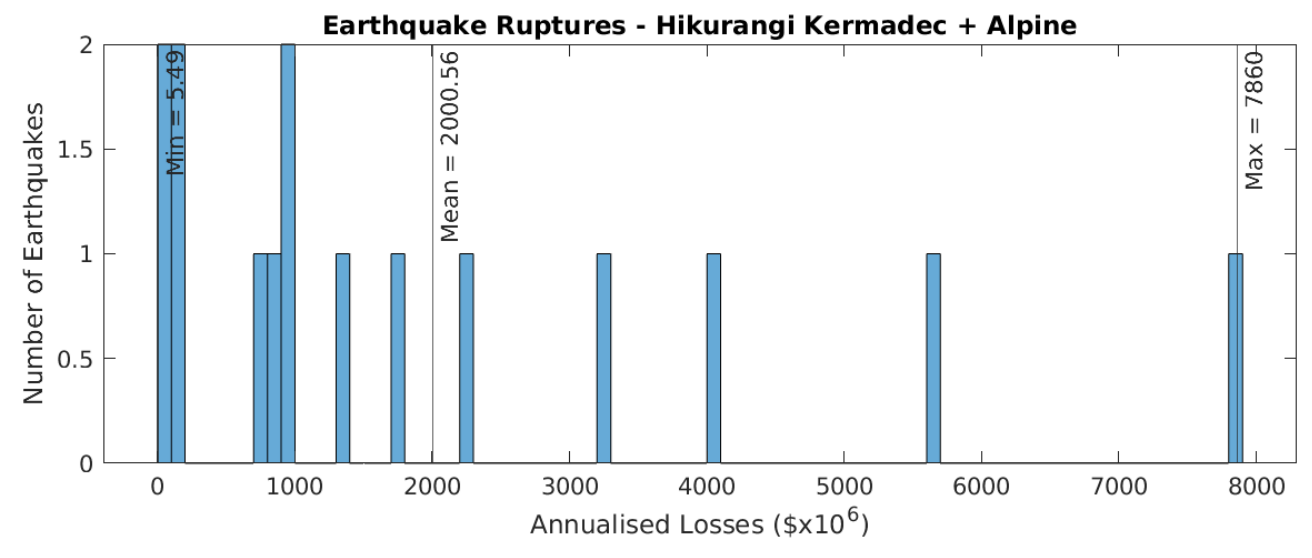


Figure 4.10 Annualised loss for pure subduction megathrust events. Note: Other faults may also be rupturing at the same time, and these events are likely to be counted in the other deaggregation plots.

# **Only Wellington Fault**

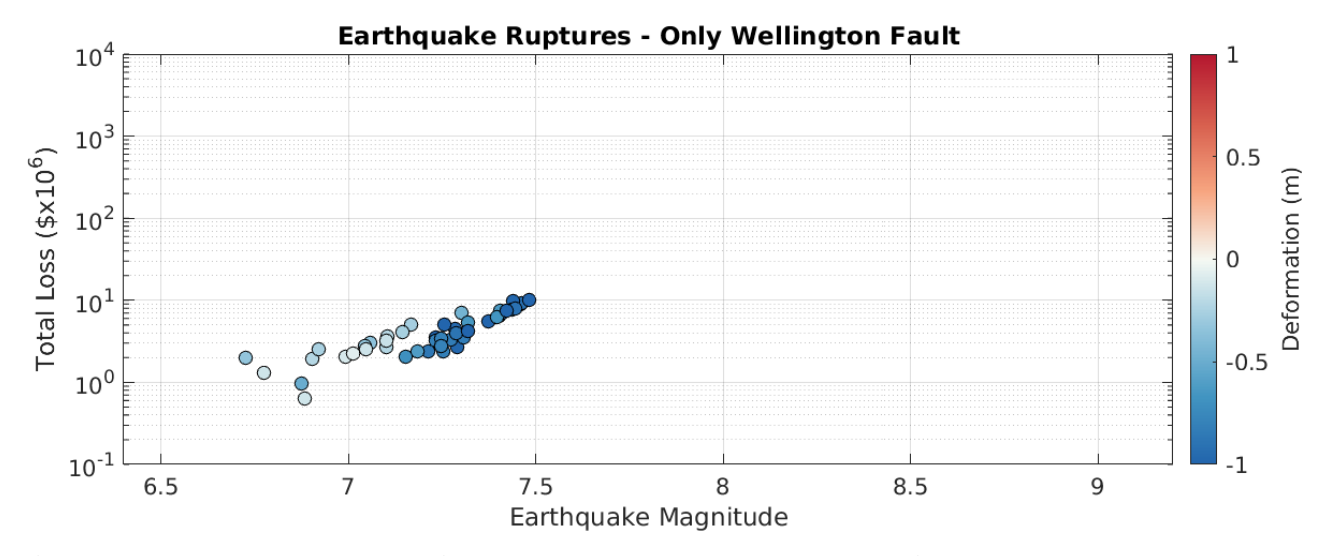


Figure 4.11 Event loss versus magnitude for events that only rupture the Wellington Fault.

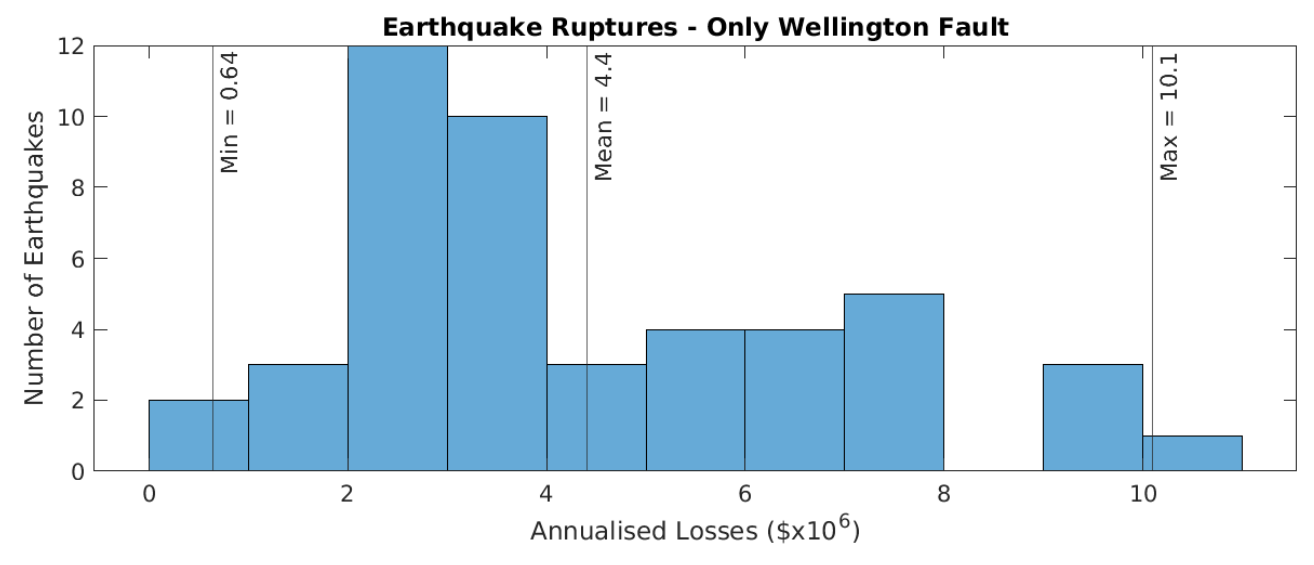


Figure 4.12 Annualised loss of events that only rupture the Wellington Fault.

## 4.4 Risk from Distant Events

While hazard and risk from distant events is outside the scope of Stage 1, we consider 20 distant  $M_W$  9.3 scenarios from the New Zealand Tsunami Threat-Level Database (Gusman et al. 2019, 2020). We observe that minimal inundation occurs from each of the earthquake scenarios (Figure 4.13).

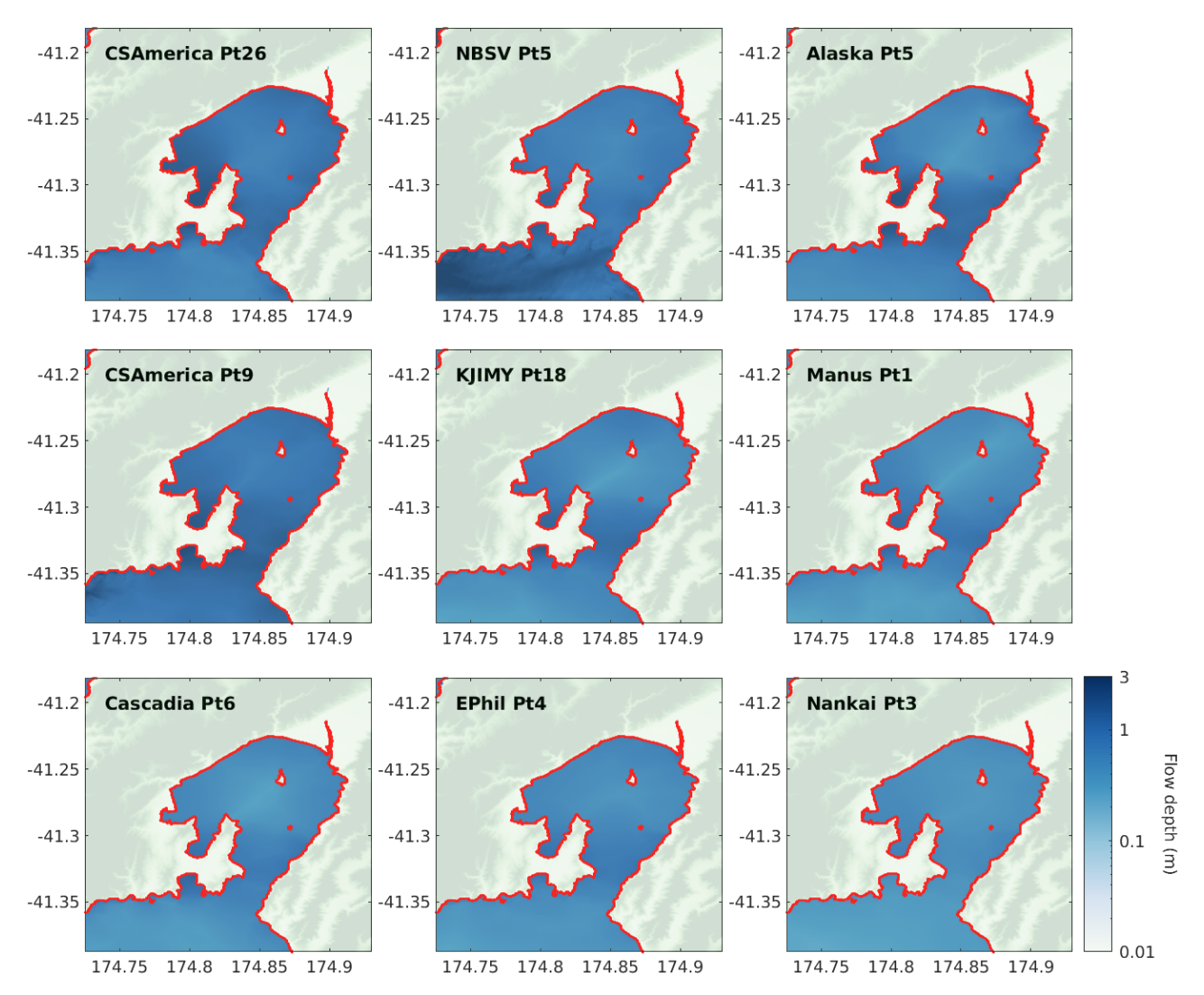


Figure 4.13 Inundation generated by a selection of nine distant source earthquakes taken from the New Zealand Tsunami Threat-Level Database (Gusman et al. 2019, 2020). Summary of the inundation is included in Table 4.3.

Inundation areas from these scenarios are predominantly focused along the coast and round the Hutt River, generating minimal loss. This is consistent across all 20 events. To better understand the extent of inundation and expected losses, we calculate the maximum area and maximum volume of inundation, as well as the total losses for each of these scenarios (Table 4.3).

Table 4.3 Summary of the inundation statistics and total loss generated by a selection of distant-source earthquakes taken from the New Zealand Tsunami Threat-Level Database (Gusman et al. 2019, 2020).

Scenario	Maximum Area of Inundation (km²)	Maximum Volume of Inundation (km³)	Total Loss (\$ x 10 <sup>6</sup> )
Alaska_Pt4_Mw9.30	0.24	8.0 x 10 <sup>-5</sup>	55
Alaska_Pt5_Mw9.30	0.33	0.00011	57
Cascadia_Pt6_Mw9.30	0.053	1.16 x 10 <sup>-5</sup>	7.7
Cascadia_Pt9_Mw9.30	0.019	2.12 x 10 <sup>-6</sup>	7.7
CSAmerica_Pt8_Mw9.30	0.71	0.00026	97
CSAmerica_Pt9_Mw9.30	0.62	0.00023	57
CSAmerica_Pt21_Mw9.30	0.24	7.91 x 10 <sup>-6</sup>	29
CSAmerica_Pt23_Mw9.30	0.89	0.00027	78
CSAmerica_Pt26_Mw9.30	0.53	0.00016	97
CSAmerica_Pt27_Mw9.30	0.43	0.0001	76
EPhil_Pt3_Mw9.30	0.016	3.07 x 10 <sup>-6</sup>	7.1
EPhil_Pt4_Mw9.30	0.029	2.5 x 10 <sup>-6</sup>	7.3
KJIMY_Pt18_Mw9.30	0.085	2.3 x 10 <sup>-5</sup>	18
KJIMY_Pt23_Mw9.30	0.046	5.6 x 10 <sup>-6</sup>	12
Manus_Pt1_Mw9.30	0.06	9.21 x 10 <sup>-6</sup>	10
Manus_Pt2_Mw9.30	0.016	3.08 x 10 <sup>-6</sup>	6.1
Nankai_Pt3_Mw9.30	0.018	2.89 x 10 <sup>-6</sup>	5.9
NBVS_Pt5_Mw9.30	0.45	0.00021	82
NBVS_Pt12_Mw9.30	0.91	0.00053	27
PNG_Pt3_Mw9.30	0.16	2.1 x 10 <sup>-6</sup>	3.4

The area and volume of inundation for distant sources is significantly smaller than the local sources, despite the larger magnitudes of the distant events. Total losses from distant events are also smaller than the local-source events. For example, the largest loss expected from the distant-source earthquakes analysed was  $$97 \times 10^6$ , which, if compared to the local-source events, sits at the  $41^{st}$  largest loss event. Where the losses for the distant-source events sit compared to the local sources becomes clear when we re-plot the earthquake magnitude against the losses but add in the distant sources (Figure 4.14).

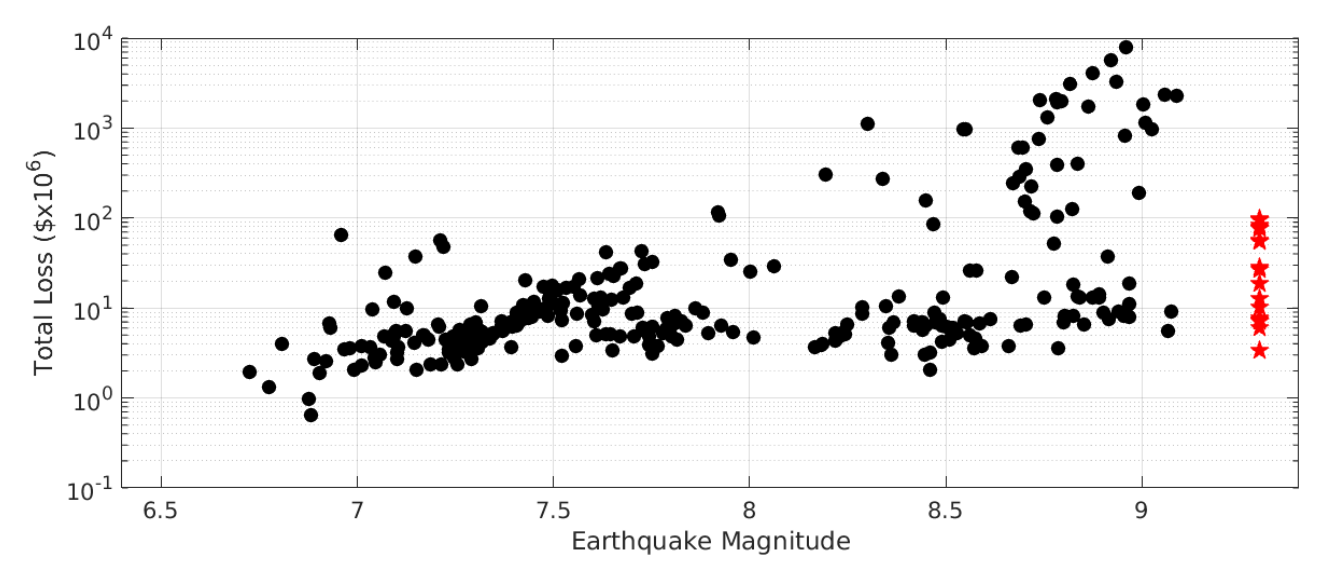


Figure 4.14 Relationship between earthquake magnitude and the total loss for each event. Black points show scenario-loss calculations, and the red stars show the  $20\,M_W\,9.30$  earthquakes from the New Zealand Tsunami Threat-Level Database (Gusman et al. 2019, 2020).

Despite the large magnitude of the distant events, losses from these are only on the scale of a Wellington-Fault-only earthquake rupture. Local-source events also dominate the largest loss events. This highlights that, for Te Whanganui-a-Tara / Wellington Region, the events that are going to generate the largest losses are the local events and so justifies our focus in Stage 1 on local events for capturing the dominant source of tsunami risk.

# 5.0 Summary

Accounting for complexity of local sources, including the simultaneous rupture of subduction megathrust and crustal faults, is crucial in determining tsunami hazard for Aotearoa New Zealand. In recognition of this understanding, we have used a physics-based source model of tsunami hazard relevant to Te Whanganui-a-Tara / Wellington Region to underpin a new probabilistic tsunami risk model. The model constitutes Stage 1 of the National Tsunami Model. Te Whanganui-a-Tara / Wellington Region is particularly well suited for this study, as (1) its tsunami hazard is dominantly generated by locally sourced tsunami and (2) its natural harbour induces many hydrodynamic effects that create a rigurous test for our physics-based approaches to tsunami inundation and risk assessment.

We use a 30,000-year synthetic earthquake catalogue to create initial conditions for tsunami simulation. Using a well-tested hydrodynamic modelling approach, we simulate inundation for the events capable of creating tsunami loss in the region. We then, on a scenario-by-scenario basis, calculate loss with the RiskScape $^{\text{TM}}$  engine. We conclude by generating probabilistic statistics of risk, including an estimate of annualised loss.

# 6.0 Acknowledgements

The National Tsunami Model, Stage 1 and 1.a are the direct result of funding from the Natural Hazards Commission Toka Tū Ake (NHC) under contract #4133. Work builds upon the Resilience to Nature's Challenges (RNC) National Science Challenge Earthquake and Tsunami Programme. Stage 1 and 1a also draw upon previous funded work including the Tsunami impact and loss modelling in Hawkes Bay project (contract #20/LM773) a study funded by the NHC (then the Earthquake Commission).

# 7.0 References

- Burbidge DR, Gusman AR, Power WL, Wang X, Lukovic B. 2021. Wellington City probabilistic tsunami hazard maps. Lower Hutt (NZ): GNS Science. 24 p. Consultancy Report 2021/91. Prepared for Wellington City Council.
- Fry B, Power W, Hughes L, O'Kane A, Howell A, Nicol A. 2024. National Tsunami Hazard Model: Stage 1 update report. Lower Hutt (NZ): GNS Science. 6 p. Consultancy Report 2024/79LR. Prepared for NHC Toka Tū Ake.
- Gusman AR, Wang W, Power WL, Lukovic B, Mueller C, Burbidge DR. 2019. Tsunami threat level database update. Lower Hutt (NZ): GNS Science. 110 p. (GNS Science report; 2019/67). https://doi.org/10.21420/QM31-NA61
- Gusman AR, Lukovic B, Peng B. 2020. Tsunami threat level database update: regional sources and tsunami warning text. Lower Hutt (NZ): GNS Science. 57 p. (GNS Science report; 2019/83). https://doi.org/10.21420/PTDC-NS18
- Horspool NA, Cousins WJ, Power WL. 2015. Review of tsunami risk facing New Zealand: a 2015 update.

  Lower Hutt (NZ): GNS Science. 44 p. Consultancy Report 2015/38. Prepared for the New Zealand Institute of Economic Research.
- Hughes L. 2024. From earthquakes to inundation: using physics-based synthetic earthquake catalogues to assess tsunami hazard in New Zealand [PhD thesis]. Wellington (NZ): Victoria University of Wellington. <a href="https://doi.org/10.26686/wgtn.27320670">https://doi.org/10.26686/wgtn.27320670</a>
- Hughes L, Power W, Lane EM, Savage MK, Arnold R, Howell A, Shaw B, Fry B, Nicol A. 2023. A novel method to determine probabilistic tsunami hazard using a physics-based synthetic earthquake catalog: a New Zealand case study. *Journal of Geophysical Research: Solid Earth*. 128(12):e2023JB027207. https://doi.org/10.1029/2023JB027207
- Hughes L, Lane EM, Power W, Savage MK, Arnold R, Howell A, Liao Y-WM, Williams C, Shaw B, Fry B, et al. 2024. Effects of subduction interface locking distributions on tsunami hazard: a case study on the Hikurangi/Tonga-Kermadec subduction zones. *Geophysical Journal International*. 240(2):1147–1167. https://doi.org/10.1093/gji/ggae441
- Kennedy AB, Chen Q, Kirby JT, Dalrymple RA. 2000. Boussinesq modeling of wave transformation, breaking, and runup. Part1: 1D. *Journal of Waterway, Port, Coastal, and Ocean Engineering*. 126(1):39–47. https://doi.org/10.1061/(ASCE)0733-950X(2000)126:1(39)
- Liao Y-WM, Fry B, Howell A, Williams CA, Nicol A, Rollins C. 2024. The role of heterogeneous stress in earthquake cycle models of the Hikurangi-Kermadec subduction zone. *Geophysical Journal International*. 239(1):574–590. https://doi.org/10.1093/gji/ggae266
- Lynett PJ. 2002. A multi-layer approach to modeling generation, propagation, and interaction of water waves [PhD thesis]. Ithaca (NY): Cornell University. 201 p.
- Macías J, Mercado A, González-Vida JM, Ortega S, Castro MJ. 2016. Comparison and computational performance of Tsunami-HySEA and MOST models for LANTEX 2013 Scenario: impact assessment on Puerto Rico coasts. *Pure and Applied Geophysics*.173:3973–3997. https://doi.org/10.1007/s00024-016-1387-8
- Magill C. 2024. Personal communication. Risk Scientist; GNS Science, Lower Hutt, NZ.

- [MCDEM] Ministry of Civil Defence & Emergency Management. 2016. Tsunami evacuation zones: Director's guideline for Civil Defence Emergency Management Groups [DGL 08/16]. Wellington (NZ): MCDEM; [accessed 2025 Apr]. https://www.civildefence.govt.nz/assets/Uploads/documents/publications/guidelines/directors-guidelines/08/16-tsunami-evacuation-zones/dgl-08-16-Tsunami-Evacuation-Zones.pdf
- Melgar D, LeVeque RJ, Dreger DS, Allen RM. 2016. Kinematic rupture scenarios and synthetic displacement data: an example application to the Cascadia subduction zone. *Journal of Geophysical Research: Solid Earth*. 121(9):6658–6674. https://doi.org/10.1002/2016JB013314
- Power WL, compiler. 2013. Review of tsunami hazard in New Zealand (2013 update). Lower Hutt (NZ):
  GNS Science. 222 p. Consultancy Report 2013/131. Prepared for Ministry of Civil Defence & Emergency Management.
- Power WL, Fry B. 2023. Tsunami impact and loss modelling in Hawkes Bay high-level summary: EQC project number 20773. Lower Hutt (NZ): GNS Science. 3 p. Consultancy Report 2023/50LR. Prepared for Toka Tū Ake EQC.
- Power WL, Burbidge DR, Gusman AR. 2022. The 2021 update to New Zealand's National Tsunami Hazard Model. Lower Hutt (NZ): GNS Science. 63 p. (GNS Science report; 2022/06). https://doi.org/10.21420/X2XQ-HT52
- Robinson R, Benites R. 1996. Synthetic seismicity models for the Wellington Region, New Zealand: implications for the temporal distribution of large events. Journal of Geophysical Research: Solid Earth. 101(B12):27833–27844. https://doi.org/10.1029/96JB02533
- Scheele FR, Syed YI, Hayes JL, Paulik R, Inglis S. 2023. Building inventory and vulnerability functions for risk modelling in New Zealand. Lower Hutt (NZ): GNS Science. 42 p. (GNS Science report; 2023/08). https://doi.org/10.21420/G34N-V958
- Seebeck H, Van Dissen RJ, Litchfield NJ, Barnes PM, Nicol A, Langridge RM, Barrell DJA, Villamor P, Ellis SM, Rattenbury MS, et al. 2022. New Zealand Community Fault Model version 1.0. Lower Hutt (NZ): GNS Science. 97 p. (GNS Science report; 2021/57). https://doi.org/10.21420/GA7S-BS61
- Shaw BE, Fry B, Nicol A, Howell A, Gerstenberger M. 2022. An earthquake simulator for New Zealand.

  Bulletin of the Seismological Society of America. 112(2):763–778. https://doi.org/10.1785/0120210087
- Suppasri A, Mas E, Charvet I, Gunasekera R, Imai K, Fukutani Y, Abe Y, Imamura F. 2013. Building damage characteristics based on surveyed data and fragility curves of the 2011 Great East Japan tsunami. Natural Hazards. 66:319–341. https://doi.org/10.1007/s11069-012-0487-8
- Wang X. 2008. Numerical modelling of surface and internal waves over shallow and intermediate water [PhD thesis]. Ithaca (NY): Cornell University. 245 p.
- Wang X, Power W. 2011. COMCOT: a tsunami generation, propagation and run-up model. Lower Hutt (NZ): GNS Science. 121 p. (GNS Science report; 2011/43).

# **APPENDICES**

This page left intentionally blank.

# APPENDIX 1 National Tsunami Model Stage 1.a

#### A1.1 Introduction

In this addendum, we report against the successful completion of all 5 contracted milestones (in addition to the 8 milestones reported against in the Final Report from Stage 1):

- 1. Formalisation and peer review of the seismic source model that underpins the National Tsunami Model (NTM) Stage 1.
- 2. Formation of a Technical Advisory Group (TAG) for the NTM.
- 3. Comparison of the Stage 1 model for the Wellington region against the existing New Zealand National Tsunami Hazard Model.
- 4. Assessment of the IT and computational resources necessary to facilitate application of the Stage 1 framework in a New Zealand-wide context.
- 5. Delivery of a final report for Stage 1.a.

# A1.2 Peer Review of the Physics-Based Source Model

**Milestone 1:** Formalisation and peer review of the seismic source model that underpins the NTM Stage 1.

Physics-based earthquake simulators are relatively new to applications in hazard and risk quantification. Underpinning work for Stage 1 has previously published in international peer-reviewed journals (Shaw et al. 2022; Liao et al. 2024; Hughes et al. 2023). We have now published our source model and made it available for community uptake.

 Howell A, Penney C, McLennan T, Seebeck H, Liao Y.-W. M, Williams C, Fry B, Nicol A. 2025. An RSQSim Synthetic Earthquake Catalogue for Aotearoa New Zealand based on the New Zealand Community Fault Model. Zenodo. <a href="https://doi.org/10.5281/zenodo.15734819">https://doi.org/10.5281/zenodo.15734819</a>.

The source model has also been presented at various international meetings including:

- Andy Nicol, SSA, April 2025 Testing and evaluation of earthquake simulations for natural hazards and risk modelling
- Andy Nicol, JpGU, May 2025, Characteristics of segmented and multi-fault earthquake-rupture models in New Zealand
- Camilla Penney, JpGU, May 2025, What role should physics-based simulators play in seismic hazard models? A case study from Aotearoa New Zealand.

We have convened a session at the annual meeting of the SSA to elicit contributions on the utility of simulators for seismic hazard studies:

• SSA session, April 2025, Testing, Testing 1 2 3: Appropriate Evaluation of New Seismic Hazard and Risk Models

We have tested the model against paleoseismic records of large central New Zealand earthquakes and published the results in the Bulletin of the Seismological Society of America. The paleoseismic evidence is consistent with the simulator results of clustering of crustal earthquakes on timelines compatible with the physics-based simulations.

- Jade Humphrey, Andrew Nicol, Andy Howell, Nicola Litchfield, Rob Langridge, Russ Van Dissen, Camilla Penney, Bill Fry; Spatial and Temporal Clustering of Large Earthquakes on Upper-Plate and Subduction Thrust Faults Along the Southern Hikurangi Subduction Margin, Aotearoa-New Zealand. BSSA 2025; <a href="https://doi.org/10.1785/0120240246">https://doi.org/10.1785/0120240246</a>.
- The paper was further highlighted by the Bulletin of Seismological Society of America (https://www.seismosoc.org/news/clustering-of-upper-plate-and-subduction-earthquakes-at-new-zealands-southern-hikurangi-margin/) in a press release.

In work aligned with the Rapid Characterisation of Earthquakes and Tsunamis (RCET) MBIE Endeavour Programme, we have successfully tested the model against empirical regressions of displacement ground motion. In this work, our catalogue is more effective at generating ground motions closer to displacement GMPE than the well-documented Fakequake (Melgar et al. 2016) algorithm.

 Solares-Colón M, Melgar D, Howell A, Crowell B, D'Anastasio E, Caballero E, Fry B. Using ruptures from earthquake cycle simulators to test geodetic early warning systems performance, submitted to Seismica.

## A1.3 Technical Advisory Group

Milestone 2: Formation of a Technical Advisory Group (TAG) for the NTM

We have established the international component of the Technical Advisory Group including four global experts of tsunami hazard and risk. The current international contingent includes:

- Stefano Lorito, head of the Tsunami Alert Centre of the INGV (Italy) and director of the Global Tsunami Model. Expertise in probabilistic seismic hazard and geophysics of tsunami genesis and wave propagation.
- Fatemeh Jalayer, coordinator of the European Tsunami Risk Service (ETRiS) and chair of the European Facilities for Earthquake Hazard and Risk (EFEHR), Professor of Geophysical Hazard and Risk at the University College London. Expertise in vulnerability modelling and loss.
- Chris Moore, Director of U.S. NOAA Center for Tsunami Research, chair of ICG-PTWS Working Group 1 (Understanding Tsunami Hazard). Expertise in computational fluid dynamics and tsunami modelling.
- Gareth Davies, Leader of the Australian Tsunami Hazard Model. Expertise in probabilistic tsunami hazard, Bayesian and logic-tree approaches.

This group is currently undertaking consideration of the Stage 1 report. We will extend the TAG in Stage 2 to domestic members.

# A1.4 Comparison of NTM Stage 1 and NTHM

**Milestone 3:** Comparison of the NTM Stage 1 model for the Wellington region against the existing New Zealand National Tsunami Hazard Model

In Stage 1, we used physics-based earthquake simulators to calculate tsunami hazard and risk for the Wellington region. Tsunami wave propagation and inundation models were calculated for large numbers of local and regional earthquakes and statistically analysed for quantitative risk.

Previously, tsunami inundation hazard assessments have been conducted using a small number of events that have been deaggregated from the 2021 National Tsunami Hazard Model (NTHM) (Power et al. 2022). For the return period of interest, scenarios are selected from the NTHM and these events are modelled through to inundation.

Here we compare the two approaches. We refer to the earthquake simulator approach as the "simulator" analysis and the NTHM deaggregation as the 'traditional' analysis. We simulate the traditional analysis using the same simulation parameters that were previously used in Stage 1 of the Nation Tsunami Model to ensure a direct comparison. We then re-estimate risk based on the traditional analysis at mean high water springs and with different resolutions and roughness parameters to ensure that traditional analysis follows the same patterns as was previously observed with the simulator analysis in Stage 1.

#### A1.4.1 Scenario Selection and Simulations

For the simulator approach, we use the earthquakes and simulations that were undertaken to complete Stage 1 of the Nation Tsunami Model. To analyse these events, we use the same approach that was previously undertaken.

For the traditional approach, we take the same approach that was undertaken in the Wellington City Council tsunami inundation report (Burbidge et al 2021). We selected four return periods, 100 years, 500 years, 1000 years and 2500 years. For each return period we deaggregate the NTHM and find the six tsunami sources that are the largest contributors to the hazard. Once we have selected the events for each return period, we scale the slip in each of the events so that the wave heights in the Wellington Warning Zone (warning zone 91) match the expected height for the corresponding return period. For each scenario, we take the re-calculated slip and the patches that make up the fault of interest and run tsunami simulations using COMCOT. Within COMCOT the slip on the patches are used to calculate the initial displacements. We use the same COMCOT set up as was previously used for the simulator approach. As the events that make up the 500-year, 1000-year and 2500-year return periods are within the same region as the simulator approach we run the simulations for 10 hours. However, for the 100-year return period there is a combination of local/regional and distant sources. For the three local/regional source we run the simulations for 10 hours but for the distant sources we run these simulations for 30 hours as the longer time is required in order to capture the waves arriving around Wellington.

Due to the different approaches, we analysed the tsunami hazard in different ways. For the simulator approach we used the same approach as was used in Stage 1. For the traditional approach, once the simulations were completed, we formed a composite hazard map for each return period. To do this we find the weighted median of the tsunami wave heights/flow depths across the simulation grid. The weights for the median calculation are taken from the deaggregation and normalised.

To move from tsunami inundation to loss, we calculate total building losses from all catalogues (simulator events, traditional composite hazard map and traditional individual events) with RiskScape.

#### A1.4.2 Hazard and Loss Comparison

We compare the two approaches to see how the tsunami inundation and associated loss vary. In Section A1.4.3 we compare the hazard at three return periods and in Section A1.4.4 we compare the losses that were calculated for the two approaches.

### A1.4.3 Return Period Hazard Comparison

With the traditional method we can go down to return periods of 100 years, but with the simulator the shortest return period is 150 years. Therefore, we only compare the tsunami inundation maps for the 500-year, 1000-year and 2500-year return periods, which were generated by running the simulations with the same parameters. In this section we are comparing the inundation generated when a 40 m resolution and one friction parameter is used in the modelling process. **Error! Reference source not found.** compares the inundation generated using the simulator and traditional methods for the three return periods and the difference between the methods.

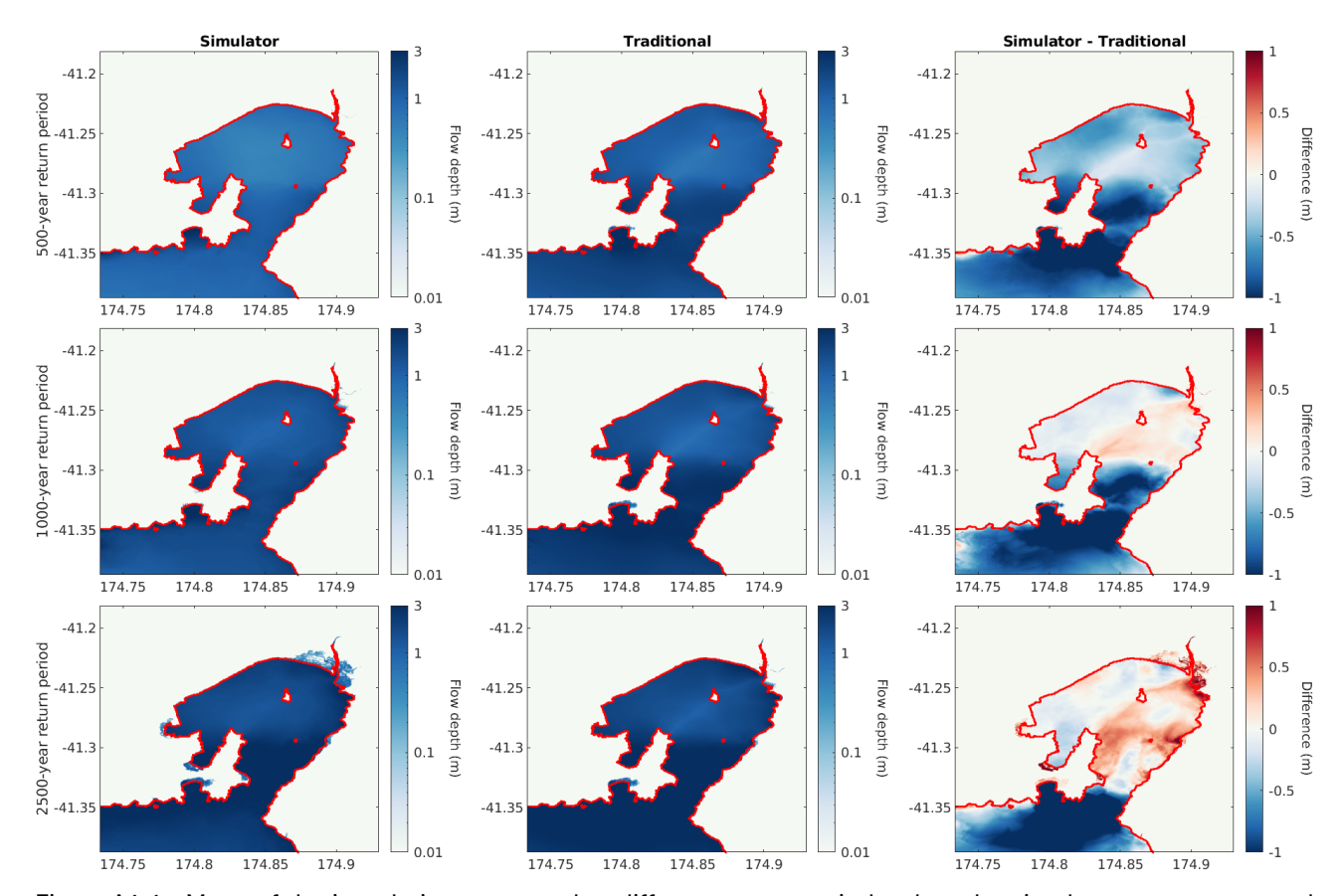


Figure A1.1 Maps of the inundation generated at different return periods when the simulator events are used and when the traditional approach to hazard is used. Left column: inundation generated when the simulator events are used. Middle column: inundation generated when the traditional approach is used. Right column: difference between the two approaches. Top row: 500-year return period. Middle row: 1000-year return period. Bottom row: 2500-year return period

From Figure A1.1 we observe the in general the inundation generated at the 500-year and 1000-year return periods is similar between the two methods around Petone and the Hutt Valley but the traditional method generates more inundation around Lyall Bay compared to the simulator method. When comparing the inundation at the 2500-year return period in general the simulator method results in more inundation across the entire region. While similar inundation extents are observed around Lyall Bay, however the flow depths generated by the simulator are slightly larger than the traditional method. The largest differences are observed around the Port, Evans Bay and Petone and the Hutt Valley. In these locations the simulator generates larger areas of inundation and flow depths compared to the traditional method. This is likely because the earthquake deformation that is generated by the simulator is more varied compared to the traditional method. Therefore, at the longer return periods we are observing greater variation in the deformation resulting in increased inundation across the Wellington Region.

# A1.4.4 Loss Comparison

Using RiskScape, we estimate the total building losses around the Wellington Region. Figure A1.2 compares the total building loss exceedance curves at different return periods estimated using the simulator outputs and the composite hazard map from the traditional approach.

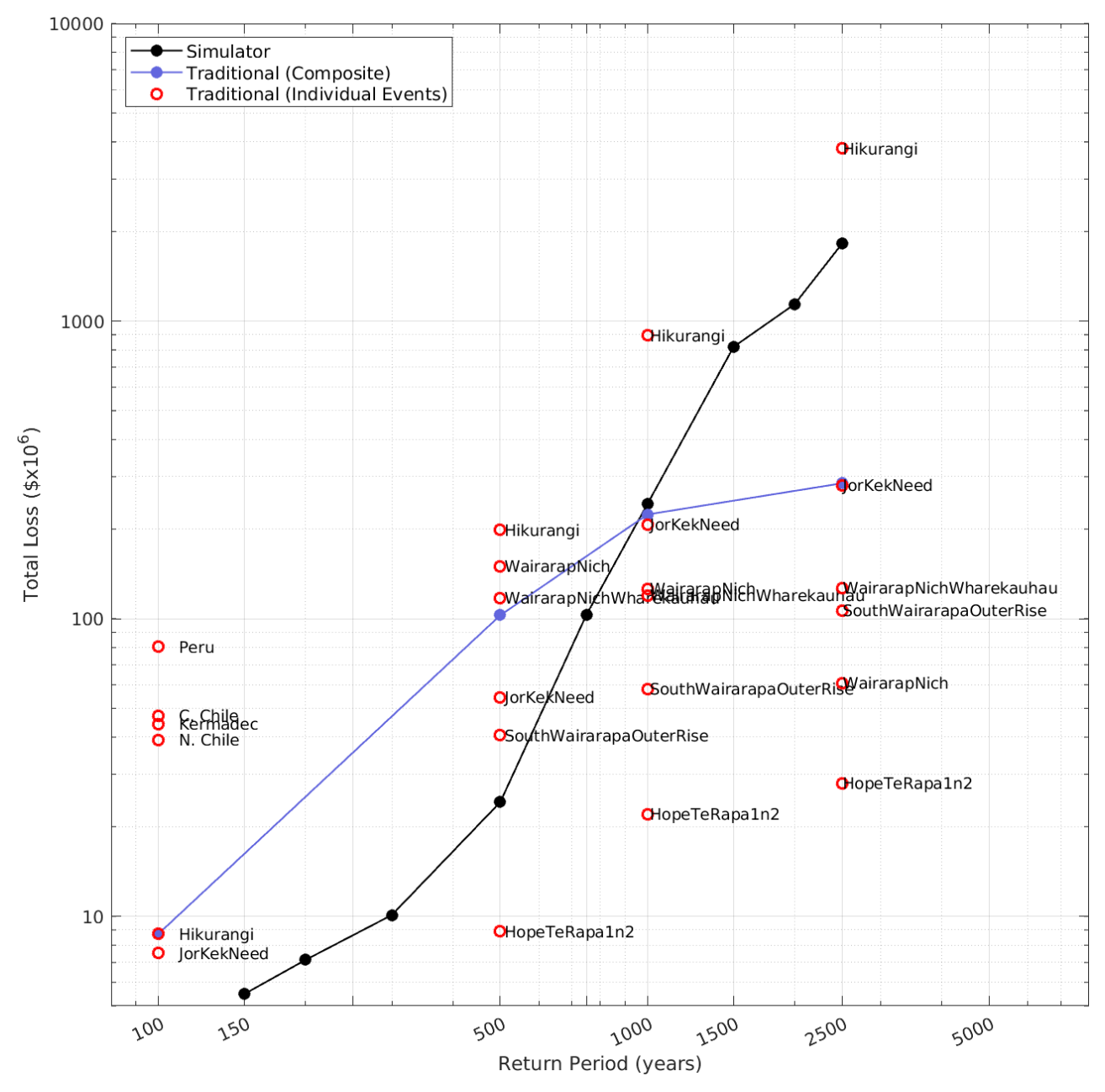


Figure A1.2 Comparison of the exceedance curves for total loss (calculated using RiskScape) for the two alternative approaches. Black line: loss calculated using the simulator events. Blue line: loss calculated using the mapped flow-depth hazard estimated by the traditional approach ('composite'). Red circles: the loss generated by each of the individual events that are used to make the composite return period hazard maps in the traditional approach. Note: due to the differences in how the events are analysed to obtain the losses at given return periods, more return periods can be readily extracted when the simulator events are used.

Like the inundation maps, similar patterns in the losses are observed. At return periods shorter than 1000 years, using the traditional method results in greater loss compared to the simulator method. However, at return periods greater than and equal to 1000 years, the losses generated using the simulator method result in larger losses compared to the traditional method. When we look at the individual events that make up each of the traditional method return periods we observe that the simulator method falls within the range of the deaggregated events.

The range of losses for events of the same return period in the traditional deaggregation is quite large. This shows that events with the same height at the coast could produce quite different losses

depending on other properties of the tsunami, such as the number and period of waves. The general trend is for distant source events, which would typically have longer periods and more waves close to the maximum height, to cause the largest losses, followed by local subduction events, with the lowest losses from crustal faults which are likely to have shorter wave periods. Also, an unusual trend is seen in the Wairarapa Fault scenarios (labelled WairarapNich), which decrease in loss with increasing return period, this is discussed further in Section A1.5.2.

We further explore the differences between the approaches by taking a different approach to estimating the risk in the traditional case. Here we calculated the loss for each scenario in the deaggregation, and then took a weighted mean of the losses. Figure A1.3 compares the results against the composite method and the simulator results.

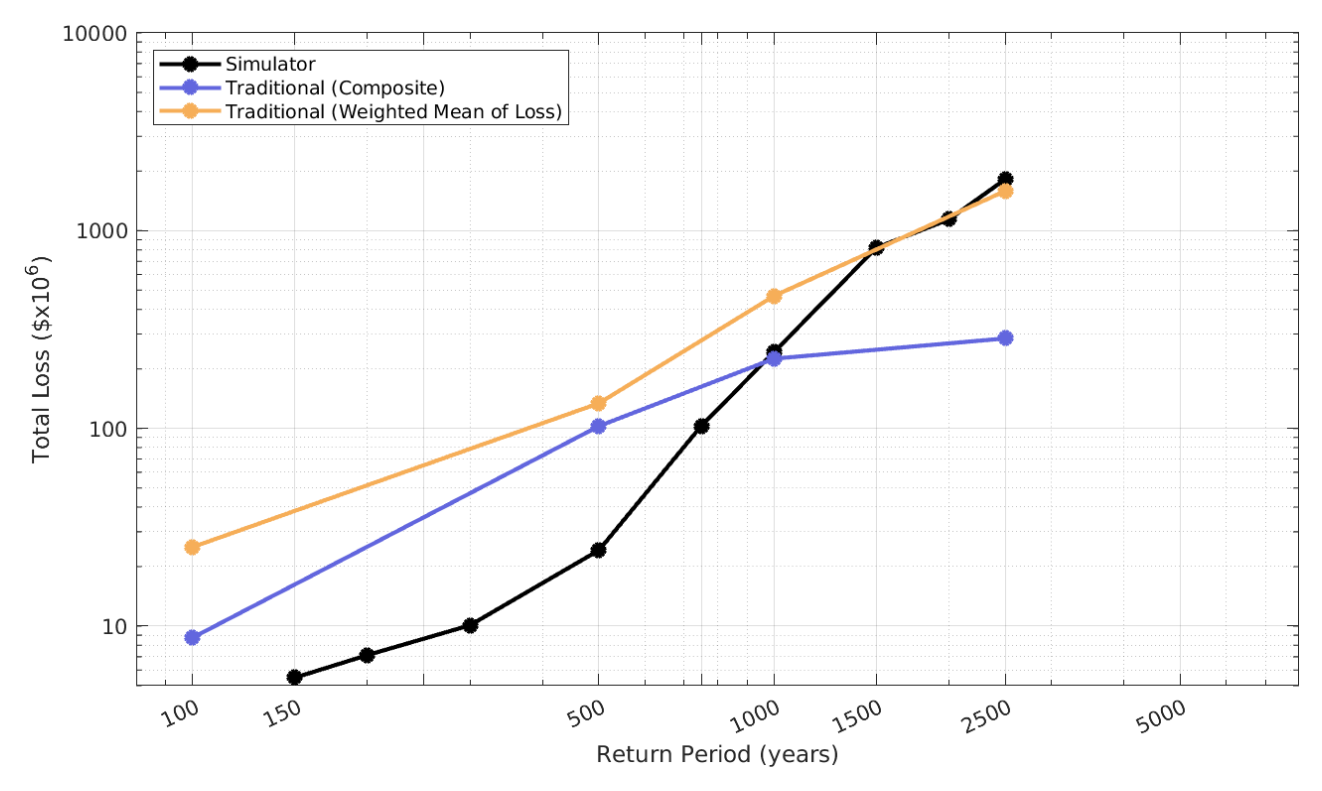


Figure A1.3 Comparison of the total loss exceedance curve (calculated using RiskScape) for the two alternative approaches. Black line: loss calculated using the simulator events. Blue line: loss calculated using the composite hazard maps from the traditional approach. Orange line: weighted mean of the loss, calculated using the estimated loss for each of the individual events that make up the hazard in the traditional approach. Red line: weighted median of the loss, calculated using the loss calculated for each of the individual events that make up the hazard in the traditional approach.

The weighted mean of loss method applied to the traditional approach produced similar trends but somewhat larger results (by around a factor of two) than the traditional composite hazard method at the lower return periods (1000 years or less), but the weighted mean estimated significantly larger losses at 2500 years. Both methods used with the traditional approach estimated larger losses than the simulator at 100 and 500 years. The weighted mean of loss method produced results more consistent with the simulator at 2500 years.

That the traditional approach produces larger losses than the simulator at the 100 year return period may be explained by the inclusion of distant sources, not currently present in the simulator model. The difference at 500 years return period appears to be related to the particular deformation model used for Hikurangi subduction earthquakes in the traditional approach, which causes subsidence of Wellington and the Hutt Valley and consequently increased losses, compared to more variable

deformation of this area in the simulator scenarios, often the result of co-rupture of upper-plate faults. This is discussed in more detail in Section 5.1.

# A1.4.5 16<sup>th</sup>, 50<sup>th</sup> and 84<sup>th</sup> Percentile Comparisons

We also identified by deaggregation the events that make up the 16<sup>th</sup> and 84<sup>th</sup> percentiles of epistemic uncertainty in the traditional approach, and calculated the losses associated with each event. Table A1.1 provides the losses and weights for each of the events that were analysed.

Table A1.1 Summary of the losses for each event, and their associated weights, divided based on percentile of uncertainty and return period.

Percentile	Return Period	Location	Loss (\$)	Weight (%)
		C. Chile	42600000.00	7.33
		Hikurangi	6497335.10	50.23
	100	Jordan-Kekerengu-Needles	13500000.00	8.57
	100	Kermadec	32600000.00	7.74
		N. Chile	32200000.00	10.71
		Peru	59800000.00	15.43
		Hikurangi	116000000.00	58.46
		Hope-Te Rapa	7894878.11	5.70
	500	Jordan-Kekerengu-Needles	45900000.00	19.93
	500	Kermadec	84500000.00	5.65
		Peru	267000000.00	5.15
4 Oth		Wairarapa	188000000.00	5.10
16 <sup>th</sup>		Hikurangi	36000000.00	47.57
		Hope-Te Rapa	9031517.03	7.09
		Jordan-Kekerengu-Needles	69700000.00	24.51
	1000	South Wairarapa Outer Rise	45000000.00	5.52
		Wairarapa	13000000.00	7.29
		Wairarapa-Wharekauhau	14400000.00	8.02
		Hikurangi	1810000000.00	41.53
	2500	Hope-Te Rapa	12700000.00	6.72
		Jordan-Kekerengu-Needles	341000000.00	22.55
		South Wairarapa Outer Rise	68500000.00	6.26
		Wairarapa	104000000.00	11.28
		Wairarapa-Wharekauhau	117000000.00	11.66
	100	C. Chile	47220916.50	7.10
		Hikurangi	8737906.56	55.65
		Jordan-Kekerengu-Needles	7518978.31	10.42
F.O+b		Kermadec	44288664.83	6.74
50 <sup>th</sup>		N. Chile	39219514.64	7.36
		Peru	80364548.87	12.73
	500	Hikurangi	198824224.05	49.98
		Hope-Te Rapa	8896705.02	7.21

Percentile	Return Period	Location	Loss (\$)	Weight (%)	
		Jordan-Kekerengu-Needles	54476858.24	23.44	
		South Wairarapa Outer Rise	40543666.84	4.85	
		Wairarapa	149832795.48	6.89	
		Wairarapa-Wharekauhau	117519300.14	7.63	
		Hikurangi	894943670.15	43.41	
		Hope-TeRapa	22024389.10	6.70	
		Jordan-Kekerengu-Needles	207283244.51	23.81	
	1000	South Wairarapa Outer Rise	58040896.81	6.29	
		Wairarapa	126059577.13	9.31	
		Wairarapa-Wharekauhau	119750351.86	10.48	
		Hikurangi	3800000000.00	39.31	
		HopeTeRapa1n2	28000000.00	5.77	
	0705	Jordan-Kekerengu-Needles	281000000.00	21.47	
	2500	South Wairarapa Outer Rise	107000000.00	6.62	
		Wairarapa	60700000.00	12.33	
		Wairarapa-Wharekauhau	127000000.00	14.49	
		C. Chile	52300000.00	6.35	
		Hikurangi	73600000.00	60.04	
		Jordan-Kekerengu-Needles	9623254.94	12.10	
	100	Kermadec	55300000.00	5.91	
		N. Chile	48800000.00	6.19	
		Peru	87800000.00	9.40	
		Hikurangi	58000000.00	46.53	
		Hope-Te Rapa	9294920.49	7.16	
	500	Jordan-Kekerengu-Needles	92300000.00	23.15	
		South Wairarapa Outer Rise	48500000.00	5.66	
		Wairarapa	109000000.00	8.55	
		Wairarapa-Wharekauhau	10300000.00	8.94	
84 <sup>th</sup>	1000	Hikurangi	2470000000.00	39.95	
		Hope-Te Rapa	16100000.00	6.80	
		Jordan-Kekerengu-Needles	271000000.00	22.72	
		South Wairarapa Outer Rise	81100000.00	6.25	
		Wairarapa	112000000.00	10.72	
		Wairarapa-Wharekauhau	113000000.00	13.56	
	2500	Hikurangi	7070000000.00	37.88	
		Hope-Te Rapa	60600000.00	6.29	
		Jordan-Kekerengu-Needles	341000000.00	16.19	
		South Wairarapa Outer Rise	232000000.00	6.49	
		Wairarapa	79200000.00	15.25	
		Wairarapa-Wharekauhau	118000000.00	17.90	

Using the losses for each of the events in Table A1.1, we calculated the weighted mean of the losses at the different percentiles and return periods. Figure A1.4 summaries these results.

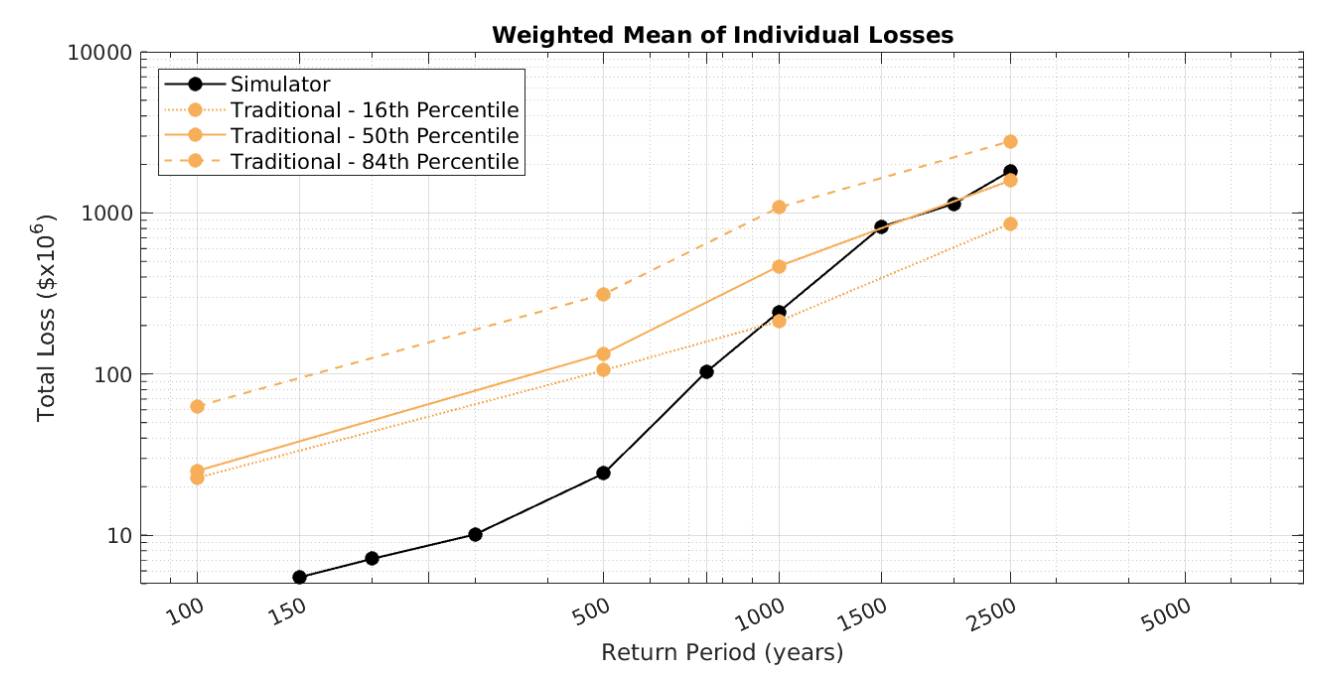


Figure A1.4 Comparison of the total loss exceedance curves (calculated using RiskScape) for the Simulator approach (black) and the weighted mean of the losses in the traditional approach (yellow) at each return period.

For the traditional approach using the weighted mean, the results largely follow the expected pattern, and converge towards the simulator results at the longer (1000+ years) return periods. The deviation from the simulator results at shorter return periods can probably be explained by the presence of distant sources (particularly at 100 years), and by specific features of the Hikurangi deformation model used for the traditional approach (see Section A1.5.1).

We also calculated the losses associated with the composite hazard maps generated by the traditional approach for each return period and chosen percentile. Figure A1.5 shows the composite map losses for each return period for the 16<sup>th</sup>, 50<sup>th</sup> and 84<sup>th</sup> percentiles, and the individual event losses are also plotted. When we look at the losses associated with the ensemble hazard, as expected the 84<sup>th</sup> percentile maps generate the largest losses, and in general the 16<sup>th</sup> percentile maps generate the smallest losses, except for an anomaly at the 500-year return period. The anomaly appears to be related to the deaggregation being of the tsunami height at the coast relative to background sea level. As mentioned previously, for a given height at the coast distant sources produce greater inundation and loss, and the inclusion of a distant source (Peru) in the 500 year 16<sup>th</sup> percentile hazard (where no distant source appears in the deaggregation of the 50<sup>th</sup> and 84<sup>th</sup> percentile at this return period) seems to be partly responsible. An unusual trend in the Wairarapa Fault scenarios, where uplift of the landscape reduces losses (see Section A1.5), may also contribute.

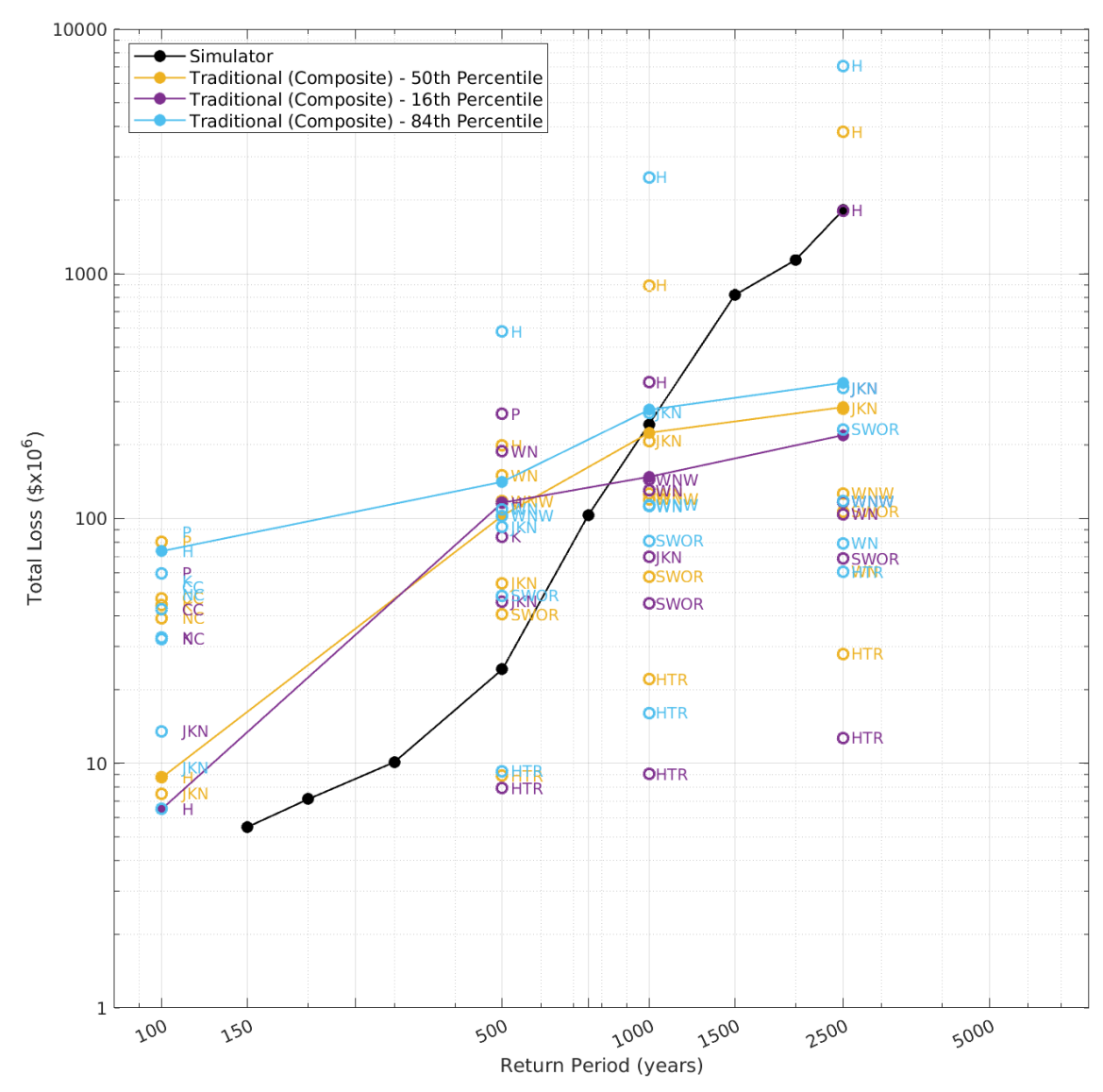


Figure A1.5 Comparison of the total loss exceedance curves (calculated using RiskScape) for the two alternative approaches (simulator and traditional composite hazard). Black line: loss calculated using the simulator events. Other colours and symbols relate to the traditional composite hazard approach. Orange line: losses calculated using the events that make up the 50<sup>th</sup> percentile. Orange open circles: individual events that make up the 50<sup>th</sup> percentile. Purple line: losses calculated using the events that make up the 16<sup>th</sup> percentile. Purple open circles: individual events that make up the 84<sup>th</sup> percentile. Blue open circles: individual events that make up the 84th<sup>th</sup> percentile. CC = Central Chile, H = Hikurangi, JKN = Jordan, Kekerengu and Needles, NC = Northern Chile, P = Peru, HTR = Hope and Te Rapa, SWOR = South Wairarapa Outer Rise, WN = Wairarapa Nicholson, WNW = Wairarapa Nicholson Wharekauhau.

# A1.4.6 Comparison of Sensitivity to Sea Level, Friction and Model Resolution between the NTHM and NTM Stage 1 Events

In the NTM Stage 1, we investigated how changing different modelling parameters influenced the tsunami inundation and loss. Section A1.4.7 compares the simulations from the simulator and traditional approaches when the simulations are run at Mean High Water Springs (MHWS) and Section A1.4.8 investigates how the traditional approach simulations respond to changes in the tsunami modelling resolution and roughness of the simulation grid.

#### A1.4.7 Simulations at Mean High Water Springs

In Stage 1 we identified the events that generated an adjusted wave height at the coast of at least 2 m and simulated those events again but at MHWS. For Wellington MHWS is 0.68 m greater than mean sea level. For the 100-year, 500-year and 1000-year return periods in the traditional approach we reran the simulations at MHWS and compared the results to the simulator results that were already analysed in Stage 1. Figure A1.6 compares the inundation maps from the simulator and traditional approaches, that are the result of running the simulations at MHWS.

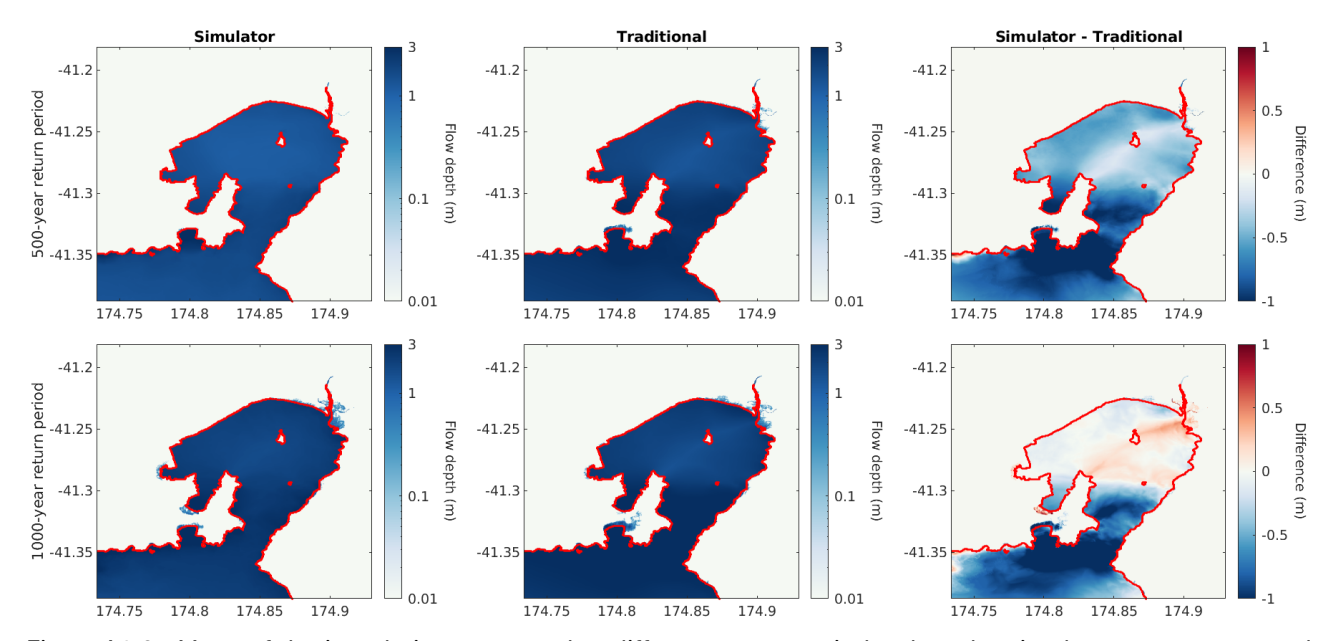


Figure A1.6 Maps of the inundation generated at different return periods when the simulator events are used and when the traditional approach to hazard is used, and modelling is undertaken at mean high water spring (mean sea level + 0.68 m). Left column: inundation generated when the simulator events are used. Middle column: inundation generated when the traditional approach is used. Right column: difference between the two approaches. Top row: 500-year return period. Middle row: 1000-year return period.

From the maps in Figure A1.6 similar patterns to the mean sea level simulations are observed when the two approaches are compared, but the areas of inundation and the flow depths are larger. In general, the traditional approach generates greater areas of inundation and flow depths compared to the simulator approach, which is most notable at the 500-year return period. For the 1000-year return period, there are some areas in which the simulator approach results in greater areas, around the Port and Evans Bay, and in some areas the simulator approach generates larger flow depths, to the east of the Hutt River, compared to the traditional approach. These differences in the areas of inundation are directly translated to the differences in the total loss that is observed for the two approaches. Figure A1.7 shows the total losses that are generated by the two approaches when the modelling is undertaken at mean high water springs.

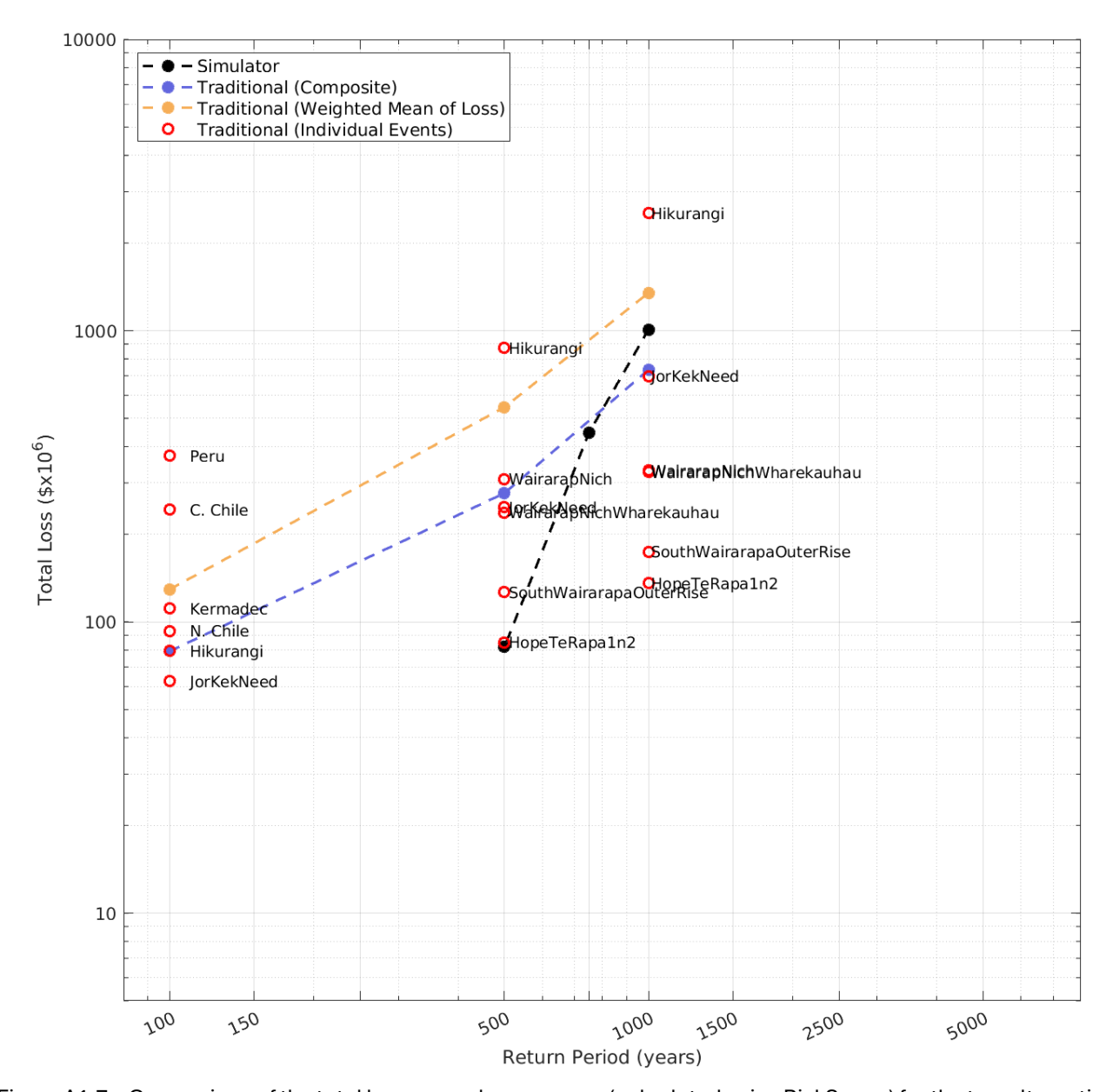


Figure A1.7 Comparison of the total loss exceedance curves (calculated using RiskScape) for the two alternative approaches, when modelling is undertaken at mean high water springs (mean sea level + 0.68 m). Black line: loss calculated using the simulator events. Blue line: loss calculated using the composite hazard maps generated using the traditional approach and composite hazard method. Yellow dashed line: loss calculated using the composite hazard maps generated using the traditional approach and weighted mean of loss method. Red circles: the loss generated by each of the individual events in the traditional approach.

For the simulations run at MHWS the pattern in the losses shows similarities to the pattern in the losses for the simulations that are run at MSL. The key difference is where the two lines intersect. For the simulations run at MSL the intersection point is at the 900-year return period and for the simulations run at MHWS it is at the 800-year return period. We also observe the same pattern when we compare individual traditional events to the simulator, with the simulator losses falling withing the range of the individual event losses. The only difference is that at the 500-year return period the simulator losses are much closer to the Hope-Te Rapa events when modelling is undertaken at MHWS compared to when modelling is undertaken at MSL.

We also compared the loss for each approach when the simulations are run at mean sea level and mean high water springs. Figure A1.8 compares the losses at the two sea levels and the two approaches.

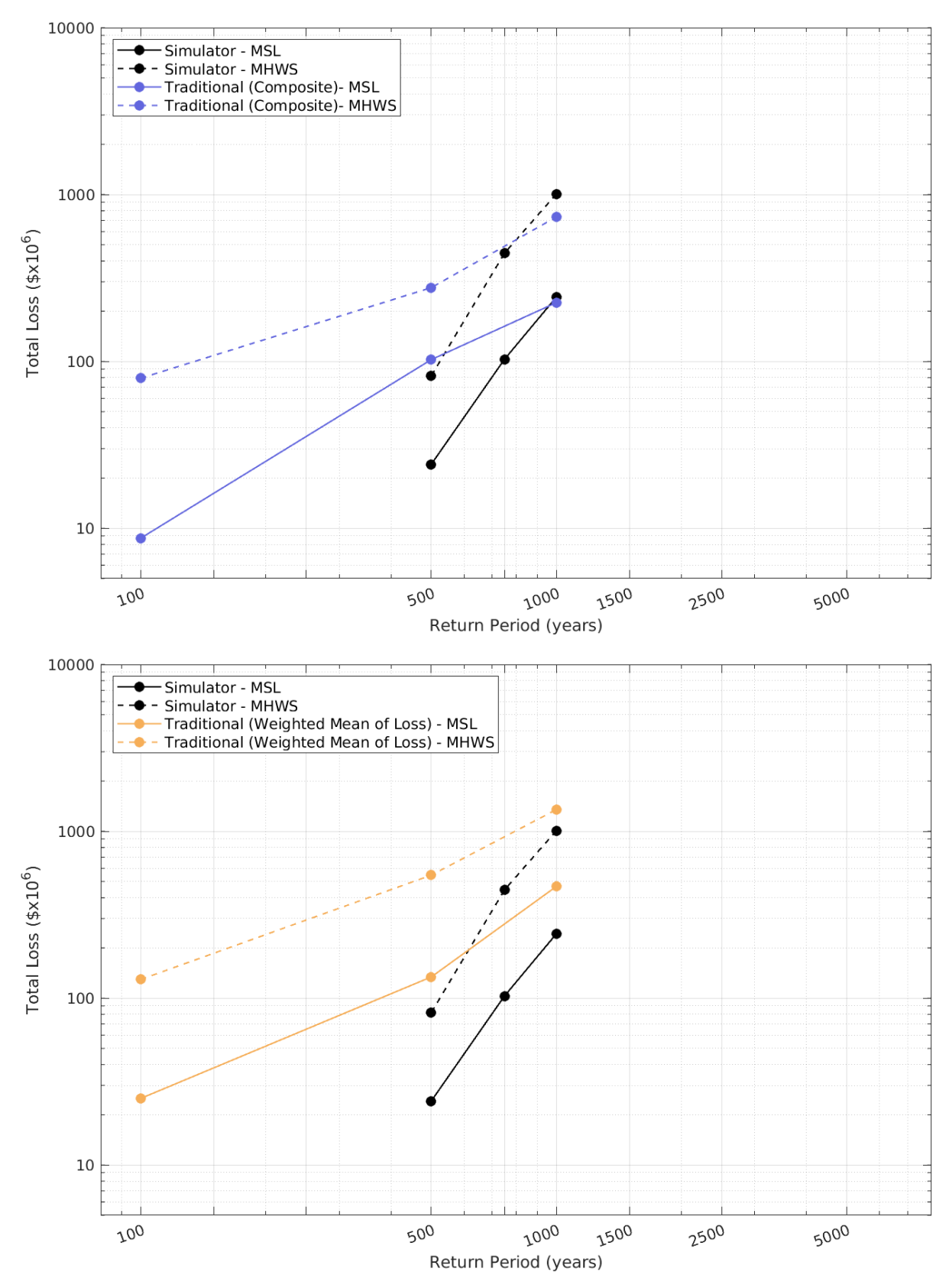


Figure A1.8 Comparison of the losses that are generated by the two approaches when modelling is undertaken at both mean sea level and mean high water springs. Black lines: losses generated when the simulator events are used. Blue lines (top): losses generated when the traditional approach is used to generate composite hazard maps. Yellow lines (bottom): losses when the traditional approach is used to calculate the weighted mean of losses. Solid lines: losses generated when modelling is undertaken at mean sea level (MSL). Dashed lines: losses generated when modelling is undertaken at mean high water springs (MHWS).

When we compare the two methodologies we observe the same patterns. For both methodologies the losses calculated when the simulations are run at MHWS is greater than the losses calculated when the simulations are run at MSL. This is consistent with what we observed in the previous analysis.

# A1.4.8 Simulations Run with Different Resolutions and Roughness Coefficients

In Stage 1 we also looked at how changing the resolution of the simulation grid and the roughness grid used in the simulation process impacted the inundation and the associated losses. Figure A1.9 compares the losses generated when the resolution is changed from 40 m to 20 m and 10 m and a multiple friction grid is used.

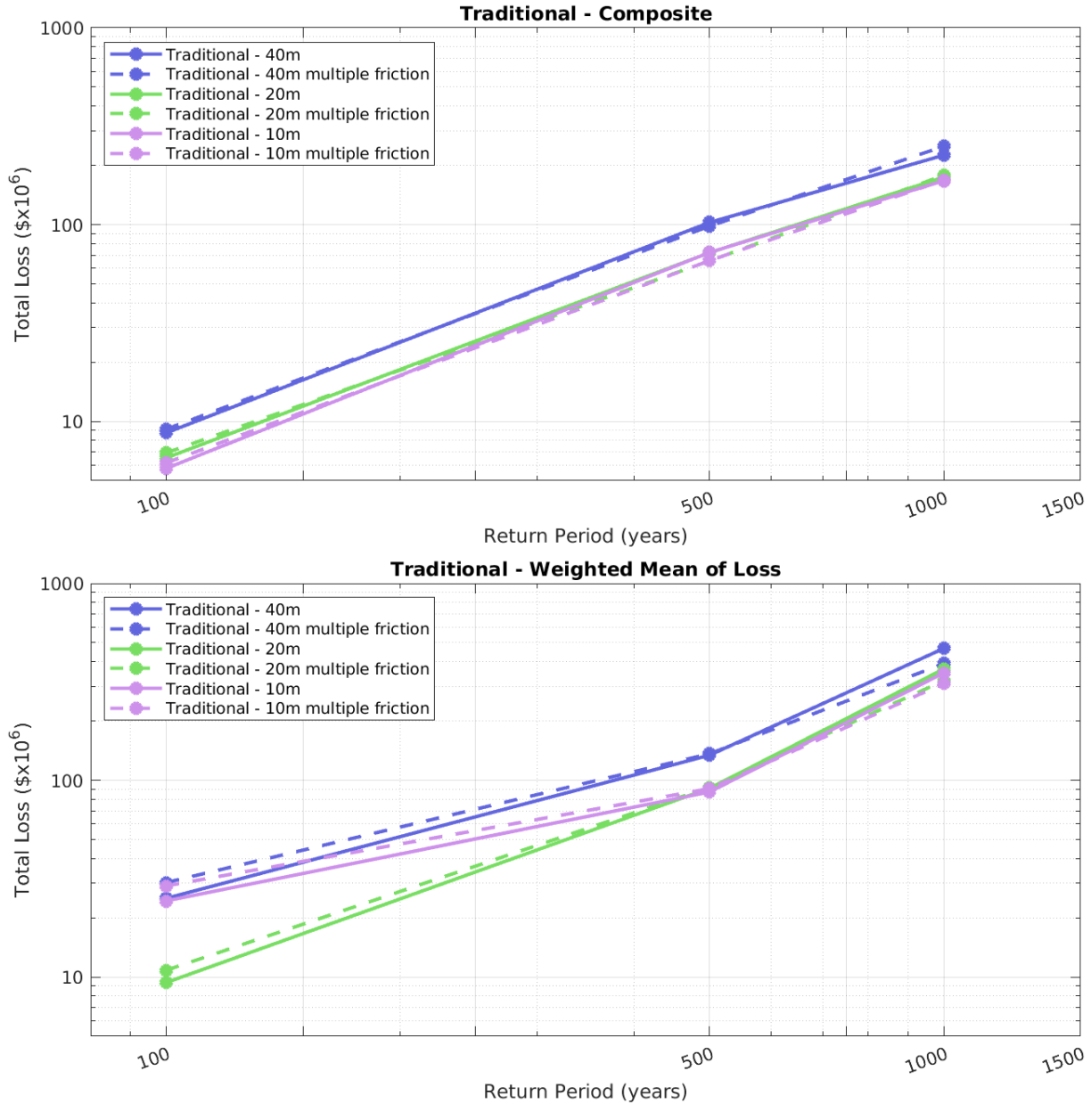


Figure A1.9 Comparison of the losses that are calculated when different modelling resolutions and friction coefficients are used. Blue lines: 40 m resolution. Green lines: 20 m resolution. Purple lines: 10 m resolution. Solid lines: one friction coefficient is used in the modelling. Dashed lines: multiple friction grid is used in the modelling. In the upper figure losses were calculated using composite hazard maps in the Traditional approach, in the lower figure losses were calculated using the weighted mean loss.

From the simulations at the different resolutions and roughness values we see that the differences in the losses between running the simulations with one friction value and a multiple friction grid are very small. However, running the simulations at higher resolutions results in the losses decreasing. While the differences are larger between the 40 m resolution and the 20 m resolution there are small to no differences between the 20 m resolution and the 10 m resolution. While increasing the simulation resolution from 40 m to 20 m would increase the time required, the computational memory requirements and the storage requirements this increase is considerably smaller than if we were to increase the resolution to 10 m. The differences between the losses calculated using the 10 m and 20 m resolutions are so small that the benefit of increasing the time and computational costs is not countered with the change in the losses.

## A1.5 Discussion of Differences between NTM Stage 1 and NTHM

While we observe similarities between the two methods, there are some differences. In this section we analyse the earthquake deformation models to see if differences in the earthquake models explain the differences.

# A1.5.1 Hikurangi Subduction Margin Events

When comparing the events the rupture the Hikurangi subduction margin from the traditional approach and the simulator there are significant differences between the rupture patterns of the events. For this comparison we have isolated events from the simulator that rupture just the subduction interface. While there are events in the simulator that hold more similarities to the traditional approach, they also involve the co-rupture of crustal faults. Table A1.2 and Figure A1.10 summarise the differences between the two approaches.

Table A1.2 Summary of the Hikurangi earthquake magnitudes from the traditional approach and the simulator.

		Simulator			
Return Period <sup>3</sup>	100	500	1000	2500	-
Magnitude⁴	8.1	8.6	8.7	8.83	6.5–8.34*

<sup>\*</sup> Not including events that rupture other faults as well.

This is the return period of the coastal tsunami hazard to which the tabulated source contributes. This is not the same as the recurrence interval for the particular source, which is always longer.

<sup>&</sup>lt;sup>4</sup> The NTHM (in the Traditional approach) uses the concept of an 'Effective Magnitude' which takes into account a range of different causes of uncertainty and variability as if they had an effect equivalent to increasing or decreasing the earthquake magnitude (see Section 6.5 of Power [2013]).

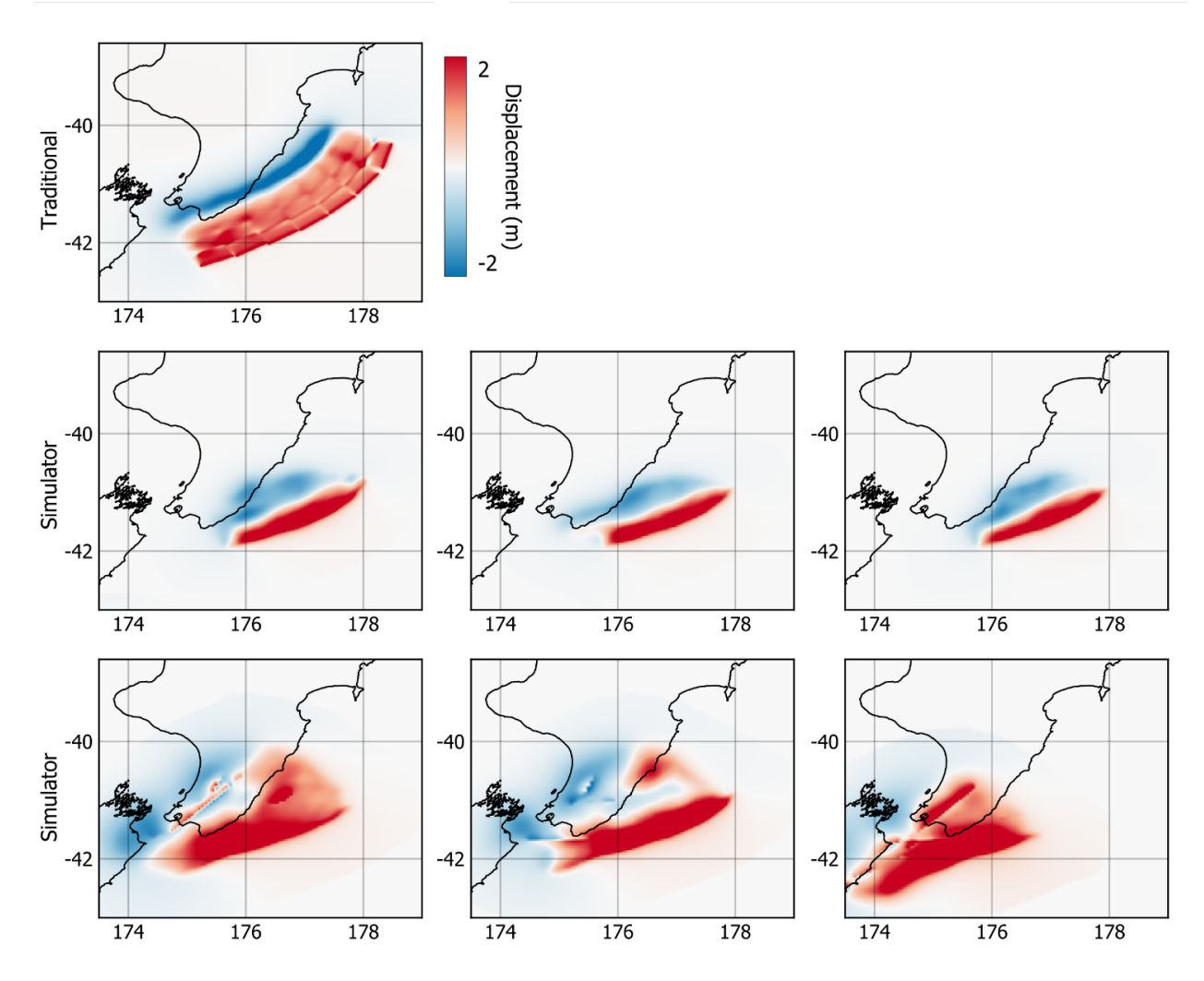


Figure A1.10 Initial surface displacements for the different scenarios modelled (Hikurangi). Top row: 1000-year return period Hikurangi event from the traditional approach using the 2021 NTHM. Middle row: Examples of the largest events taken from the simulator that only rupture the Hikurangi Subduction Margin (Mw~8.3). Bottom row: Examples of events from the simulator of similar magnitude (Mw~8.7) to the 1000-year return period Hikurangi event from the traditional approach, showing combined rupture of the Hikurangi Subduction Margin and upper plate faults.

The first difference is the magnitude range of the two approaches and the second difference is the deformation that is occurring across the Wellington Region. Here we observe that the traditional approach 1000-year event generates more subsidence around the region compared to the similar (but in this case lower magnitude) interface-only simulator events. If we include simulator events that also involve the rupture of crustal faults, then we can include events with magnitudes that are closer to the traditional approach. The inclusion of the multi-fault rupture events also allows deformation of similar degree (but wider variation) to that observed in the traditional event to be observed in the simulator events. Therefore, we observe greater variation in the deformation models of the simulator events that are incorporated into the longer return periods which likely explains why the simulator generates comparable, or sometimes greater (especially if the composite method is used), losses than the traditional approach at longer return periods.

#### A1.5.2 Wairarapa Fault Events

There are also obvious differences between the simulator events and the traditional events that involve the rupture of both the Wairarapa and Wharekauhau Faults. **Error! Reference source not found.** Table A1.3 and Figure A1.11 compare the different events from the two approaches.

Table A1.3 Summary of the Wairarapa earthquake magnitudes from the traditional approach and the simulator.

		Simulator			
Return Period	100	500	1000	2500	-
Magnitude	NA*	8.3	8.4	8.45	6.5–7.76**

<sup>\*</sup> No events that involve Wairarapa or Wharekauhau Faults make up the top six events in the deaggregation.

<sup>\*\*</sup> Not including events that rupture other faults as well.

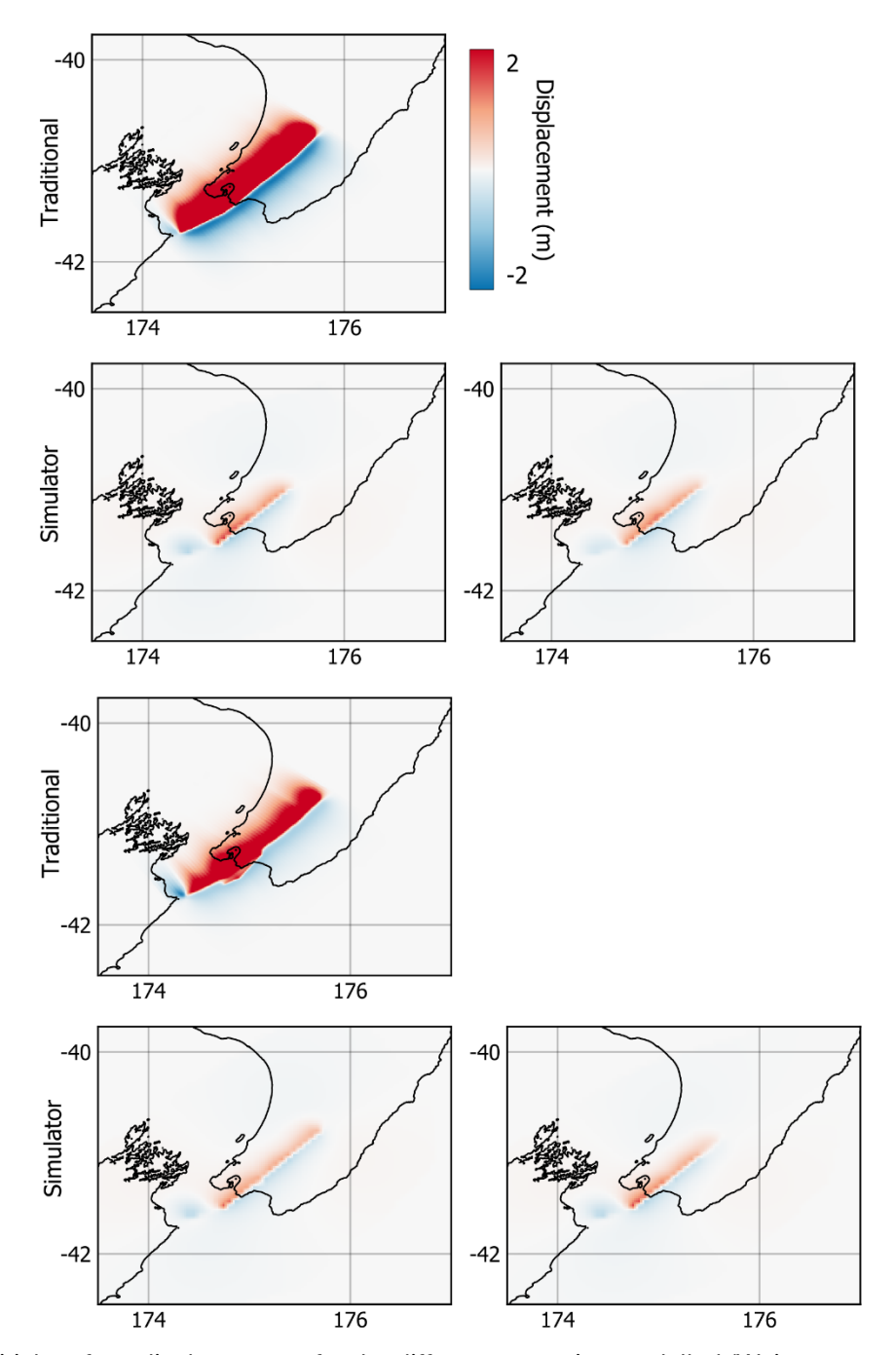


Figure A1.11 Initial surface displacements for the different scenarios modelled (Wairarapa and Wharekauhau).

1st row: 1000-year return period Wairarapa event from the traditional approach. 2nd row: Events taken from the simulator that also only rupture the Wairarapa Fault. 3rd row: 1000-year return period Wairarapa and Wharekauhau event from the traditional approach. 4th row: Events taken from the simulator that also only rupture the Wairarapa and Wharekauhau Faults.

For both types of Wairarapa fault ruptures, the initial surface deformation of the events in the traditional approach are significantly larger than that observed by the events from the simulator. The magnitudes of the earthquakes in the two approaches also are very different, with the largest magnitude event in the simulator that does not involve other faults being smaller by around 0.5 magnitude units than the smallest event in the traditional approach. The surface deformation that occurs in the Wellington Region is also significantly smaller for the simulator earthquakes compared to the traditional approach earthquakes.

The surface displacement of the earthquakes in the traditional approach could also explain the counterintuitive result that the losses from Wairarapa Fault events decrease with increasing return period. As the magnitude of the event increases, with increasing return period, the uplift that occurs in the Wellington Region also increases. This results in both a larger tsunami (relative to background sea level) but also a higher landscape. As the tsunami propagation is partially non-linear, while the effect of raising the terrain is linear, the effect of the raised terrain leads to a net reduction in the impacts of the waves that are generated.

### A1.5.3 Jordan-Kekerengu-Needles Fault Events

Like both the Hikurangi Subduction Margin events and the Wairarapa Fault events, the events that rupture the Jordan-Kekerengu-Needles Faults alone also differ in magnitude, but the differences in the surface deformation is smaller. Table A1.4 and Figure A1.12 compare the events from the two approaches.

Table A1.4 Summary of the Jordan-Kekerengu-Needles earthquake magnitudes from the traditional approach and the simulator.

		Simulator			
Return Period	100	500	1000	2500	-
Magnitude	7.7	7.9	8.0	8.1	6.5–7.78

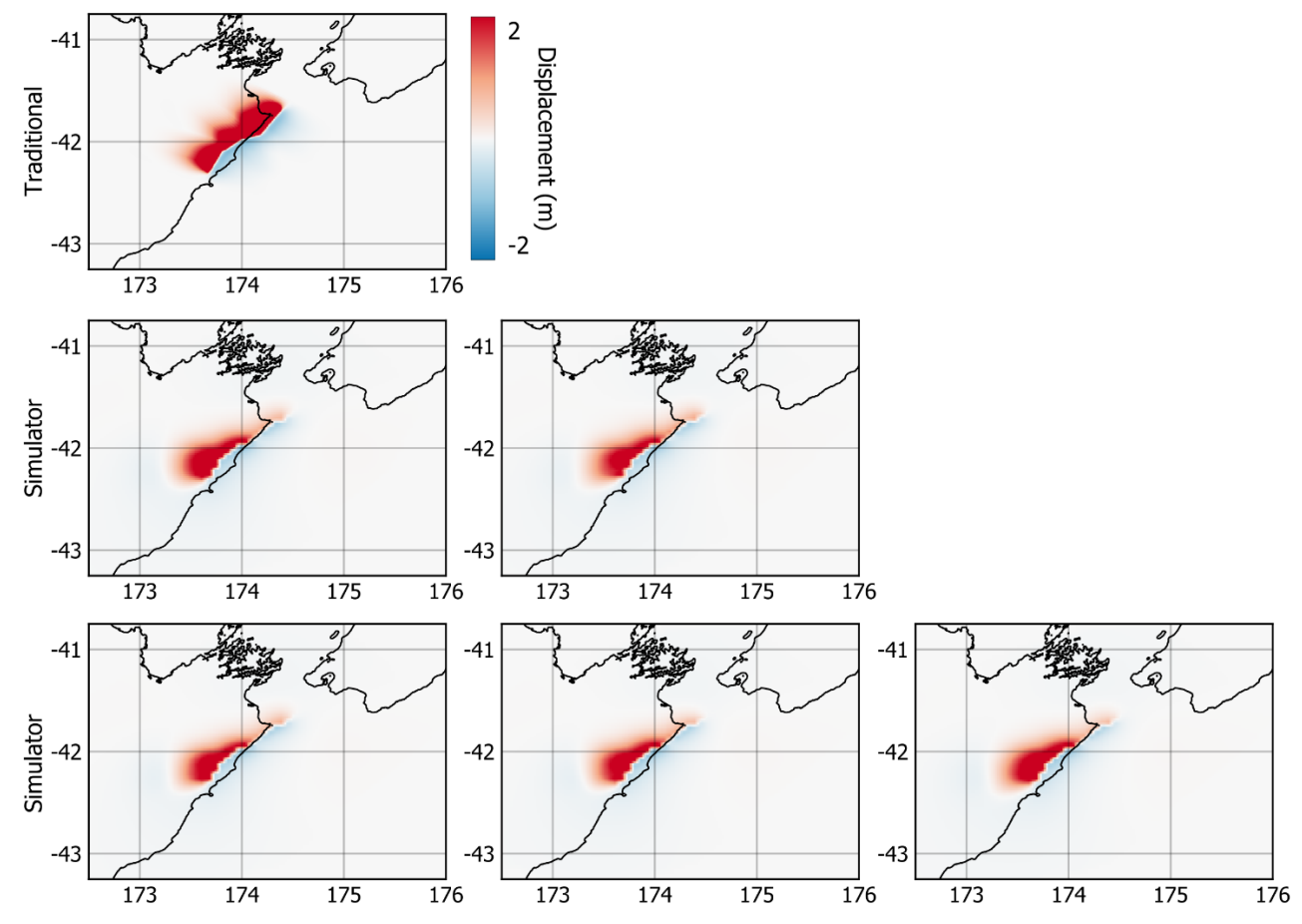


Figure A1.12 Initial surface displacements for the different scenarios modelled (Jordan-Kekerengu-Needles). Top row: 1000-year return period Jordan-Kekerengu-Needles event from the traditional approach. Middle and bottom rows: Events taken from the simulator that also only rupture the Jordan-Kekerengu-Needles faults.

While the earthquake deformation is similar for both the traditional and simulator approach, there is slightly more deformation around the Needles Fault in the traditional approach compared to the simulator approach and the magnitudes of the traditional approach are usually larger than the equivalent events in the simulator unless other faults are involved.

## A1.5.4 Hope-Te Rapa Fault Events

As previously discussed both the magnitude and surface deformation of the events that rupture the Hope and Te Rapa Faults in the traditional approach are larger than that in the earthquake simulator. There is also only one event in the simulator that ruptures exactly the same faults as that in the traditional approach. Table A1.5 and Figure A1.13 compares the events from the different approaches.

Table A1.5 Summary of the Hope-Te Rapa earthquake magnitudes from the traditional approach and the simulator.

		Simulator			
Return Period	100	500	1000	2500	-
Magnitude	NA*	7.8	7.9	7.9	7.29

<sup>\*</sup> No events that involve Hope Te Rapa Fault make up the top six events in the deaggregation.

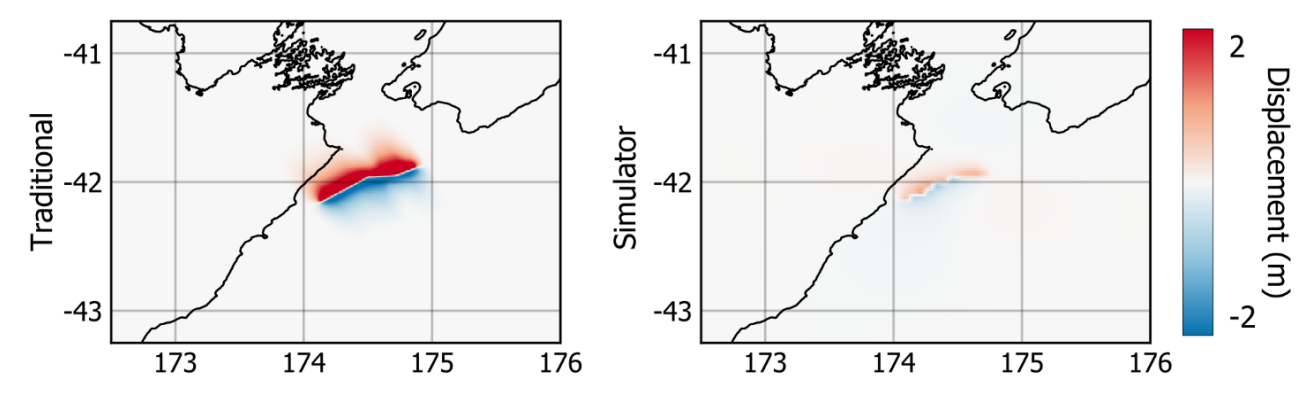


Figure A1.13 Initial surface displacements for the different scenarios modelled (Hope – Te Rapa). Left: 1000-year return period Hope – Te Rapa event from the traditional approach. Right: Event taken from the simulator that only ruptures the Te Rapa Fault.

This event in the traditional approach generates the smallest inundation and losses, and the event presented in Figure A1.13 from the simulator has not modelled through to inundation in Stage 1 because it did not produce wave heights that met the threshold established.

# A1.6 IT Infrastructure Necessary for Nation-Wide Probabilistic Tsunami Risk Calculation with Hydrodynamic Tsunami Simulations

**Milestone 4:** Assessment of the IT and computational resources necessary to facilitate application of the Stage 1 framework in a New Zealand-wide context

The NTM approach requires two computationally intensive steps: (1) earthquake cycle simulations and (2) hydro-dynamic tsunami propagation and inundation modelling.

We have completed all necessary earthquake cycle simulations for local and regional events under aligned RNC2 and NHRP programmes. Work to extend our distant source models is relatively computationally "light" and can be completed on New Zealand supercomputer resources with only moderate effort, within the anticipated budget of Stage 2.

Hydrodynamic modelling of inundation is necessary to capture inundation from complex earthquake scenarios in which deformation from local faulting creates complex patters of coastal vertical deformation, including non-linear interaction with tsunami waves. In NTM Stage 1, this computationally expensive modelling was undertaken with New Zealand supercomputing resources utilising our parallel CPU Comcot software. For nation-wide implementation, computationally cheaper hydrodynamic modelling is necessary. In Stage 2, we will compare inundation estimates from our existing CPU Comcot workflow with calculations made by GPU software. Candidate codes include GPU HySEA, a software package in common use in the European community and GPU BGFlood, a software package developed by NIWA and used in the national flood model. We anticipate approximately 3 months of computational time for calculation of inundation with either of the GPU codes.

# A1.7 Summary

We have undertaken an extension of the NTM Stage 1 project as part of NTM Stage 1.a. This addendum to the Stage 1 Final Report documents successful completion of that work. We present a comparison of the Stage 1 probabilistic tsunami risk model for the Wellington Region and risk derived from the previous National Tsunami Hazard Model. Our results highlight key improvements over the previous source model through the inclusion of complex scenarios involving locally generated coastal vertical deformation from simultaneous rupture of the Hikurangi megathrust and crustal events. Our estimates suggest total risk of the Wellington region is less than previously estimated, however, Stage 2 work

including distant sources must be undertaken before final conclusions are drawn. We further present programme infrastructure that contributes to the design and implementation of Stage 2. This includes establishment of a Technical Advisory Group and exploration of computational resources necessary for undertaking nation-wide modelling.